Water-Based Drill-In Fluid Optimization Using Polyelectrolyte Complex Nanoparticles as a Fluid Loss Additive

By

Lucas Brandon Whatley

Submitted to the graduate degree program in Chemical and Petroleum Engineering and the Graduate Faculty of the University of Kansas in partial fulfillment of the requirements for the degree of Master of Science in Petroleum Engineering

_____

Chairperson: Dr. Reza Barati

_____

Dr. Jyun Syung Tsau

_____

Dr. Shapour Vossoughi

Date Defended: 01/29/2017

The Thesis Committee for Lucas Brandon Whatley

certifies that this is the approved version of the following thesis:

Water-Based Drill-In Fluid Optimization Using Polyelectrolyte Complex Nanoparticles as a Fluid Loss Additive

_____

Chairperson: Dr. Reza Barati

Date approved: 01/29/2017

Abstract

It is well known within industry that conventional drilling fluids can damage the well's producing zone. Damage mechanisms occur due to leakage of drilling fluid into the formation even after the formation of a filter cake. This filtrate contains entrained particulates that can enter the pore spaces of the rock and restrict flow through the pore throats resulting in reduced permeability during production. Cleaner drill-in fluids with low solids content have been developed for use when drilling through a producing zone in an attempt to mitigate the extent of damage caused by leak-off. These fluids should not only provide excellent fluid loss prevention, but also exhibit the rheological characteristics needed to perform the traditional functions of conventional fluids. Even though these fluids reduce the amount of particulates entering the formation by containing less solids, the filtrate that is still able to flow through the filter cake can be equally as damaging. Reduction of filtrate volumes can be further achieved by introducing nanoparticles to bridge across the nano-sized gaps within the filter cake. This research focuses on the application of polyelectrolyte complex nanoparticles (PECNP) as a fluid loss additive to further enhance the filter cake filtration properties of a general drill-in fluid. A baseline fluid is formulated consisting of a sodium chloride brine, biopolymers for rheology and fluid loss purposes, and calcium carbonate as a density and bridging agent. The ratio and pH of polyelectrolytes were optimized in order to create stable PECNPs for this system. Different dilutions of PECNPs were added and tested in a static fluid loss setup, where filtrate volumes were compared to determine the best system of $1/8^{th}$ diluted nanoparticles. The chosen system was then taken to be tested in the dynamic fluid loss setup "Quasimodo" where fluid loss volumes were successfully reduced and wall building coefficients lowered. Analysis of cleanup curves after testing revealed that the PECNP drill-in fluid was less damaging to the core permeability than when the baseline fluid was used.

Acknowledgments

I would like to thank my advisor Dr. Reza Barati for his guidance, support and encouragement throughout the process of completing the research for this project. I would also like to thank my committee members Dr. Jyun Syung Tsau and Dr. Shapour Vossoughi for their comments and suggestions for the improvement of this thesis.

A special thank you to Zach Kessler and Scott Ramskill for the countless hours they put into fixing and assembling the dynamic fluid loss setup "Quasimodo" as well as help with any technical or mechanical needs involved with the other laboratory equipment. I would also like to thank Schlumberger for the donation of "Quasimodo" and the static fluid loss setup, Drilling Specialties Company for donation of the Flowzan® biopolymer and GEO Drilling Fluids for the donation of the sized calcium carbonate.

I sincerely appreciate all the friends I have made during my time here at KU, especially those involved in Dr. Barati's research group. Their friendship and motivation helped me from beginning to end of this journey.

I am grateful for Maddie McCaffrey and her family whom I now consider to be family of my own. They helped make Lawrence, KS my home away from home.

Finally, I dedicate this thesis to my parents (Thomas and Gail Whatley), sister (Angel Whatley), and brother (Matt Whatley) for always being there for me to provide reassurance and encouragement when needed the most. Without their love and support, this thesis would not have been possible.

Table of Contents

List of Figures

List of Tables

1. Introduction

1.1 Drilling Fluids and the Transition into Cleaner Drill-In Fluids

One of the main components of producing successfully from an oil well is the fluid used when initially drilling the well. Much research has gone into drilling fluid technology since the first success of the rotary drilling bit (1). History has shown that drilling fluid optimization is a key constituent in the process of saving time and money when drilling a well. Between the years of 1947 and 1957, a lot of focus was placed on drilling fluid products that could effectively produce ideal viscosity and fluid loss properties which would help increase the penetration rate (2). However, within the past few decades "expense versus value" drilling has become a topic of discussion between oilfield operators (3). The "expense" refers to the actual cost of drilling a well while the "value" denotes how much worth is to be gained once the well is in production. The early days of drilling prioritized drilling quickly and doing it cheaply. This is no longer the case as drilling and completions engineers agree that safeguarding the reservoir from damage is more important (3). One of the most influential sources of reservoir damage near the wellbore is fluid loss to the formation while drilling the wellbore. This leakage of fluid into the rock matrix carries particulates from the drilling fluid into the pore spaces of the rock. When flow back to the wellbore is attempted during the production, these particles can bridge across pore throats severely reducing the near-wellbore permeability, in some cases up to 90% (4). It is necessary to form a thin impermeable filter cake on the borehole wall as quickly as possible to prevent migration of filtrate and particles into the formation. To mitigate this problem, cleaner brine based drill-in fluids, also known as reservoir drilling fluids (RDF), have been developed with minimal solids content to reduce damage when drilling through a productive formation. This becomes exceptionally important in regards to horizontal wells considering that the drilling fluid will have contact with a

producing zone over extensive distances and extended periods of time (5). The use of drill-in fluids has and will become increasingly important as the drilling of horizontal wells continues to rise. Many drill-in fluids are water or brine based with biopolymers added to reach the desired viscosity. Sized calcium carbonate particles in the micrometer range are included to serve as a bridging agent for fluid loss prevention. This however leaves nanometer sized void spaces between calcium carbonate particles when bridging across pore throats. Macro and micro sized fluid additives often fall short of fulfilling essential tasks in difficult drilling and production environments due to their insufficient characteristics (6). In recent years, application of nanotechnology in the oilfield has been a topic of discussion (7). Researchers have looked to use of nanoparticles as a fluids loss agent to build thinner filter cakes at a faster rate in areas of fracturing as well as drilling fluids. Specifically, polyelectrolyte complex nanoparticles have proven to be a successful fluid loss additive in tight and ultra-tight hydrocarbon bearing formations for hydraulic fracturing applications (8).

1.2 Thesis Statement

This research aims to investigate the application of polyelectrolyte complex nanoparticles (PECNP) in cleaner drill-in fluids to further prevent fluid loss and formation damage so that drilling through pay zones can result in optimized production. A baseline drill-in fluid is formulated and fluid loss tests are performed under static conditions with varying concentrations of PEC nanoparticles to determine the optimal systems which are then tested under dynamic conditions. A core flood setup is utilized to define initial permeability and assess any associated damage caused during fluid loss testing by analyzing clean up curves created from gathered data. The fluid is tested against limestone and sandstone cores of low and high permeability in the range

of 0.1 – 10 mD. This will allow for a somewhat broad scope view of the fluid's performance with different rock types and permeability ranges.

2 Literature Review

2.1 Drilling Fluid Basics

The drilling fluid, frequently referred to as drilling mud, can be water or oil-based in most situations. Water-based fluids are most commonly used considering the higher cost and environmental issues associated with oil-based fluids (9). They are used in drilling of approximately 80% of all wells (10). Drilling fluids perform many functions to facilitate the rotary drilling process. The most basic of these functions include but are not limited to: (3) (9)

1. Clean the rock cuttings from the borehole and bring them to the surface;
2. Apply adequate hydrostatic pressure to prevent formation fluids from entering the wellbore;
3. Keep the newly drilled hole from collapsing;
4. Lubricate and cool the rotating drill bit and pipe;
5. Form a thin, low permeability filter cake that prevents drilling fluid from entering the formation.

In order to perform these duties, the fluid must have specific rheological properties that allow it to perform the aforementioned duties without causing any detrimental side effects to the equipment or well. The most important properties are viscosity, density, and fluid loss control which are all governed by specific components within the fluid. A properly balanced viscosity allows the rock cuttings to be transported to the surface without causing too much resistance to the drilling equipment. Sufficient fluid density creates the hydrostatic pressure needed to prevent formation

fluids from entering the wellbore and also prevents borehole collapse. Fluid loss control agents prevent drilling fluids from entering the formation and causing damage by creating a filter cake on the wellbore walls.

Formulation of drilling fluids can be highly complex depending on the nature of the environment being drilled. However, the most basic components of a water-based drilling fluid which affect its rheological properties are salt, bentonite, barite and organic polymers. Salts are added to drilling fluids for density control and inhibition of clays encountered in formation. Bentonite is an insoluble and hydratable clay solid added to increase the fluid viscosity and help with the filter cake formation. Density of the fluid can be increased by adding insoluble barite, due to its high specific gravity. Lastly, organic polymers are added to reduce filtration and increase fluid viscosity.

2.1.1 Formation Damage

Since the focus of this research is to reduce fluid loss and formation damage, it is important to develop a general understanding of the damage types and their underlying mechanisms. It should be noted that there are many types of formation damage, however only those induced by fluid loss from water based drilling fluids will be discussed. The following damage types caused by drilling fluid leak-off are listed and briefly discussed below:

1. Particle invasion from the drilling fluid
2. Formation clay swelling
3. Changes in fluid saturation

One of the primary causes of formation damage by drilling fluids is particulate invasion (11). Invasion of drilling fluid particles into the formation rock typically occurs during the time before

the formation of the filter cake and is referred to as spurt loss (3). As the filter cake builds, the size of particles invading the formation decreases until only filtrate with no colloids can pass through. The particles that invade the formation prior to an established filter cake can fill pore spaces of the rock and bridge across pore throats forming an internal filter cake. This can severely reduce near-wellbore permeability since removal of the internal filter cake by production flow alone proves to be quite difficult (4). Adsorption of these particles onto the formation face contributes to the damage and is a particular concern with polymers. As a result of their high molecular weight, polymers are prone to be adsorbed on the surface of the formation matrix where they can restrict flow area thus reducing permeability (12).

Water-based filtrates invading the reservoir rock can come into contact with native clays within the pore space. This causes hydration and swelling of the clay particles which can lead to a reduction in permeability. The degree to which permeability is reduced depends on the amount, type and location of clay minerals present, however it is nearly impossible to predict a clay's response to water flow without testing (4). Clay swelling tends to be an intrinsic problem in sandstones containing water sensitive clays but may be reduced depending on the type of saline filtrate entering the pore space due to ion exchange properties between clay minerals and salts in the filtrate (13).

In the case of water-based drilling fluids, an influx of filtrate into the formation can change the near-wellbore water saturation of the reservoir. Reservoir rocks are typically water-wet and comprehensive research and testing has revealed that water-based filtrates do not modify wettability (14) (15) (16) (17). However, the increasing saturation of water and decreasing saturation of oil in the pore space causes a decrease in relative permeability of oil (18). As oil flows

through this lowered permeability zone during production, it could take a substantial amount of time before the oil can displace the filtrate (14).

Once the permeability has been diminished by one of the aforementioned damage mechanisms, it is improbable that the reservoir permeability will ever return to its initial condition (5).

2.2 Drill-in Fluids & Additives

It is well known within industry that conventional drilling muds cause formation damage to the well's producing zone by allowing mud filtrate to seep into the formation. The leakage of filtrate is inevitable as a result of the necessary hydrostatic pressure of the drilling fluid column which prevents inflow of formation fluids into the wellbore (5). Pressure of the fluid column must surpass the pore pressure of the formation by at least 200 psi to prevent previously mentioned inflow (3). This pressure differential between the wellbore and the formation is responsible for the creation of a thin impermeable filter cake meant to reduce leak-off of filtrate containing particle fines that clog pore throats and reduce the near wellbore permeability.

Conventional drilling fluids described in section 2.1 contain non-degradable solids that can fill pore spaces and bridge across pore throats during production. Cleaner drill-in fluids have been developed for use when drilling through the producing zone to reduce the amount of damage done to the formation. Typical practice is to drill to the top of the producing zone using conventional drilling mud, then switch to drill-in fluids to drill through the producing zone (19). This technique is used in vertical as well as deviated and horizontal wells. Use of drill-in fluids for horizontal wells has become increasingly important since the pay zone is exposed to drilling fluids over longer intervals and time periods (5). Since the surface area of contact between the formation and drilling fluid is larger than in vertical wells, the consequences of a damaging fluids are significantly

greater. Selection of proper additives is key to formulating a drill-in fluid that not only performs the duties of drilling fluids but also prevents any damaging effects to the reservoir. Although the formulation of a drill-in fluid is highly dependent on the reservoir rock and conditions, it should exhibit the following features and associated properties (20):

1. Formation damage control: There should be no inert solids that could invade pore spaces and block pore throats. Additives for fluid loss control should be acid-soluble for easy clean-up. Fluid should be compatible with native reservoir fluid to prevent any changes in chemistry.
2. Drilling performances: The drill-in fluid should perform all the duties of a conventional fluid while still allowing for an adequate rate of penetration.
3. Completion compatibility: Drill-in fluids should be compatible with completion fluids.

There are many types of drill-in formulations composed of a base fluid with additives. The selection of which to use is based on cost, technical performance and environmental impact. Drill-in fluids can be categorized into the following:

- Water-based
- Oil-based
- Synthetic-based

Additives include:

- Viscosifiers
- Fluid loss additives
- Bridging agents
- Inhibitive salts

- Bactericides

Water-based fluids are most often used simply because of the higher cost and environmental issues related with oil and synthetic-based fluids.

2.2.1 Salts

The addition of salt to drill-in fluids can serve many purposes ranging from density control to inhibition of clay swelling. High concentration brines have been used to control hydrostatic pressures without suspended solids while maintaining an ultra-fine filter cake (21). Sized salt particles can be used as a bridging agent in the prevention of fluid loss. Many horizontal wells have been drilled using sized sodium chloride particles for bridging and polymers for viscosity control (22). Salts are also used for their inhibitive properties when drilling through shales or sandstones that contain interstitial clay particles. Studies of sandstone permeability using brines composed of different polyvalent salts have shown that clay particle shrinkage occurs when a beneficial ion exchange occurs between the brine salt and formation clay (23). If reservoir properties have been previously attained, salts can be used to mimic the native reservoir brines to dampen any changes in chemistry that might occur from mixing with drilling fluid filtrate.

2.2.2 Xanthan Gum

Xanthan gum is a natural polymer derived through the fermentation process of simple sugars using the bacteria Xanthomonas campestris and is used in many industries ranging from food to oilfield applications (24). It is an anionic polysaccharide consisting of a glucan backbone connected by β-1,4 glycosidic links with side chains composed of β-D-mannose, β-1,4-D-glucuronic acid and α-1,2-D-mannose resulting in a high molecular weight ranging from 2×10^6 to 2×10^7 Da (25) (26).

When added to water in small concentrations, xanthan gum produces a viscous gel with shear thinning capabilities. Its rheological properties paired with its environmentally friendly nature have made xanthan gum a much desired additive for use in many oilfield applications ranging from enhanced oil recovery to drilling fluids. Use of xanthan as a viscosifier in drilling fluids is popular due to its ability to carry cuttings to the surface as well as suspend them when circulation of the drilling fluid has stopped. In regards to suspending ability, xanthan gum is described as being the top of its class when compared to other biopolymers used in drilling fluids (27).

Xanthan gum is a versatile additive in oilfield fluids as it performs well with low and high salt concentrations and still maintains its stability over a wide pH range (28) (25). However it does have its limitations when it comes to temperature. Breakdown of its rheological properties tend to occur at temperatures above 90° C, therefore it is not recommended for high temperature drilling applications (29).

Effective clean-up methods for xanthan polymer are necessary when it is used for reservoir drilling. Polymeric damage to reservoir permeability has been known to occur as a result of leak-off when xanthan was used as a viscosifier. Fortunately, use of acid as a clean-up method is a viable option considering xanthan is 50% acid soluble (3). Polymer specific enzymes have been developed in recent years to act as a breaker by hydrolyzing the polymer into non damaging fragments (30).

2.2.3 Guar Gum and Its Derivatives

Guar gum is a non-ionic polysaccharide produced from the endosperm of guar beans and was one of the first polymers used to viscosify water for hydraulic fracturing purposes (31). The structure of guar consists of a linear chain backbone of D-mannose bonded together by 1, 4-β-glycosidic

linkages with D-galactosyl substituents randomly arranged along the backbone (32). This long chain high-molecular-weight polymer can be used in low concentrations as an additive not only for fracturing fluids, but for drilling fluids as well.

Like xanthan gum, guar is processed into a fine powder which can be added to water in desired concentrations. When added to water, the guar particles swell and hydrate allowing the polymer molecules to unfold and extend out into solution giving a rise in viscosity. It is also noted for its fluid loss prevention capabilities when polymer strands are deposited on the rock face forming a filter cake. Studies on annular flow of guar gum and xanthan gum mixtures have shown that these polymers improve desired characteristics of a drilling fluid which include shear thinning ability, yield stress and solids transport capabilities especially when the guar is crosslinked with borax (33).

For clean-up purposes guar gum will degrade when an enzyme is incorporated into the formulation. However, the process that produces guar powder does not completely remove all plant material which are not soluble in water (31). This results in up to 9% remaining residue after degradation which is enough to cause severe impairment to the reservoir (3). Guar derivatives have been developed by exposing guar powder to high pH water at high temperature to swell the powder so that a derivatizing agent such as propylene oxide can be used (34). This process generates hydroxypropyl guar (HPG) which is found to contain only 1-2% residue after breakage of the gel (35). Even though recent studies suggest that the damage caused by guar is more or less the same as HPG, derivatizing the guar into HPG makes it more suitable for use in wells with temperatures higher than 150° C (31) (36).

2.2.4 Sized Calcium Carbonate

Calcium carbonate ($CaCO_3$) is a chemical compound commonly found in rocks as the minerals calcite and aragonite. It is the main component in rocks such as limestone, chalk and marble. Having uses in many industrial applications such as oil and gas, calcium carbonate is an additive to drilling fluids as a fluid loss control agent and a weighting material. High purity marble and calcite are ground into a fine powder of varying mesh sizes depending on the preferred particle size. Calcium carbonate is desired for its usefulness in reservoir drilling and completion fluids as it is highly soluble in acid allowing for an easy clean-up. Industrial powders such as Geo Drilling Fluid's CalCarb brand are claimed to be 98 to 99.5% soluble in 7.5 – 15% hydrochloric acid solution (37).

When used for fluid loss control, calcium carbonate particles act as a bridging agent to plug the pore throats and help in the formation of an impermeable filter cake. In order for proper bridging to occur, it is necessary to have a particle size distribution that aligns closely with the pore throat diameters in the rock attempting to be plugged. Extensive research and studies have gone into optimizing methods for choosing a non-damaging particle size distribution. Abrams' rule is regularly used as a basis for selecting particle size. The rule states that the bridging agent's median particle size must be slightly greater than or equal to $1/3^{rd}$ of the median pore size and that the concentration should be 5% by volume in the final mud mix (38).

Figure 1 demonstrates the process of particle bridging. While Abrams rule serves as a good guideline, others have taken the "shotgun" approach by selecting a particle size distribution covering a broad spectrum of permeabilities and pore throat sizes that may be encountered in the wellbore (39).

Calcium carbonate as a weighting agent is useful mainly for drill-in, completion and workover fluids considering its solubility in acid. With a lower specific gravity of 2.7 compared to barite and iron-based weighting material, it is acceptable to use when drilling conditions do not require the mud to provide a high degree of weight (37) (3). Mud weights of 10 lb/gal can be achieved when using finely ground calcium carbonate in brine solutions and can be further increased to 14 lb/gal with a saturated brine by the addition of more salt (2) (3) (40). Typical concentrations of calcium carbonate added for bridging and fluid loss purposes are in the 10 to 50 lb/bbl range (41).

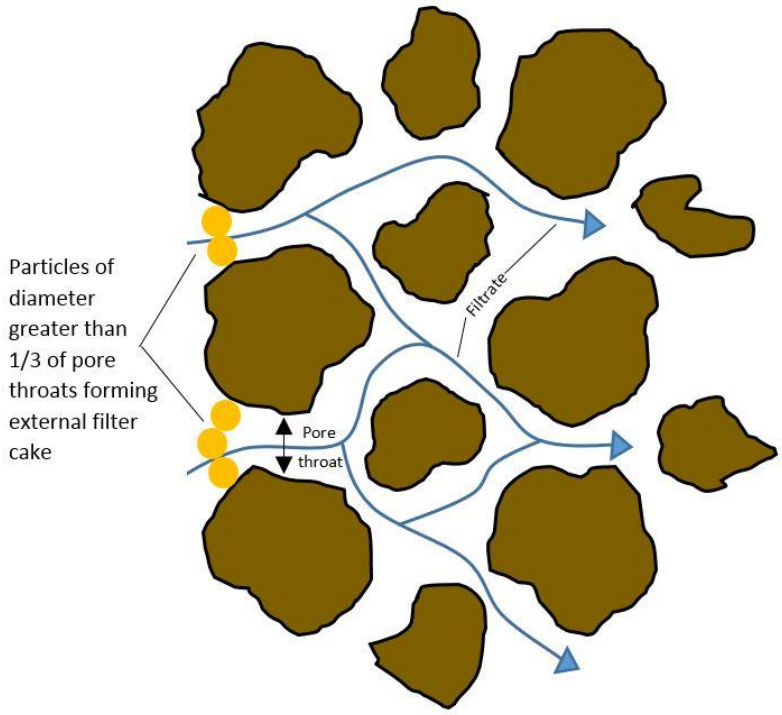

Figure 1: Schematic of particle bridging at formation surface

2.3 Clean-up Methods

Though the goal of non-damaging drill-in fluids is to prevent formation damage or any hindrance to production, successful clean-up methods are required for filter cake removal whether internal or external. Insufficient clean-up of the filter cake from drill-in fluids can result in a significant

impedance of flow at the wellbore wall which in turn reduces the well productivity or injectivity (30). In an optimal scenario, natural flow back to the wellbore and draw-down pressures during production would be strong enough to remove the filter cake without any prior clean-up treatment. However, this is seldom the case. It has been observed that using only draw-down pressures to lift the filter cake results in only partial removal reducing the total flow area on the wellbore wall (42). Therefore the application of breaker systems for filter cake removal have become standard practice before starting production on a well.

Acid and oxidative treatments are commonly used breakers for filter cake degradation. Acids such as HCl have the capability to dissolve calcium carbonate bridging particles as well as polymers within the filter cake. Acidizing with HCl typically has good results in vertical wells with short production intervals. Oxidizers such as sodium hypochlorite can degrade polymers in the same manner as acids by reacting with active sites on the polymer chains breaking it at key linkages and degrading it to its base units (43). Aside from their successes, acids and oxidizers have problems that should be taken into consideration. Both are highly non-specific reactive species that will react with almost anything they encounter including hydrocarbons, downhole equipment and formation components (44). This could result in the breaker being consumed before it ever reaches the damaged zone. Regarding polymer degradation, the non-specific reaction tendency of acids and oxidizers may cause them to react with non-critical polymer linkages or miss the polymer backbone entirely resulting in partially degraded polymer strands left behind (43). Studies conducted by Burnett indicated that carbonate particles used as a bridging agent may be resistant to degradation by acid when they are coated with unbroken polymers (45). Acids also have a habit of producing wormholes by reacting on a path of least resistance which leaves behind significant areas of unremoved filter cake. All of the issues associated with the effectiveness of acids and

oxidizers as breakers become more accentuated when applied to horizontal wells. Considering the large target zone area and extended length of horizontal wells, use of these conventional breakers have proven to be less than satisfactory when trying to produce horizontal completions at their full potential.

Polymer specific enzymes have been the focus of several studies in recent years as a means to effectively degrade polymers used in oilfield fluids from drilling applications to fracturing jobs. Unlike acids and oxidizers, enzymes are environmentally friendly and react with specific linkages of polymers to break it down into non damaging fragments. Enzymes are specialized proteins that act as catalysts in the promotion of specific reactions. Since the structure of an enzyme is unchanged during the reaction it encourages, its reactivity is basically infinite as long as it does not become denatured by chemical, thermal or mechanical means (30). Because of its polymer-specific reactive nature, it will not react with anything on its way to the target zone ensuring full reactivity upon arrival. Once the polymers involved in the formation of filter cake have been degraded they cannot function as a glue holding the calcium carbonate particles together. No longer being shielded by the polymers, the calcium carbonate can now be dissolved by acid. This two stage filter cake removal system involving an enzyme treatment followed by an acid treatment has shown good results in the lab with cores reaching near 100% initial permeability values and a 3-fold increase in production for wells treated with this system in the field (30). There are several biopolymers used for drill-in fluids such as starches, derivatized-guar and xanthan gum. To accompany the range of biopolymers, linkage specific enzymes have been developed and include amylase, cellulose, glucosidase, xanthan depolymerase and pectinase. Xanthan depolmerase, as its name suggests, has shown to successfully cleave the backbone linkages of xanthan significantly reducing its viscosity (46). Depolymerization of guar by the enzyme pectinase was observed in

research done by Shobha et al. (47) and Barati (34) demonstrated the use of pectinase as a breaker of hydroxypropyl guar in fracturing fluid applications.

In a case where removal of the filter cake does not improve flow to the well, it is possible that solids in the filtrate have invaded the formation causing damage. Typically, unless the formation permeability is very high, this damage is contained within a few centimeters of the wellbore (12). If the aforementioned treatments are unable to reach the particulates, perforations may be used to bypass the damaged zone.

2.4 Fluid Loss

The stages of fluid loss during drilling can be broken down into three cases according to Ferguson and Klotz (48):

1. Static filtration - Occurs when the mud is not in circulation. Rate of filtration is controlled by the filter cake permeability
2. Dynamic filtration - Drilling fluid is in circulation and flowing up the annular space past the filter cake surface. Rate of filtration is controlled by the filter cake thickness and both become constant depending on circulation rate and drill string rotation.
3. Filtration below the drill bit - No filter cake is formed beneath the drill bit. Filtration is controlled by plugging of the formation by particles in the mud.

Fluid loss volume is highly dependent on the quality of the filter cake and how fast it can be formed. During formation of the filter cake, an initial volume of fluid known as spurt loss is leaked into the formation before the filter cake is fully formed. After the spurt loss, Carter established a linear relationship between the leak off volume and the square root of exposure time of the fluid to the rock face (49). **Figure 2** is a fluid loss curve from static testing of fracturing fluids and serves

as an example of this linear relationship. It should be noted that fluid loss curves generally take this shape whether the fluid is for fracturing or drilling applications. If the linear trend line is extended to the y-axis of the chart, this indicates the spurt loss volume. The wall building coefficient can also be calculated using the slope of the trend line by dividing it through the cross sectional area of the rock face.

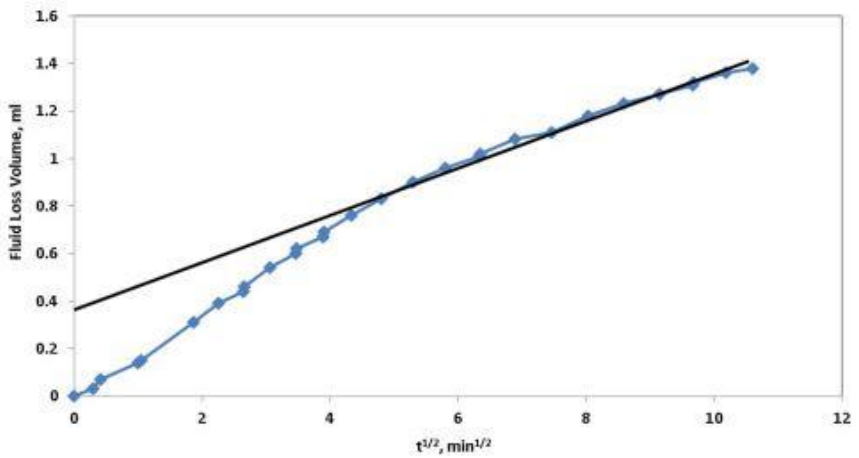

Figure 2: Typical Fluid loss curve (8)

2.4.1 Static Fluid Loss Tests

Static filter cake formation is studied by filtering the fluid in question while its flow path is perpendicular to the rock surface. A widely accepted way to gauge a fluid's filtration properties in the lab as well as the field is the standard API fluid loss test. It involves filtering the fluid through standard filter paper with 100 psi at ambient room temperatures for 90 minutes using a static filter press. Though this may be a quick and easy way to determine a fluid's filtering capabilities, it is not very representative of actual reservoir conditions. High pressure and high temperature (HPHT) fluid loss cells are used in conjunction with rock cores to effectively simulate the pressures, temperatures and permeabilities the fluid will encounter. Using this setup a core is placed into the core holder, the fluid is heated up to desired temperatures, differential pressure is applied across

the core using nitrogen and the rate of filtrate volume forced through the core is measured versus time (50). Most fluid loss data are obtained under static testing conditions yet these data may be misleading to the actual fluid loss happening in a wellbore. As mentioned earlier, static fluid loss during drilling will only occur when drilling fluid circulation has stopped. Prior to this, formation of a filter cake has already been in development but under the erosional forces of the circulating fluid. In order to more closely replicate the fluid loss during circulation, testing under dynamic conditions becomes necessary.

2.4.2 Dynamic Fluid Loss

As long as drilling fluid circulates or the drill string rotates in the wellbore, fluid filters into the formation under dynamic conditions (48). Drilling fluid flowing perpendicular to the wellbore wall continuously erodes the low shear strength transition layer that exists between the solid filter cake and the fluid mud (48). Thickness of the filter cake is controlled by the shear stress caused by the drilling fluid flowing past the borehole wall. This process is essentially the same when applied to fracturing fluids flowing along a fracture face. In **Equation 1**, Prud'homme and Wang (51) mathematically presented three stages of filter cake buildup when fracturing fluid flows perpendicularly to the direction in which the filter cake forms.

$$\frac{dM}{dt} = \begin{cases} \omega u \ldots\ldots\ldots\ldots\ldots\ldots\ldots\ldots\ldots\ldots\ldots\ldots\ldots\ldots\ldots\ldots\ldots \tau_w < \tau_{fc} \\ 0 \ldots\ldots\ldots\ldots\ldots\ldots\ldots\ldots\ldots\ldots\ldots\ldots\ldots\ldots\ldots\ldots\ldots \tau_w = \tau_{fc} \\ rate\ of\ erosion \ldots\ldots\ldots\ldots\ldots\ldots\ldots\ldots\ldots\ldots\ldots \tau_w > \tau_{fc} \end{cases} \quad \text{Equation 1}$$

Where:

ω= Mass fraction of solids in the fluid phase

M= Mass/area of the filter cake

$\tau_{fc=}$ yield stress of the filter cake

u= velocity of solvent through the filter cake

τ_w= fluid stress

The first stage where fluid stress is less than yield stress of the cake can be simulated by static fluid loss conditions. The third stage must be simulated in dynamic conditions as the rate of erosion is dictated by how much greater the fluid stress is than the yield stress of the filter cake. Growth or erosion of the filter cake will cease when the fluid stress becomes equal to the yield stress of the cake. There are many designs for dynamic fluid loss cells with varying geometries. However, some are unnecessarily complex and difficult to characterize, therefore Navarrete et al. (52) chose a slot flow through a rectangular geometry bounded by a non-permeable wall and a circular rock core. Using this type of fluid loss cell, Navarrete et al. (52) designed a reciprocating dynamic fluid loss simulator that would allow continuous unidirectional flow of the test fluid to pass in front of a rock core where a filter cake could be formed under dynamic conditions while measuring fluid loss. The setup also includes a shear history loop to simulate the shear forces a fluid encounters in the wellbore which preconditions the fluid before it reaches the fluid loss cell. Although this setup was used to simulate fluid loss in fractures with fracturing fluids, it can also be applied to drilling fluids where the shear history loop may simulate the fluid traveling through the drill string and the fluid loss cell would mimic the fluid flowing past the borehole wall during circulation

2.5 Nanoparticles

Nanoparticles are microscopic particles with at least one dimension falling in the range of 1 – 100 nanometers. When compared to macro and micro-sized particles, nanoparticles have a significantly higher surface area to volume ratio which is expected to play a huge role in fluid properties with

only a small concentration of nano-material added (53). The oilfield application of nanotechnology is somewhat new, and its application to drilling fluids is even more recent. Several studies have investigated the addition of nanoparticles to water-based bentonite muds with promising results that led to improved rheology under HPHT conditions and improvement in reducing fluid loss (53) (54) (55) (56). Although these studies project a positive outlook for nanoparticle applications in conventional drilling fluids, little work has been done in regard to the use of nanoparticles for cleaner drill-in fluids with low solids content.

2.6 Polyelectrolytes

Polyelectrolytes are polymers that carry multiple ionic groups. Their dual character of highly charged electrolytes and macromolecular chain molecules make them unique in the fact that they have the electrical charge of an electrolyte while exhibiting the viscosity of a polymer (57). The ionic groups will dissociate in an aqueous solution such as water which will give charge to the polymer. Polyelectrolytes can be categorized into natural, modified natural and synthetic polymers while further subcategorized by their charge of being a polycation, polyanion or polyampholyte (57). Polyelectrolytes that have a broad range of size, shape and mass characteristics are said to be "polydisperse" (34). The polyetheylenemine/dextran sulfate system described in the next section is a synthetic polyelectrolyte system.

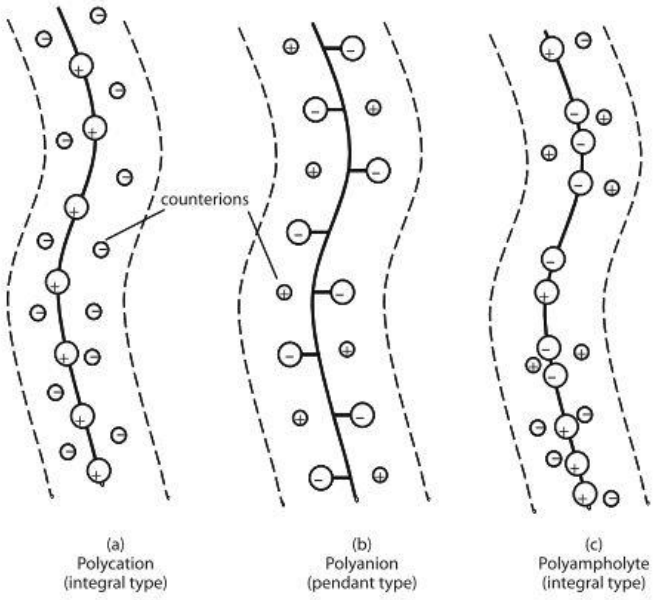

Figure 3: Different classifications of polyelectrolytes based on their charge (57). The above figure is reprinted with permission from Springer.

2.7 Polyethylenemine/Dextran Sulfate System of Tiyaboonchai

When the solutions of polyanions and polycations are mixed, spontaneous formation of insoluble polyelectrolyte complexes (PECs) occur under certain conditions (58). On this basis, Tiyaboonchai developed a polyelectrolyte complex system consisting of polyethylenemine (PEI) as the polycation and dextran sulfate (DS) as the polyanion to serve as a drug delivery vehicle for pharmaceutical applications (59). PEI is a polymer known for its water soluble nature and is available in linear and branched form for use in several industrial applications from paper making to pharmaceuticals. DS is a combination of the polymer dextran of anhydroglucose with approximately 17 % sulfur and is supplied as a sodium salt form which makes it soluble in water (60). The structures of PEI and DS are shown in **Figure 4** and **Figure 5**. Tiyaboonchai was able to create a stable nanoparticle system with particle size of 200 nm by adding PEI solutions of pH 8 with DS solution in a PEI:DS mass ratio of 2:1 (59). She observed that the particle size seemed to be effected by the ratio of PEI to DS with particle size decreasing as the ratio of polymers

increased (61). This may be a result of excess PEI preventing coalescence of the nanoparticles by acting as a colloidal protective agent (59). It was found that charge of the nanoparticles was determined by the ratio as well in that ratios of PEI:DS greater than 1:1 resulted in positively charged nanoparticles while ratios less than 1:1 resulted in a negative charge (62).

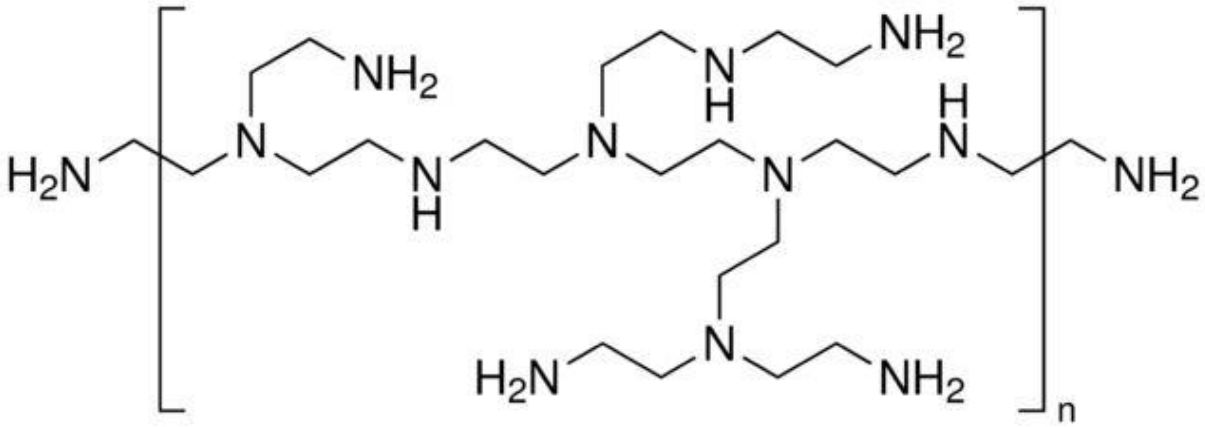

Figure 4: Chemical structure of PEI (Sigma Aldrich Specification Sheet) (63)

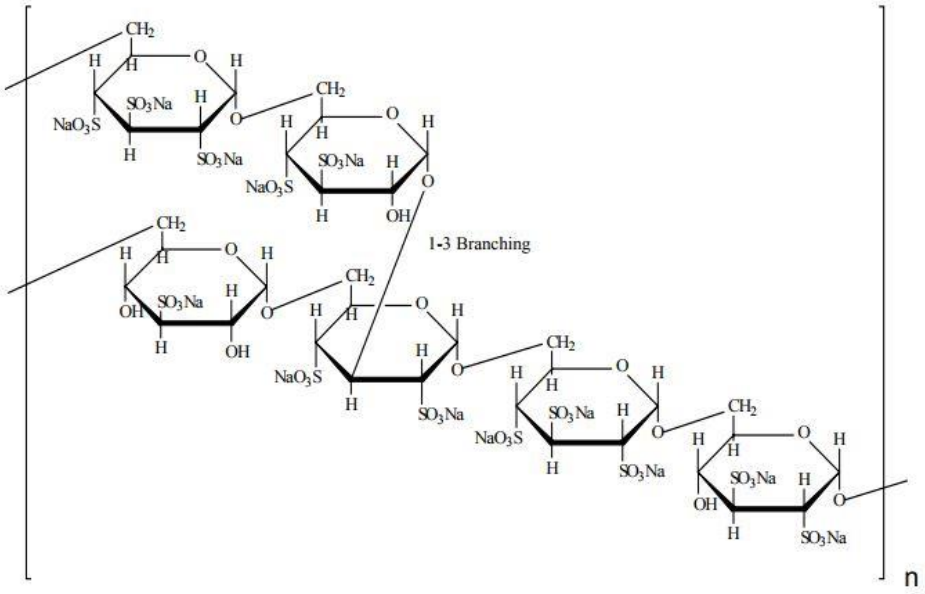

Figure 5: Chemical structure of DS (Sigma Aldrich product information sheet) (75)

2.7.1 Polyelectrolyte Complex Nanoparticles as a Fluid Loss Agent

Fluid loss reducing agents are routine additives meant to lessen the volume of filtrate that leaks off into the formation when drilling through a prospective producing zone. As discussed in section 2.2.4, sized calcium carbonate is added as a fluid loss agent so that its particles may bridge across pore throats, forming a filter cake and restricting filtrate from leaking into the formation. When a bridge is initiated by two particles, smaller particles may then form a bridge in the openings between the original larger particles. Theoretically, if this trend persisted and enough smaller particles were present to continue bridging smaller gaps in the filter cake, the void space left would be too small for even a water molecule to fit through (13). That's where polyelectrolyte nanoparticles become useful. Since calcium carbonate particles are in the range of 1-1000s of micrometers, the void spaces left by even the smallest particles can be bridged by nanoparticles ≥ one-third their size. Polyelectrolyte nanoparticles have previously been used to prevent fluid loss in hydraulic fracturing applications. Barati (8) applied PEC nanoparticles as a fluid loss additive in a hydroxypropyl guar solutions for tight and ultra-tight sandstone cores. He successfully reduced the fluid loss volume of HPG fluids during static testing by adding PEC nanoparticles with a mean particle size of 545 nm as shown in **Figure 6**. Bose (64) also used PEC nanoparticles with success in reducing fluid loss volumes for both limestone and sandstone cores of high, low and tight permeability. The average size of the PEC nanoparticles he used was around 500 nm. **Figure 7** shows the results of a static fluid loss test he performed for Indiana limestone cores.

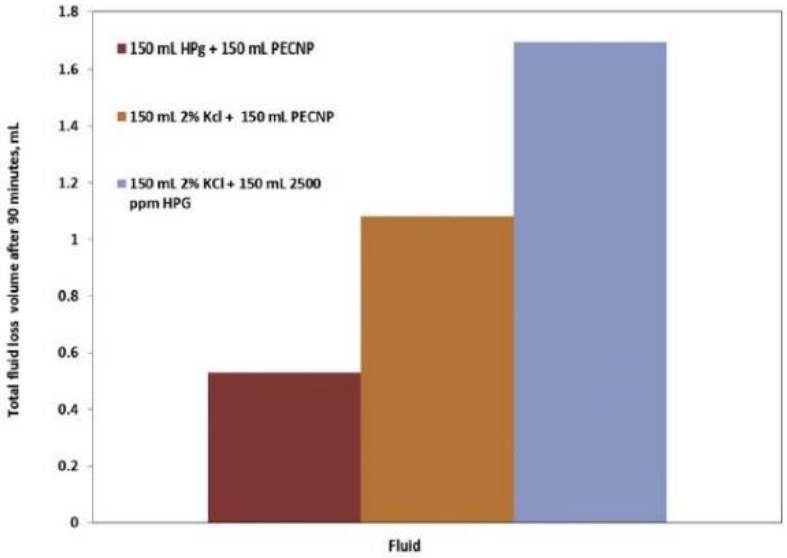

Figure 6: Barati's fluid loss results of HPG solutions with and without PEC nanoparticles (8)

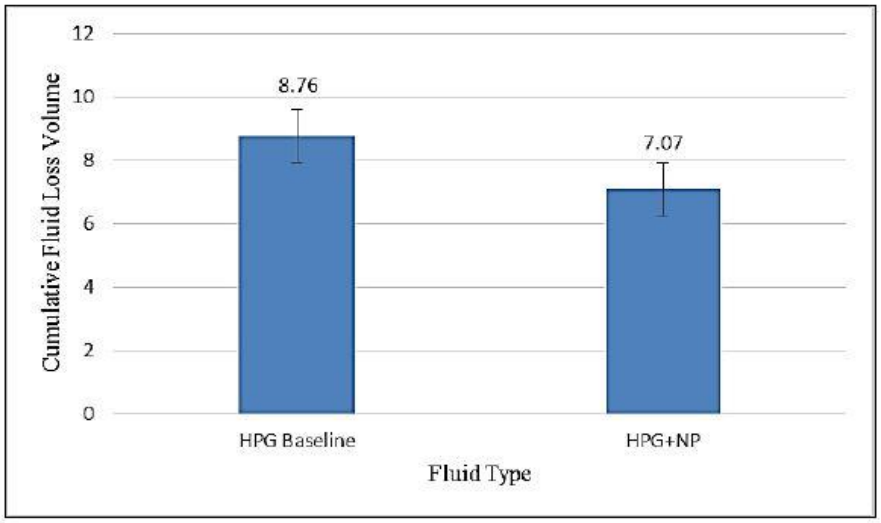

Figure 7: Bose's fluid loss results of HPG solutions with and without PEC nanoparticles

2.8 Drill-in Fluid Rheology

The rheology of a drill-in fluid is vital to its performance in various functions required during drilling. Drilling fluids typically follow a shear thinning or pseudo plastic rheological model based on their shear stress behavior in response to shear rate. Shear thinning fluids will become less viscous as the shear rate applied is increased resulting in a non-linear curve on a graph of shear stress vs. shear rate. However, drilling fluid rheological properties are generally tested and reported in the field using the Bingham Plastic Model. This model assumes a linear trend in viscosity with a minimum shear stress needed for flow to occur. Measurements of the fluid are taken using a rotational viscometer. From these measurements, three parameters known as plastic viscosity, yield point and gel strength can be calculated and used to characterize the fluid. The plastic viscosity is simply the slope of the Bingham Plastic line and serves as an indicator of size, shape, distribution and quantity of solids as well as the viscosity of the liquid phase (40). The yield point, typically reported in lbf/100 ft^2, is the shear stress required in order to initiate flow of the fluid. Gel strength, also reported in lbf/100 ft^2, is an indication of how well the fluid will be able to suspend cuttings in the wellbore annulus if circulation is stopped. Plastic viscosity and yield point are two properties whose significance is firmly engrained in drilling technology, yet they follow the Bingham Plastic Model which does not accurately describe most drilling fluids (40). The Power Law Model shown in **Equation 2** more accurately describes drilling fluids, however it does not include a yield stress like the Bingham Model. Its two terms *K* (consistency factor) and *n* (flow behavior index) are easily calculated with data obtained from rotational viscometer measurements.

$$\tau = K(\gamma^n) \qquad \text{Equation 2}$$

Drilling fluids typically behave in a pseudo plastic manner with a yield stress which are characteristics from both the Bingham Plastic and Power Law Models. The Herschel-Bulkley Model shown in **Equation 3** includes a yield stress parameter while also describing the pseudo plastic behavior of the fluid. This model is solvable with the use of computers where τ_0 is the yield stress, *K* is the consistency factor, γ is the shear rate and *n* is the flow behavior index.

$$\tau = \tau_0 + K(\gamma^n) \qquad \text{Equation 3}$$

2.9 Drill-in Fluid Field Studies of Horizontal Wells

Relative to vertical wells, horizontal wells take a greater amount of time to drill considering the depth to pay zone along with the added lateral section. Lateral sections through the producing formation are known to extend thousands of feet. Because of this, drilling fluids are in contact with the formation for prolonged periods of time which could potentially result in formation damage with deeper invasion at the heel and lessening towards the toe as shown by **Figure 8** . Fluid contact time with the formation is said to have 5 to 10 times that of a vertical well (44). Considering the

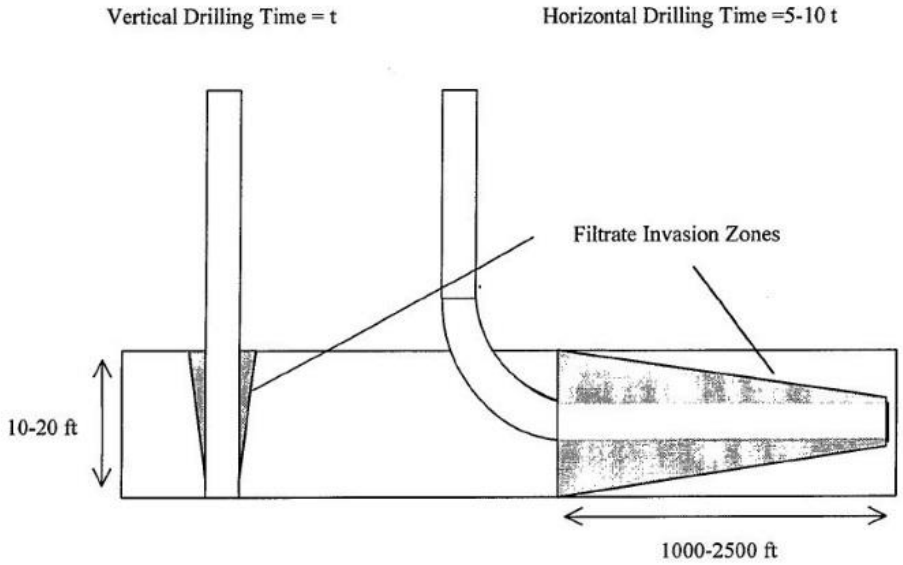

Figure 8: Schematic of a vertical damage profile versus horizontal damage profile (44). The above figure is reprinted with permission from the Society of Petroleum Engineers

consequences of formation damage over a long producing interval, use of a non-damaging drill-in fluid is key to unlocking the full potential of horizontal wells. Several case studies documenting the use of these fluids for drilling of horizontal sections show how successful they can be after completion of the well. One such case is as follows:

An offshore Dutch development well showed better than expected results after a drill-in fluid system was used to reduce formation damage (65). The fluid itself was brine based containing calcium carbonate as a bridging agent, xanthan biopolymer as a rheology modifier and a modified starch for fluid loss control. The low solids content and plastic viscosity of the system provided less friction and allowed for faster penetration rates which resulted in drilling the section 8 days ahead of schedule. The sandstone formation was predicted to produce gas at 1.5 million m^3/d, however when the well was put onto production without any stimulation or remedial work, production rates achieved 2.1 million m^3/d (65). This specially formulated drill-in fluid was used in lieu of mineral oil-based muds used to drill previous wells.

2.10 Summary

Successful application of reservoir drilling fluids has become a logical practice whether drilling a vertical or horizontal well. When considering the cost versus value of drilling a well, it is clear that the benefits of a non-damaged formation clearly outweigh the extra costs associated with developing and implementing a cleaner drill-in fluid. Still, there is work to be done for improving these non-damaging fluids by further increasing their fluid loss prevention capabilities. To this author's knowledge, little research has been done regarding the addition of nanoparticles specifically to reservoir drill-in fluids for fluid loss purposes. This work aims to investigate the use of PEC nanoparticles as a fluid loss additive to further improve the success of drill-in fluids.

3 Materials

3.1 Brine

A 3% w/w sodium chloride (NaCl) solution was prepared using purified deionized water and used as the base fluid for all other solutions. The brine had a measured density of 1.0128 g/cm^3 at 25°C and viscosity of 1.06 cP at 40°C. NaCl was purchased from Fisher Chemical (Fair Lawn, NJ. Lot No. 168160, ACS Grade).

3.2 Xanthan Products

Xanthan gum powder (Flowzan® Biopolymer, Chevron Phillips Chemical Company LP, The Woodlands, TX. Lot #FZ16291AB) was provided by Drilling Specialties Company and used in all experiments and formulations of the drill-in fluid. Flowzan® is a high purity xanthan gum biopolymer that disperses easily in brines while providing excellent viscous and suspension without formation of fisheyes (28).

3.3 Guar Products

Hydroxypropylated guar (HPG) gum powder (ECOPOL-400DS, Economy Polymers & Chemicals, Houston, TX,) was used for all experiments and formulations of the drill-in fluid. ECOPOL-400DS is a self-hydrating chemically modified non-ionic natural polysaccharide that is easily dispersible into solution (66).

3.4 Calcium Carbonate Products

Sized calcium carbonate ($CaCO_3$) powder (CalCarb-80, GEO Drilling Fluids Inc., Bakersfield, CA) was provided in a 50 pound bag. CalCarb-80 has a particle size distribution represented by **Figure 9**. It provides fluid loss prevention by acting as a bridging agent and may also be used as a

weighting agent with some limitations as its specific gravity is only 2.7 (37). Due to its acid soluble nature, pH of the drilling mud should be kept above 7.0 to preserve its effectiveness as a lost circulation material.

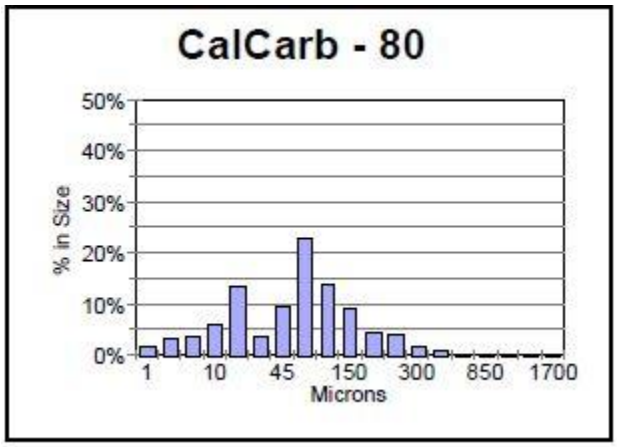

Figure 9: Schematic of CalCarb-80 particle size distribution (37)

3.5 Polyethylenimine (PEI)

Branched polyethylenimine in liquid form (Sigma Aldrich, Lot #MKCB1222V, CAS 9002-98-6) was used as the polycation in the generation of PEC nanoparticles for this research. PEI has an average molecular weight of 25,000 measured by light scattering, a density of 1.030 g/mL at 25°C, and a viscosity of 13,000-18,000 cP at 50°C as reported by Sigma Aldrich.

3.6 Dextran Sulfate (DS)

Dextran sulfate sodium salt (Sigma Aldrich, Lot #156852, CAS 9011-18-1) was used as the polyanion in the generation of PEC nanoparticles. It has an average molecular weight of 500,000.

3.7 Core Materials

To test the fluid loss capabilities of a drill-in fluid with PEC nanoparticles, static and dynamic fluid loss tests were performed on Indiana limestone and Kentucky sandstone cores. The limestone cores

were meant to represent high permeability reservoirs while the sandstone cores were meant to represent tight reservoirs. Core measurements were approximately 1 inch in both length and diameter. The cores were purchased from Kocurek Industries of Caldwell, TX. Kocurek estimated the porosity to be between 14 and 19% for Indiana Limestone cores and 14% for Kentucky sandstone.

3.8 Bleach for Core Restoration

Clorox® bleach containing 1.84 % sodium hypochlorite was diluted 3× with 3% NaCl brine for use when flooding cores after fluid loss tests to restore them to initial permeability.

4 Equipment and Experimental Procedures

4.1 Preparation of Polyelectrolyte Nanoparticles

PEC nanoparticles were generated using the same method demonstrated by Cordova et al. (62) in which different ratios of PEI:DS solutions are mixed to form the nanoparticles. First, solutions of 1% w/w PEI and DS are batched separately in 3% NaCl brine. PEI solution is adjusted with HCl to change the pH to 8.5, 8.0, and 7.5. Positively charged PEC nanoparticles were generated by rapidly adding DS to PEI of each pH in ratios of PEI:DS ≥ 1 and allowing to stir at 600 rpm on a magnetic stir plate for 20 minutes. Likewise, negatively charged particles were generated in the same manner, however the ratio of PEI:DS must be ≤ 1. Some ratios were not compatible and immediately produced precipitates indicating it to be non-stable. If a solution did not immediately produce precipitates upon mixing, it was taken for size and zeta potential analysis to determine the most stable system.

4.2 Size and Zeta Potential Measurement of Polyelectrolyte Complex Nanoparticles

Size and zeta potential were measured using a Brookhaven NanoBrook Omni particle sizer and zeta potential analyzer. For particle size analysis, samples of the nanoparticle system were diluted 40× by adding 3.9 mL of deionized water to 0.1 mL of nanoparticles. The sample was then analyzed by the Brookhaven instrument with a light scattering angle of 172.5°. The software recorded three measurements and an average of the three was taken for mean particle size. Values of previously measured viscosity and pH of the nanoparticle system were input into the software prior to analyzation by the instrument. Zeta potential samples were diluted 20× by adding 1.9 mL of 1.0 mM KCl solution to 0.1 mL of nanoparticles. Samples were then evaluated by phase analysis light scattering using the same instrument for particle size analysis. Values of viscosity, pH and particle size were input into the software. Using the Smoluchowski approximation, zeta potential

could then be calculated after sample analyses. Three measurements were recorded, and an average was taken for the mean zeta potential. Zeta potential itself is a measure of the magnitude of the electrostatic repulsion or attraction between particles and is a fundamental parameter that affects stability (67). Stability of the system decreases as the zeta potential approaches zero as shown by **Table 1.**

Table 1: Relation of particle stability to zeta potential (68)

Zeta Potential (mV)	Stability behavior of the colloid
From 0 to ±5	Rapid coagulation or flocculation
From ±10 to ±30	Insipient instability
From ±30 to ±40	Moderate stability
From ±40 to ±60	Good stability
More than ±61	Excellent stability

4.3 Preparation of Drill-In Fluid for Static Testing

After consulting with literature and case studies, a drill-in fluid was formulated consisting of 3% NaCl brine as a base, 0.3% Flowzan® biopolymer, 0.4% Hydroxypropyl guar, and 10% $CaCO_3$. This is the base formulation to be used for all subsequent experiments. Preparation of the drill-in fluid starts by slowly adding 0.24 grams of xanthan gum to the shoulder of a vortex in 80 mL of brine being generated by a magnetic stir plate at 600 RPM. Then, 0.32 grams of HPG is slowly added to the mixture while increasing the stirring speed to 800 RPM to achieve the necessary shear for thorough mixing and hydration of the polymers. It is essential that xanthan and HPG are added very slowly, to avoid generating “fisheyes” which are coagulations of the polymers. 8.0 grams of $CaCO_3$ can then be added, again increasing the speed from 800 RPM to 1200 RPM as by now the

solution has become very viscous. All mixtures are allowed to stir for a minimum of 20 minutes before the addition of the next additive. 25 mL of nanoparticle solution was then added and allowed to stir for an additional 20 minutes. For testing of a baseline fluid, 25 mL of brine was added instead of the nanoparticles. The same ratio of nanoparticle solution to drill-in fluid was scaled up for other tests such as dynamic fluid loss.

4.4 Measuring Rheology of the Drill-In Fluid

Rheology measurements were taken using a FANN® Model 35 viscometer, pictured in **Figure 10**, which is the standard method used for measuring drilling fluid viscosity in the field. The model 35 is a Couette rotation viscometer that utilizes a rotational bob and torsion spring to measure the viscous drag created by the fluid contained in the annular space between the rotating bob and outer wall (69). Standard R1-B1-F1 rotor-bob-torsion spring combination was used which is necessary to know for later calculations. The viscometer has six speeds with known shear rates at each speed which are given in **Table 2**. The shear stress can be calculated with **Equation 4,** provided in the viscometer manual, using the dial reading, shear stress constant and torsion spring constant. Shear stress versus shear rate values are plotted in Excel and a Power Law trendline is applied to obtain an equation for the curve containing *K* (consistency factor) and *n* (flow behavior index). Drilling fluid properties typically reported in the field such as apparent viscosity, plastic viscosity and yield point were calculated and compared to values of commercially available drill-in fluids using **Equation 5**, **Equation 6** and **Equation 7** respectively which are available via the viscometer manual (69).

Table 2: Shear rates for FANN Model 35 viscometer (69)

RPM	Shear Rate (sec^{-1})
600	1021
300	511
200	340
100	170
6	10.2
3	5.1

$$\tau = k_1 k_2 \theta \quad \text{Equation 4}$$

$$\mu_a = 300 \times \frac{\theta_N}{N} \quad \text{Equation 5}$$

$$\mu_p = \theta_{600} - \theta_{300} \quad \text{Equation 6}$$

$$\tau_y = \theta_{300} - \mu_p \quad \text{Equation 7}$$

Where:

τ = shear stress, dynes/cm^2

k_1 = spring torsion constant, (386 for R1-B1-F1 combination) dyne-cm/degree of reflection

k_2 = effective bob surface shear stress constant, (0.01323 for R1-B1 combination) cm^{-3}

N = Rotor speed, RPM

θ_N = Dial reading at N rotor speed

μ_a = Apparent viscosity, cP

$\mu_{p=}$ Plastic viscosity, cP

τ_y = Yield point, lbf/100 ft^2

Figure 10: Photo of FANN Model 35 viscometer used for viscosity and rheology analysis

4.5 Core Saturation and Porosity Measurement

Core dimensions were measured using a pair of Mitutoyo digital calipers and recorded for calculation of bulk volume V_B. They were dried in a 70 °C oven for 48 hours until they reached a constant weight which was then recorded as W_D. Cores were then put in a desiccator attached to a vacuum pump and evacuated for 1 hour at 30 Hg vacuum pressure. The vacuum was then turned off and an inlet valve connected to a line pre-filled with 3% NaCl brine drawing from a beaker filled with the same brine was opened to allow the flow of brine into the vacuum chamber where the cores would then become saturated. After a minimum saturation time of 2 hours, the cores were weighed and recorded as W_S. Knowing the dry weight, saturated weight and saturating fluid

density, the pore volume PV can be calculated using **Equation 8**. After calculation of the pore volume, **Equation 9** can then be used to calculate the porosity. **Figure 11** shows a photo of the core saturation setup.

PV= Pore volume, cm^3

Φ = Porosity, %

W_D = Dry weight of core, g

W_S = Saturated weight of core, g

ρ = Density of saturating fluid, g/cm^3

V_B = Bulk volume of core, cm^3

$$PV = \frac{W_D - W_S}{\rho} \quad \text{Equation 8}$$

$$\Phi = \frac{PV}{V_B} \times 100 \quad \text{Equation 9}$$

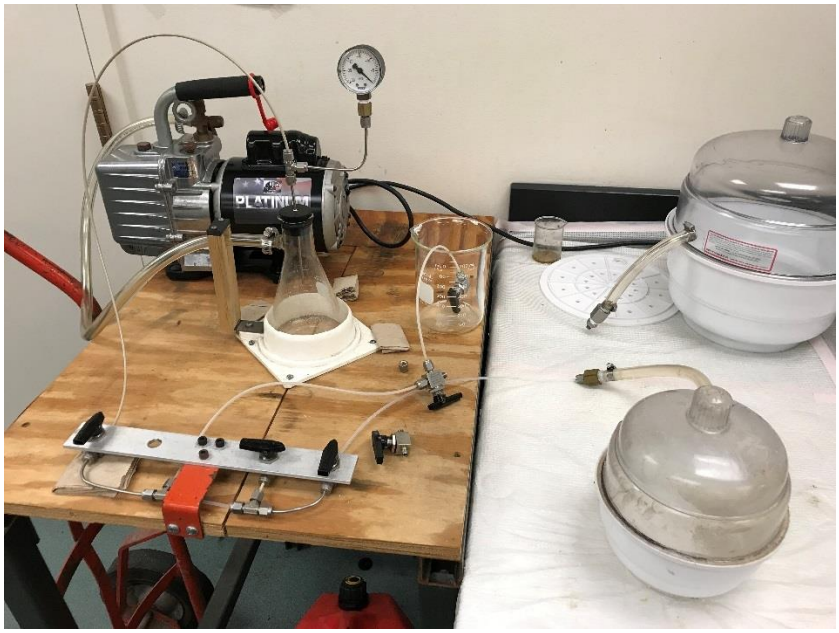

Figure 11: Photo of core saturation setup used for porosity measurement

4.6 Permeability Measurements for Static and Dynamic Fluid Loss

Permeability of each core was measured using a core flooding setup depicted in **Figure 12**. Initial core permeability was recorded for comparison to permeability measured after fluid loss tests had been performed on a core. An ISCO pump filled with SOLTROL-130 was connected to a transfer cylinder filled with SOLTROL-130 and 3% NaCl brine. Two Hassler type core holders were used depending on the expected core permeability and confining pressure needed to prevent flow around the core. A Honeywell transducer was connected to the inlet and outlet sides of the core holder to measure the pressure drop across the core during flow. The core flooding apparatus was contained in a temperature controlled unit kept at 40°C. When high permeability cores were flooded, a transducer capable of measuring 100 psi differential pressure was used. A transducer capable of measuring 3000 psi differential pressure was used for cores of low permeability. Using a known flow rate, measured pressure drop, viscosity of brine and dimensions of the core, Darcy's law was applied for calculation of permeability. Comparison of a core's permeability before and after a fluid loss test is used to assess the damage caused by the drill-in fluid.

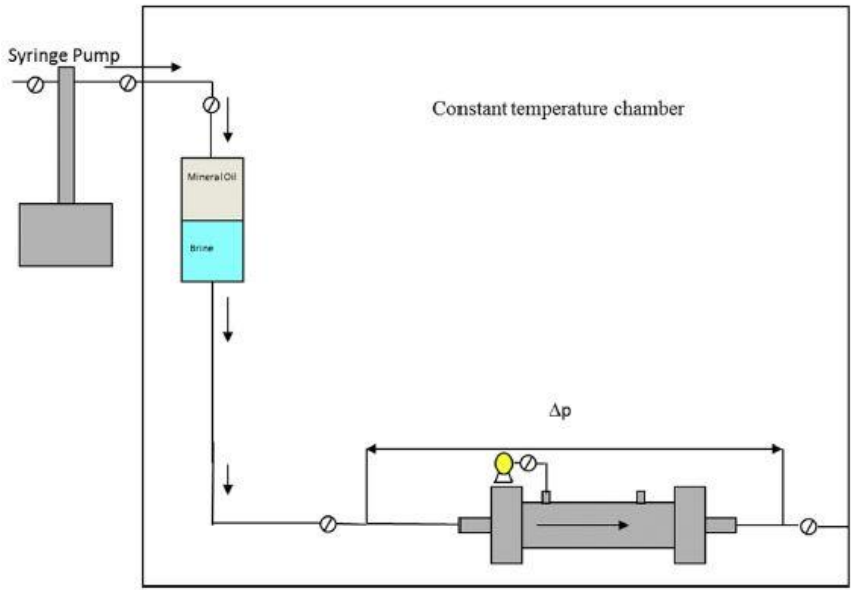

Figure 12: Schematic of core flooding setup for permeability measurement (8)

4.7 Brine Viscosity and Density

A Brookfield digital cone-and-plate viscometer was used for measuring the 3% NaCl brine viscosity. The viscometer makes use of a spindle spinning against the fluid sample and a plate. The force required to overcome the resistance to flow is measured by the viscometer and reports the viscosity in cP. An Anton Paar densitometer was used to measure the density of the brine. Both viscosity and density were measured and reported at 40 °C. Brine viscosity was measured to be 1.06 cP and density was measured to be 1.01 g/cm^3.

4.8 Static Fluid Loss Testing

Static fluid loss testing was performed on Indiana limestone cores as well as Kentucky sandstone cores using a static fluid loss cell obtained from Schlumberger. First, a baseline test was established using the baseline drill-in fluid described in section 4.3. Then tests with the addition of polyelectrolyte complex nanoparticles in dilutions of 1/2, 1/4, 1/8 and undiluted were performed to study the nanoparticle's effect on fluid loss prevention. Cores were inserted into the core holder and the drill-in fluid was place on top. The core holder was placed in a heating jacket, shown in **Figure 13**, which kept a constant temperature of 40 °C using a thermocouple and user entered temperature. The lines below the core were filled with brine to ensure that every drop of filtrate invading the core resulted in a drop out. Nitrogen was used to apply 500 psi differential pressure to the core. 550 psi of pressure was applied to the fluid and 50 psi of fluid loss back pressure as applied to prevent any vaporization of fluid at the outlet. Fluid loss was collected on a balance at the outlet and communicated with a computer which recorded balance values over time. After applying pressure, the outlet leak off valve was opened and data collection began. The test and formation of a filter cake was allowed for 90 minutes before closing the leak off valve and stopping data collection. A graph of filtrate volume versus square root of time was prepared using the data

collected and analyzed to determine the nanoparticles effect on fluid loss. The core and its filter cake are weighed, the filter cake is scraped then the core is weighed again. The difference is taken as the weight of the filter cake. **Figure 14** shows a photo of the static fluid loss setup used for these tests. A flow schematic of the setup is shown in **Figure 15**.

Figure 13: Heating Jacket for constant fluid loss cell temperature

Figure 14: Static fluid loss setup without fluid loss cell inserted

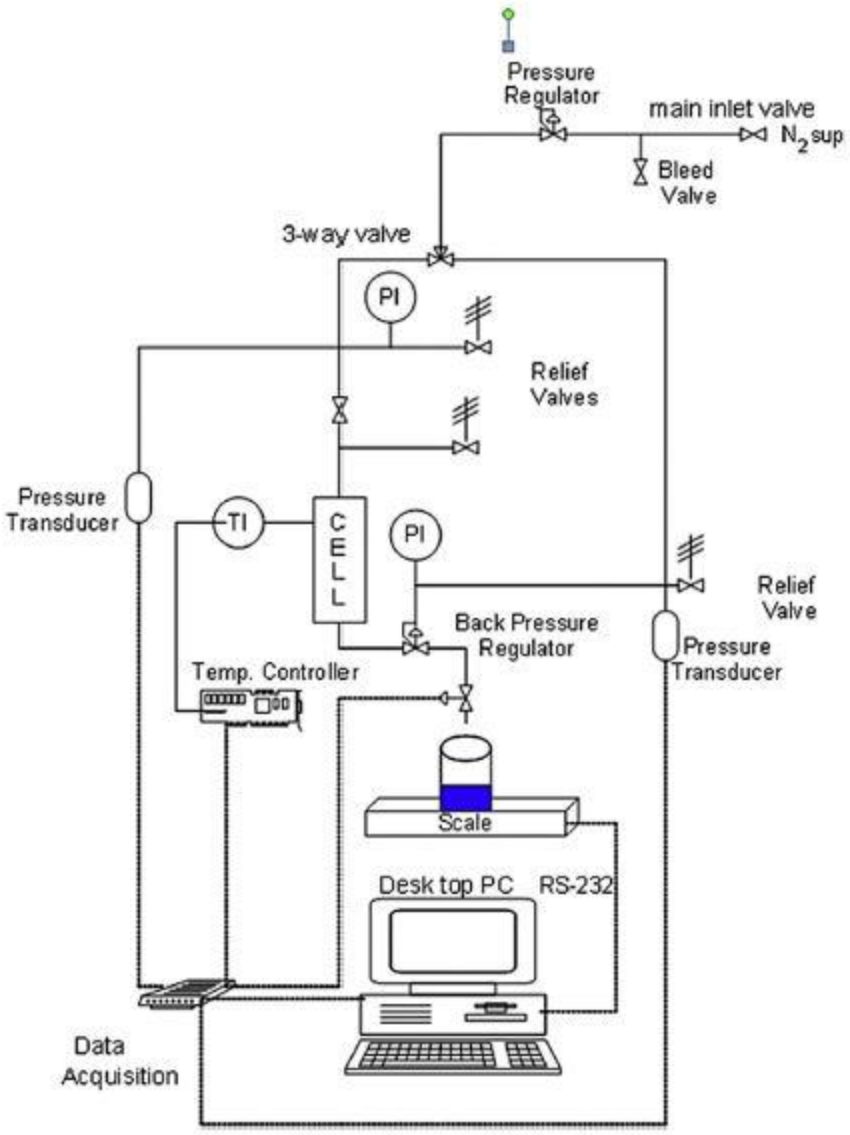

Figure 15: Static fluid loss setup flow schematic. Diagram drawn by Richard Hutchins (78)

The static fluid loss cell provided by Schlumberger is a long stainless steel cell marked PV-324. The cell was designed to handle three bottom endcaps for use in testing filter papers, ceramic discs or 1 inch cores. The bottom endcap for 1 inch cores was used and a photo of the cell with its dis-assembled bottom endcap is shown in **Figure 16**. Assembly of the endcap and core holder is described by the following:

1. Insert the core into the rubber sleeve making sure to leave room on the end opposite of flow direction.
2. Insert the rubber sleeve into the tapered cone with the excess end of the rubber sleeve on the thicker end of the taper.
3. Insert the excess of the rubber sleeve into the circular slot of the endcap in a twisting motion to ensure entry of the sleeve into the slot. Make sure the sleeve is evenly distributed in the slot. The tapered end of the plastic cone should be facing upward.
4. Push the core down flush with the endcap and place the stainless tapered collar over the plastic cone.
5. Screw the collar to the endcap using the three screws provided. It is necessary that the screws are tightened in increments of a few turns each to ensure the assembly is even and not crooked. Screws should be incrementally tightened until the bottom of the tapered cone touches the endcap. A photo of this assembled endcap is shown in **Figure 17**.
6. Insert an O-ring into the bottom end of the core holder followed by the endcap. Secure the endcap to the core holder by inserting and tightening six grub screws around the perimeter.
7. Place the core holder upright on the corner edge of a sink being careful not to let it fall.
8. Place test fluid inside the core holder over the face of the core, insert the two O-rings then place the top endcap onto the cell. Tighten with six grub screws and the cell is now assembled.

Figure 16: Dis-assembled static fluid loss core holder

Figure 17: Assembled static fluid loss cell bottom endcap

The fully assembled cell is taken to the static fluid loss setup and placed into the heating jacket at 40 °C. The nitrogen line is hooked up to the inlet and the thermocouple is inserted as well. Both of these connections are on the top endcap. The outlet is connected to the prefilled fluid loss line with the fluid loss valve closed. With desired pressures applied, the test can commence as described earlier. It should be noted that the cell should not be used in excess of 1000 psi and should be inspected periodically for cracking, pitting or corroding (70). Thorough cleaning of the cell and its assembly should happen after a test and certainly before starting another one.

4.9 Dynamic Fluid Loss Testing

After analysis of the static fluid loss data, the best system was determined and taken to be tested in a dynamic fluid loss (DFL) setting. In a real world scenario, formation faces are exposed to moving fluids and filter cakes are formed under shearing conditions when drilling fluid is in circulation. When drilling is stopped and circulation ceases, fluid loss occurs under static conditions. Testing under dynamic and static conditions allows for accurate fluid loss volume representation for each case encountered during the drilling process. The DFL setup used for these experiments helps to recreate these conditions by pre-conditioning the fluid in a shear history simulation loop before it is allowed to flow past the core face at a desired flow and shear rate. As with static testing, the filtrate volume is measured over time for a period of 90 minutes. A graph of filtrate volume versus square root of time is generated and analyzed to determine the spurt volume, wall-building coefficient and total fluid loss. Using the fluid loss curve of filtrate volume versus square root of time, McGowen et al. (71) determined the spurt volume (V_{SP}) to be the extrapolated y-intercept from the linear part of the curve at time equal to zero. They also determined the wall-building coefficient (C_W) following the linear trend in the curve by **Equation**

10 (71). The data is plotted using Excel and the slope of the linear portion of the curve is fitted with a trend line to obtain the slope and y-intercept used for calculating V_{SP} and C_W.

$$C_w = \frac{0.0164m}{A} \quad \text{Equation 10}$$

Where:

C_W = wall-building coefficient, $ft/min^{1/2}$

m = slope of volume versus $t^{1/2}$

A = core cross-sectional area, cm^2

4.9.1 Dynamic Fluid Loss Setup "Quasimodo"

The dynamic fluid loss apparatus aptly named "Quasimodo" was developed by Schlumberger to better simulate fluid loss in an actual hydraulic fracturing environment. Quasimodo has several functions that allow it to simulate this environment, from the surface pumping equipment, through the tubulars, into the wellbore and into the fracture. It consists of five separate units that include: 1) pumping units, 2) shear history simulator, 3) near wellbore, reservoir simulator, 4) a fracture simulator and, 5) the leak off monitoring equipment. The last known use of Quasimodo was in 2009 when improvements were made to the system in an attempt to automate it. These attempts proved successful, and in 2014 the setup was generously donated to Barati's Research Lab at the University of Kansas. The setup remained inoperable with missing equipment until 2017 when it was restored. The restoration and modifications will be discussed later in section 4.9.2. The following information in subsections of 4.9.1 describing the units and equipment was obtained from Navarrete et al. (52) and Hutchins et al. (72) along with some edits made since restoration:

4.9.1.1 Pumps

Originally there were three pumps used with this equipment; two Milton Roy Model B simplex piston pumps and one ISCO syringe pump. The Milton Roy pumps are still used however, each for a different purpose. The "load pump" is used to load the test fluid through the shear history, reservoir and fracture simulators before ultimately filling the accumulators. It is also used to circulate water through the system for cleaning purposes. The other pump referred to as the "reciprocating pump" is used to drive the oil to the top of the accumulators which reciprocate the test fluid through the fracture simulator. The Milton Roy pumps have a reported capability of delivering 800 ml/min at 3150 psi at 100% stroke. Pump rates measured with water after the arrival at KU indicate that the load pump has a capacity to pump 1300 mL/min and the reciprocating pump at 1020 mL/min at 100% stroke at ambient pressure. Each pump has a pressure release valve that is set to relive pressure at 2100 psi.

4.9.1.2 Shear History Simulator

The shear history simulator (SHS) is comprised of almost 800 feet of ¼ inch stainless steel tubing with an inner diameter of 0.194 inches. The capacity of the loop is 5.73 mL/ft for about 4584 mL total volume. The shear history loop is included to replicate the shear a fluid goes through as it flows through the wellbore on its way to the reservoir. For the purposes of this research, it is used to simulate the shear experienced by a drill-in fluid down the inner diameter of a drilling pipe before expulsion through the drill bit. A photo of the shear history loop can be seen in **Figure 18**.

4.9.1.3 Fracture Simulator

The near wellbore reservoir simulator and fracture simulator are both grouped into this section of the equipment. It is designed to provide shear and temperature conditioning of the test fluid by cycling the fluid through coils submerged in a temperature controlled oil bath. The fracture simulator is comprised of two 2,700 mL floating piston accumulators and two, 32-ft coils of 3/8 inch diameter stainless steel tubing with an inner diameter of 0.31 inches. At 14.8 mL/ft the coils yield approximately 947 mL of volume. The coils submerged in the temperature controlled silicone oil bath should not be operated above 300°F. There are two 3/8 inch hoses used to connect the accumulators to the fluid loss cells. They are both insulated and have flowline heaters to heat and keep the test fluid at a constant desired temperature. The test fluid is reciprocated from accumulator 1 through a coil in the oil bath to a Whitey 4-way valve which directs it through the other coil in the oil bath before it starts to fill accumulator 2. The hydraulic oil in the top of the accumulators is also directed by another Whitey 4-way valve. Unidirectional flow through the core holders is maintained by the two Whitey valves attached to an actuator signaled by magnetic proximity switches at the bottom of both accumulators. When the piston of one accumulator reaches the bottom, the magnetic proximity switch activates the actuator turning the Whitey valves. Location of the pistons can be monitored via magnets attached outside the accumulators. During a test the accumulators should be ran in automatic mode, but can be ran manually if necessary by switches on the front panel. Use of manual mode will be necessary during loading and clean out of the system. For the purposes of this research the oil bath was not used for heating purposes as tests were performed at 40°C and the flowline heaters were capable of heating and maintaining the fluid to these temperatures. A photo of the accumulators with heated hoses and fracture simulator coils can be seen in **Figure 19**, **Figure 20** and **Figure 21** respectively.

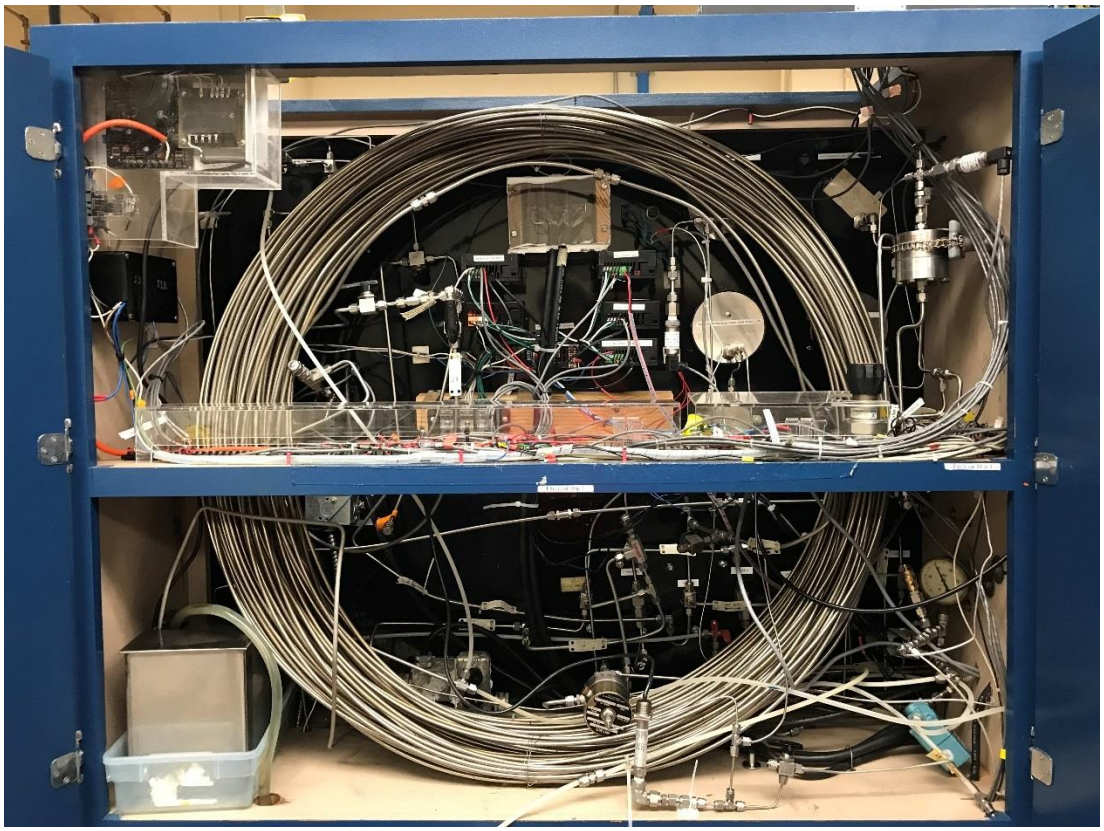

Figure 18: Dynamic fluid loss shear history simulator loop

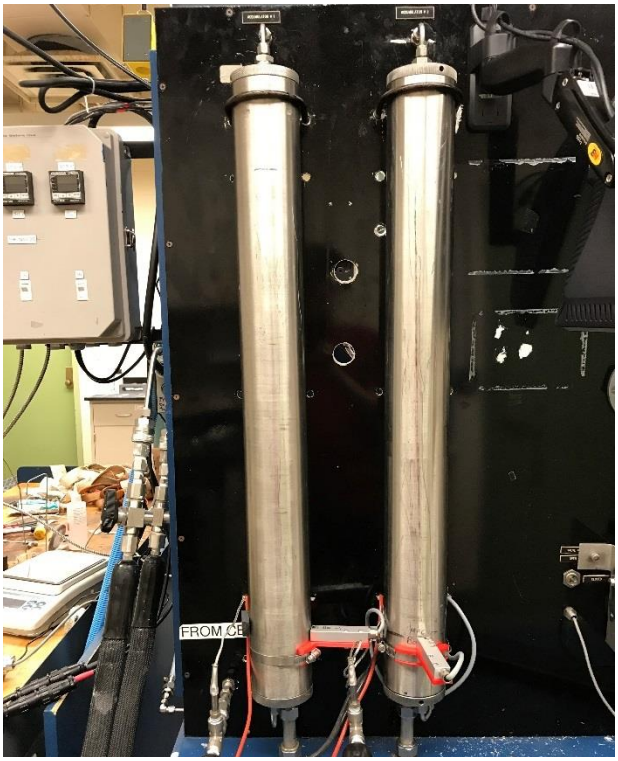

Figure 19: Dynamic fluid loss floating accumulators with proximity switches at the base and flowline heated hoses

Figure 20: Fracture simulator coils in empty oil bath with Whitey valves and actuator above. The top Whitey valve is for circulation of hydraulic oil while the bottom valve is for test fluid circulation

Figure 21: Both fracture simulation loops sitting in the empty oil bath

4.9.1.4 Dynamic Fluid Loss Cells

Originally there were three dynamic fluid loss short cells that were meant to be connected in series so the test fluid could flow through each one before returning to an accumulator. However when donated from Schlumberger only two of the three remained. The two remaining core holders can still be connected in series for running two tests at once. The core holders were designed to simulate flow through a fracture with a slot flow rectangular geometry bounded by one impermeable wall and a circular core face opposite for fluid loss to be measured through. The dimensions of the slot are 2.205 inches long, 1 inch wide with a 1/8 inch gap. The width of the slot was designed for 1 inch diameter cores to ensure that flow of the fluid could never go around the building filter cake, only above and over it. The core holder utilizes a tapered rubber sleeve that holds a 1 inch by 1 inch core. The core holder back fits over the tapered sleeve and has a conduit that allows filtrate to exit out the back of the core. These two pieces are held together by a ring that screws into the front core holder part and secures the back core holder part down with pressure. The ring can be tightened using a pin spanner wrench. The core holders slide into a heating jacket during testing which keep them at a constant temperature. A thermocouple inserted in the front of the cell monitors the internal core holder temperature. **Figure 22** is a schematic drawing of the core holder. A photo of a disassembled core holder can be seen in **Figure 23**.

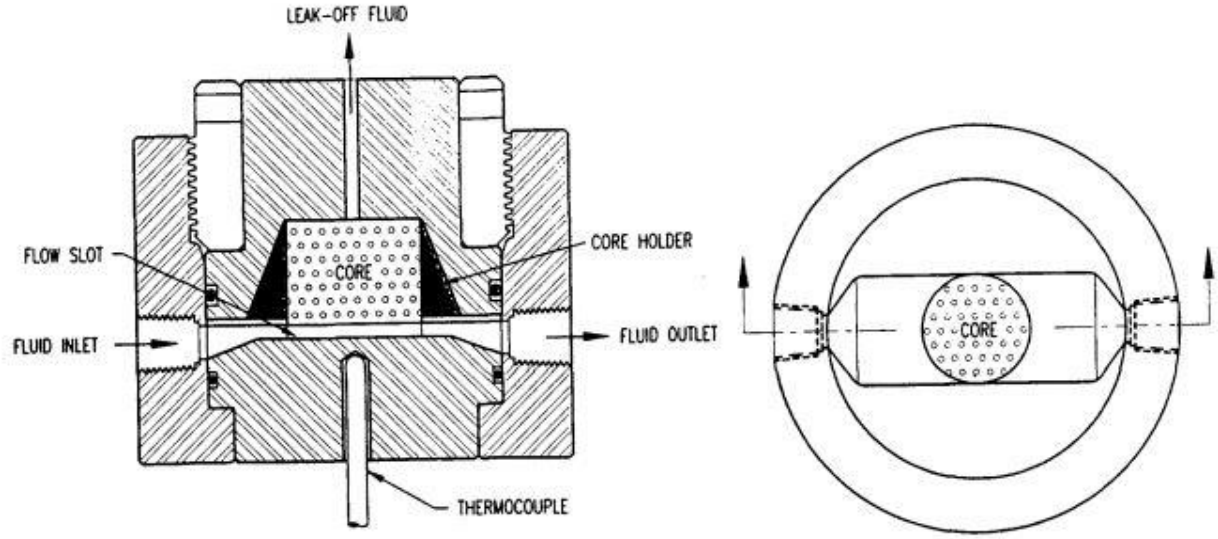

Figure 22: Schematic drawing of a dynamic fluid loss core holder used with the Quasimodo setup (52)

Figure 23: Photo of a dynamic fluid loss core holder used with the Quasimodo setup

4.9.1.5 Dynamic Fluid Loss Software

As of 2009 the software for Quasimodo was outsourced to Omnia who upgraded it to its current interface which can be seen in **Figure 24**, a screenshot of the DFL main screen. The main screen consists of four sections: Controls, Cell Data, Automatic Controls, and Facility data.

The controls section allows the user to toggle between automatic and manual mode. The controls section has preset valve commands that switch the valves to configurations using solenoids and air powered actuators for various stages during the operation of Quasimodo. This feature currently does not work as the preset stages selected will open or close valves that should or should not be activated. For selection of the correct valve configurations, the manual feature must be used then switched back to automatic mode before running a test, otherwise the fluid loss valves will not open automatically when the test begins. Clicking the manual button to the right of the valve command presets will open a window where desired valves can be activated as seen in **Figure 25.**

The cell data section monitors the fluid loss cell temperatures and filtrate weight captured by the balances. It also toggles a green light under each cell number to indicate that the sample valve has been opened while running a test.

The facility data section monitors various pressures and temperatures of the system. It also gives an indication of what the reciprocation pump % stroke is in relation to its set point as seen in **Figure 26**.

The automatic controls section is where the user can prepare and run a test. Test parameters such as starting temperature and maximum leak off can be set so that the test will commence only after a desired temperature is reached. The maximum leak off parameter will stop the test in the event that fluid is flowing around the core. The “load/edit recipe” button opens a window where the user

can select the reciprocating pump output and length of duration. Several pump outputs may be entered, and after the duration of one segment during a test, the reciprocation pump will adjust its stroke and continue for the next length of time. **Figure 28** shows a screenshot of the build recipe pop out window. The "create experiments" button opens a window shown in **Figure 27** that allows the user to enter information about the experiment for each fluid loss cell to be tested. It should be noted that a file name is the minimum about of information that needs to be entered in order to activate a cell for testing. Another important glitch to be noted with the software is that it writes data to a file in a sort of sequential manner. For example, if cell one and cell three are the only ones to undergo testing, all three cells must be activated in the "experiment" tab. If not done so, the software will write data to a file for cell one but not cell three. As a general rule to prevent this from happening, all three cells should be activated in the software as indicated by the green lights next to their names. The "additives" and "comments" tabs in this window are for user purposes only and have no effect on running of the software.

There are three tabs at the top of the main screen. The "view results" tab shown in **Figure 29** allows the user to open files from completed tests and view plots created from experimental data. Plots are of fluid loss versus both time and square root time. The software plots a regression line on the linear part of the square root of time curve and uses this to calculate a spurt value and filter cake coefficient (C_W). The graph is interactive in a way that two points can be clicked and dragged to create a best fit line while recalculating spurt and C_W. Charts plotted by the software using real data from experiments can be seen in the appendix. The "view chart" tab allows the user to see a real time plot of fluid loss weight versus time which can be viewed during a test. The "calibrate" tab allows for point calibration of the transducers. At this point in time, this calibration window does not work, and manual calibration of the transducers must be performed.

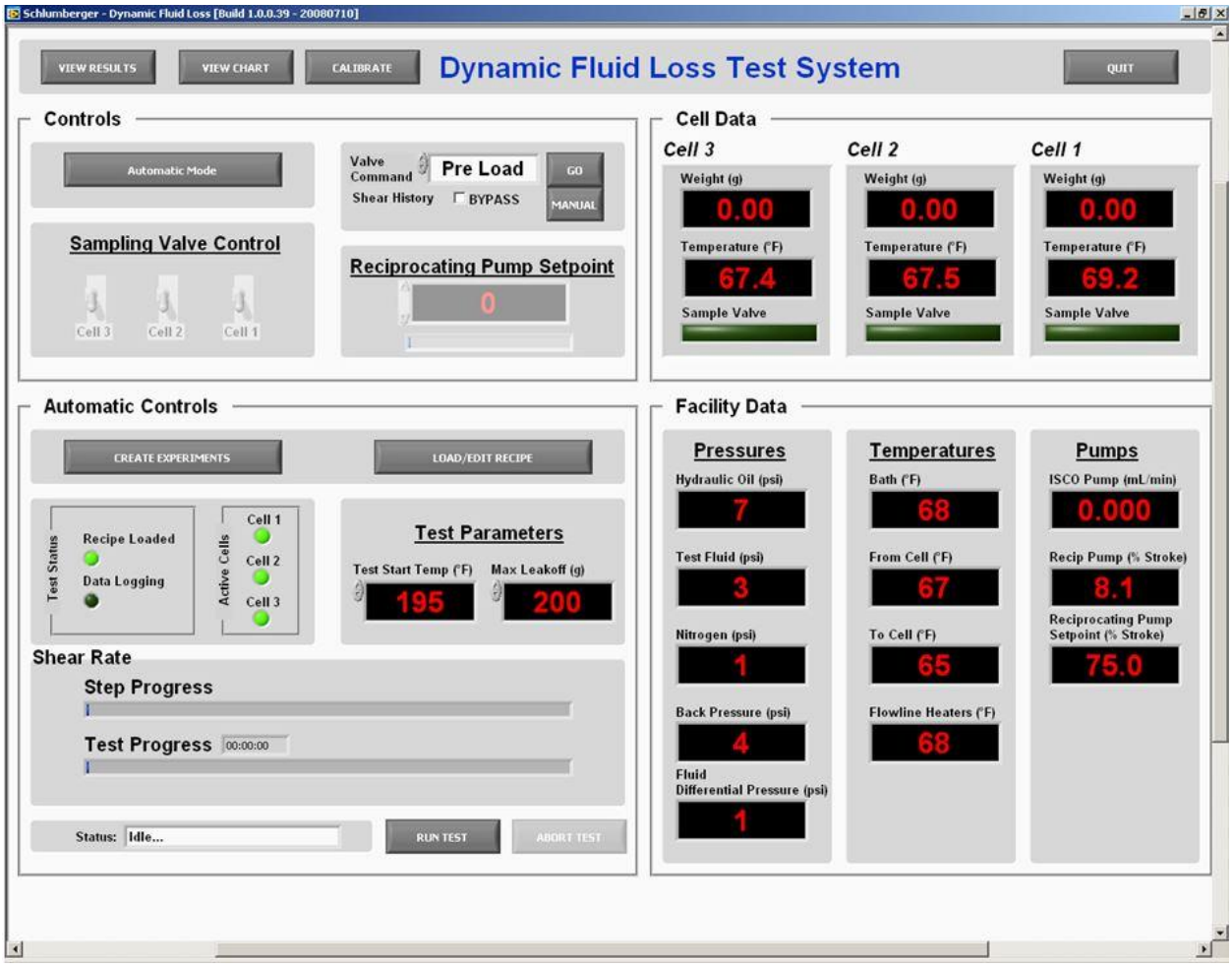

Figure 24: DFL screenshot of the software's main screen

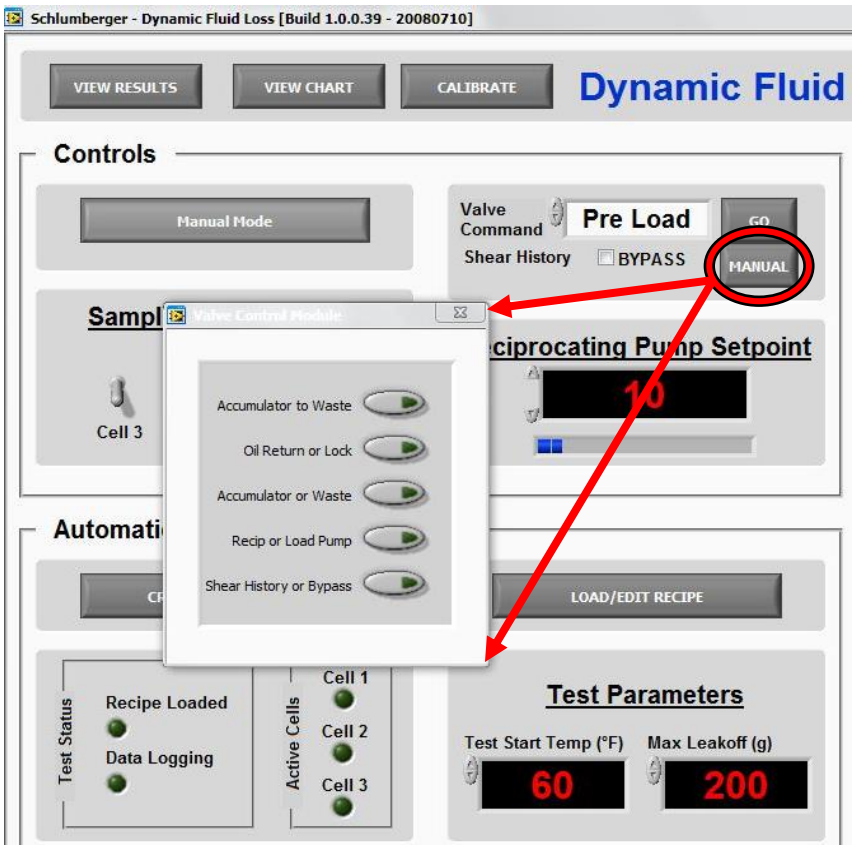

Figure 25: DFL software manual valve configuration button with resulting pop out window

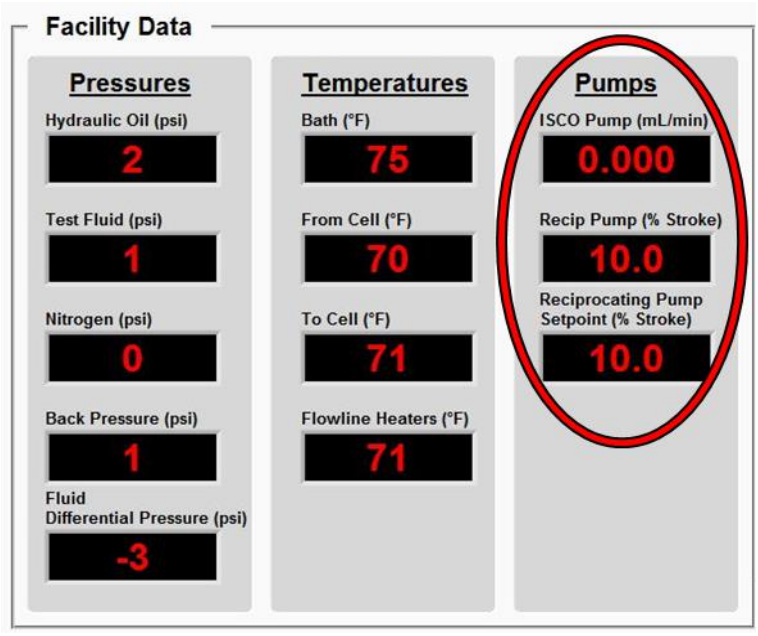

Figure 26: Facility data showing reciprocating pump stroke % in relation to its setpoint

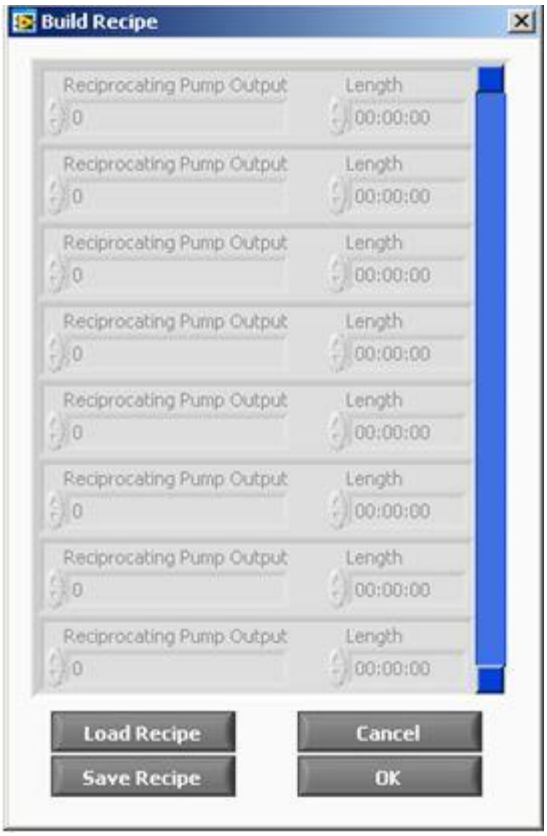

Figure 28: DFL software pop out screen for building a "recipe" that allows the user to set pump output for a given duration

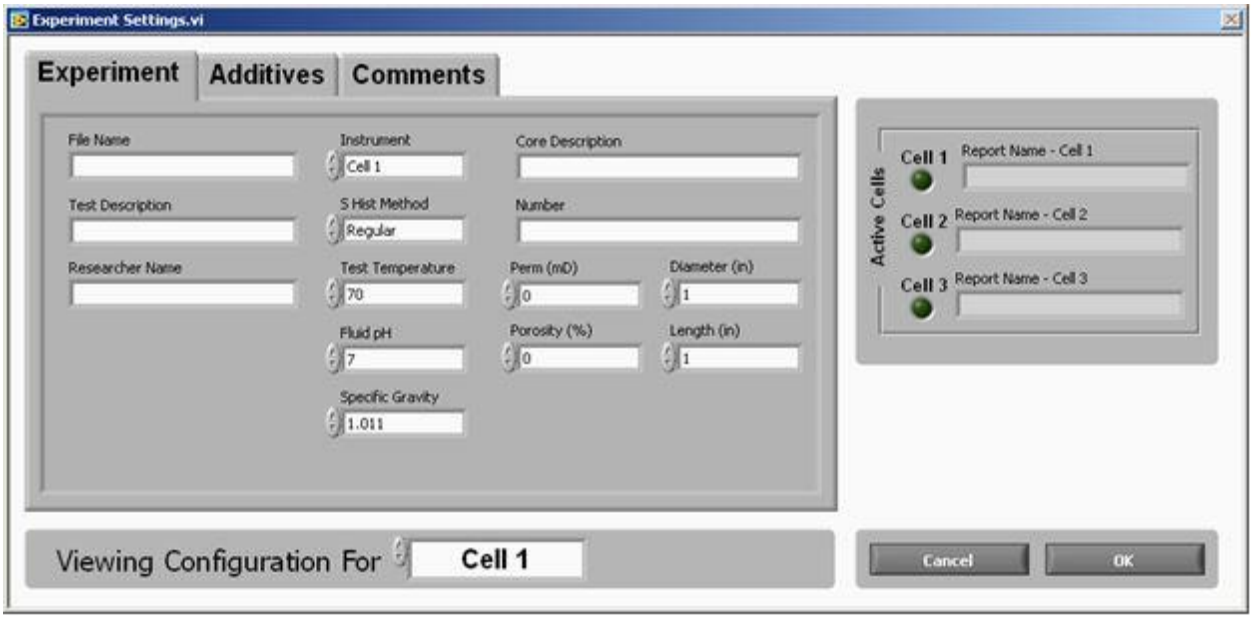

Figure 27: DFL screenshot of Create Experiment pop out window

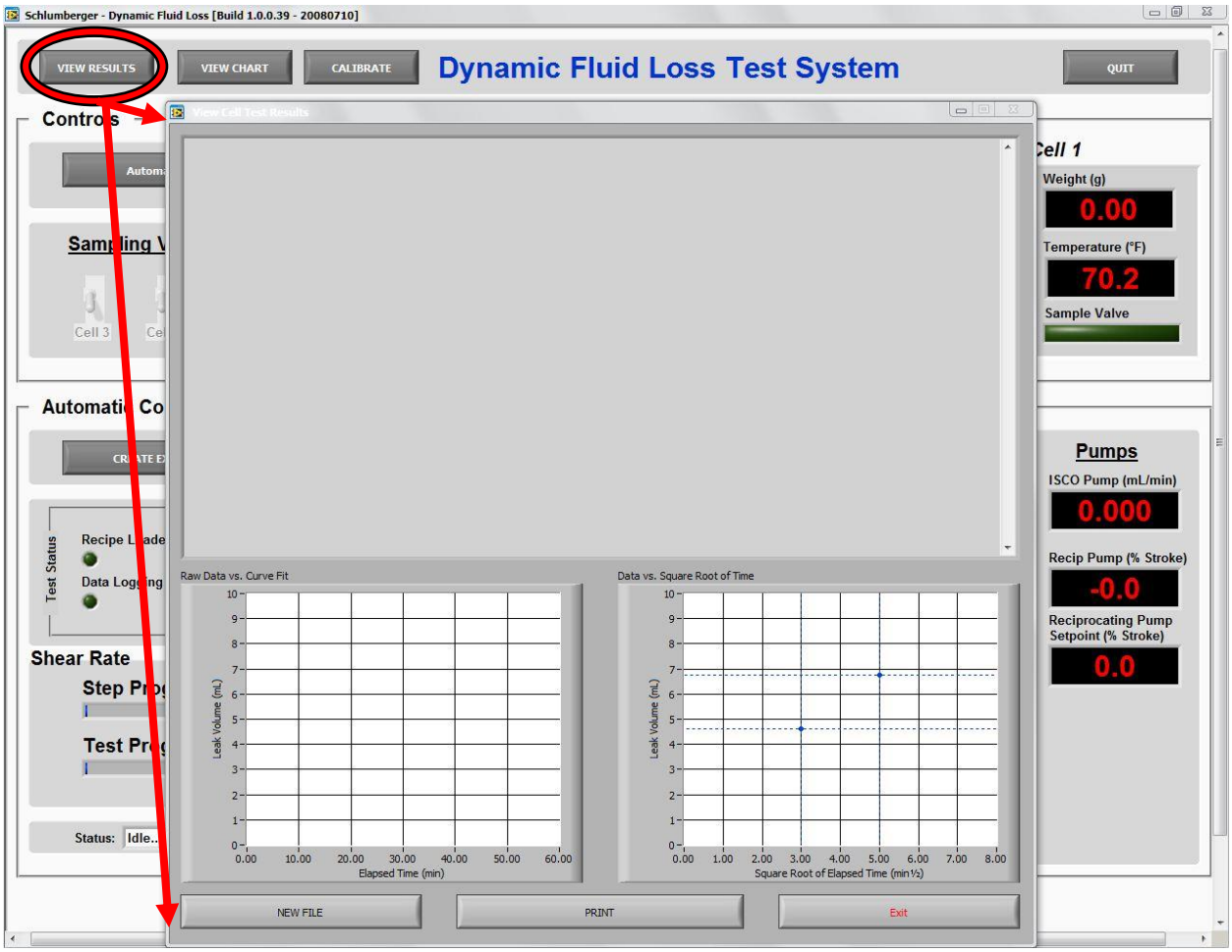

Figure 29: DFL software "view results" pop out window where files of completed tests can be selected to populate the charts and display data values.

4.9.2 Equipment Repairs and Modifications

Upon initial inspection of Quasimodo, there were many missing pieces of equipment, unconnected flow lines and cut electrical wires. Some rewiring of the electrical strip in the back cabinet had to be done in order for certain electrical components to work such as the thermocouples and temperature control units. Several flow lines were unconnected and had been rerouted or just gone missing. Below is a list of hardware modifications and missing or broken parts that were replaced:

1) AND GS3000 Balances were missing and replaced.
2) One transducer was missing and replaced while all others had to be reconnected.
3) A differential transducer that measures pressure drop within the circulating loop was missing and replaced.
4) Waste lines that were no longer in use were capped
5) Valves connecting the ISCO pump to the system were closed since it was no longer being used.
6) A valve was added to the beginning of the shear loop before Valve 5 so that if the shear loop was to be bypassed there would be no chance of losing any fluid to the shear loop on its way to bypass.
7) Flow lines connecting the fracture simulation coils to the accumulators had cracked and needed replacing.

4.9.3 Preparation of the Drill-in Fluid

Scaling up from static fluid loss testing to use of Quasimodo would require much greater volumes of fluid. In order to determine the amount of drill-in fluid needed to run a test, calculations were done by adding up the volumes of all the plumbing to be used during a test. It was decided that a fluid volume of 10 liters was needed to run a test without the fear of running out before an accumulator could be fully filled. Fluids were mixed in a five gallon bucket with an air powered stirrer pictured in **Figure 30**. The stirrer came with the DFL setup and is from Arrow Engineering Company out of Hillside, New Jersey. Formulation of this drill-in fluid is the same as that during static fluid loss testing with the exception of being scaled up. 7,619 mL of 3% NaCl was added to the bucket and allowed to stir while 22.857 g of xanthan gum was slowly added to the shoulder of the vortex and allowed to mix for 20 minutes. The air stirrer speed was increased to keep an established vortex and 30.476 g of HPG was slowly added to the shoulder of the vortex and allowed to mix for 20 minutes. 761.9 g of $CaCO_3$ was then added via a funnel to prevent introducing large clusters of the powder at once. After mixing for 20 minutes, 2,381 mL of PECNPs solution was added as the final ingredient. In the baseline case where no nanoparticles were used, the same volume of brine was added instead.

Figure 30: Air powered stirrer and mixing bucket used for mixing drill-in fluid

4.9.4 Determining Shear Rate of Dynamic Fluid Loss System

In order to create an accurate shear history using different segments of Quasimodo, some calculations were explored in an attempt to translate real world shear rates a fluid experiences during drilling and simulate them using the DFL system. The shear history loop would be used to simulate shear rates experienced by the drilling fluid as it travels down the drill pipe to the drill-bit. Although the core holder was designed to simulate shear rates within a fracture, it would be attempted to simulate shear rates within the annulus of the drill pipe and borehole wall. To follow a realistic scenario, a 5.5 inch diameter drill pipe in an 8.5 inch diameter hole was taken from literature and used for calculations (73). The inner diameter of a 5.5 inch drill pip was taken as 4.778 inches from a drill pipe supplier specifications sheet (74). A flowrate of 500 gal/min was taken from the Baker Hughes Drilling Fluids Manual section on extended reach wells (40). In order to calculate the shear rate, average velocities within a pipe and annulus should be calculated using

Equation 11 and **Equation 12** respectively. The shear rate of a power law fluid flowing through a pipe and annulus can then be calculated with **Equation 13** and **Equation 14** respectively.

$$v_p = \frac{(q,gal/min)}{2.448d^2} \quad \text{Equation 11}$$

$$v_a = \frac{(q,gal/min)}{2.448(d_2^2 - d_1^2)} \quad \text{Equation 12}$$

$$\gamma_{pw} = \frac{24v_p}{d}(3 + \frac{1}{n}) \quad \text{Equation 13}$$

$$\gamma_{aw} = \frac{48v_a}{d_2 - d_1}(2 + \frac{1}{n}) \quad \text{Equation 14}$$

Where:

v_p= velocity in the drill pipe, ft/sec

v_a= velocity in the annulus, ft/sec

γ_{pw}= shear rate in the drill pipe, sec^{-1}

γ_{aw}= shear rate in the annulus, sec^{-1}

q= flowrate, gal/min

d= inner diameter of the drill pipe, inches

d_2= borehole diameter, inches

d_1= outer drill pipe diameter, inches

n= flow behavior index

Using the values obtained from literature, shear rate in the pipe and annulus was calculated to be approximately 255 sec^{-1} and approximately 364 sec^{-1} respectively. The same equations were used to back calculate the flow rate needed within the shear history loop to produce the same shear rate. This was found to be 127 mL/min which was achievable by adjusting the load pump to perform at 17 % stroke.

Navarrete et al. (52) used Quasimodo and the dynamic fluid loss cells to study the effect of shear rate on the dynamic fluid loss behavior of fracturing fluids. Using **Equation 15** and assuming a power law model, they calculated the shear rate at the walls of a fracture (34). During back calculations to determine the flowrate required through the core holder to achieve this shear rate, it was discovered that the reciprocating pump was not capable of achieving such a high flowrate. With the equipment having just been restored and concerns of pushing the accumulators and equipment beyond its limits, it was decided that a 10 % stroke would be used for the reciprocating pump which results in a flowrate of approximately 82 mL/min and a shear rate of 6.2 sec^{-1} through the core holder and 40.3 sec^{-1} through the fracture simulator coils.

$$\gamma_{wf} = \frac{\left(4+\frac{2}{n}\right)Q}{h^2 W} \qquad \text{Equation 15}$$

γ_{wf} = shear rate at the fracture wall, sec^{-1}

Q = flowrate, $in.^3/sec$

h = height of the fracture (in this case height of the core holder slot), inches

W = width of the fracture (in this case width of the core holder slot), inches

n = flow behavior index

Flowrates of both pumps should be checked using the fluid to be tested and a graduated cylinder before testing is performed to determine what stroke percentages to use for achieving desired flowrates. This will vary based on the viscosity of the fluid in use especially for the load pump. A graduated cylinder can be used in conjunction with a stopwatch to measure the flowrate of the load pump out the sample port on the front panel of Quasimodo. This can similarly be done for the reciprocating pump by measuring the from the hydraulic oil return line which empties into the oil reservoir in the back panel. Calibration curves for both pumps are shown in **Figure 31** and **Figure 32**.

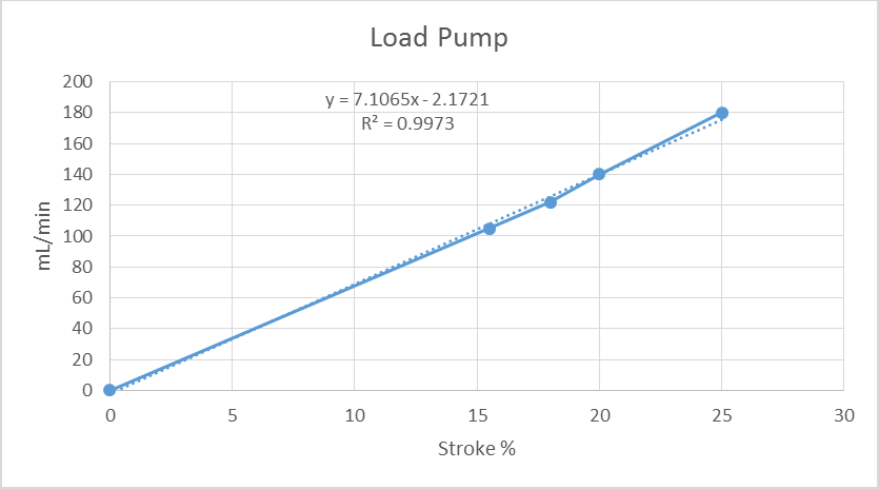

Figure 31: Load pump calibration curve

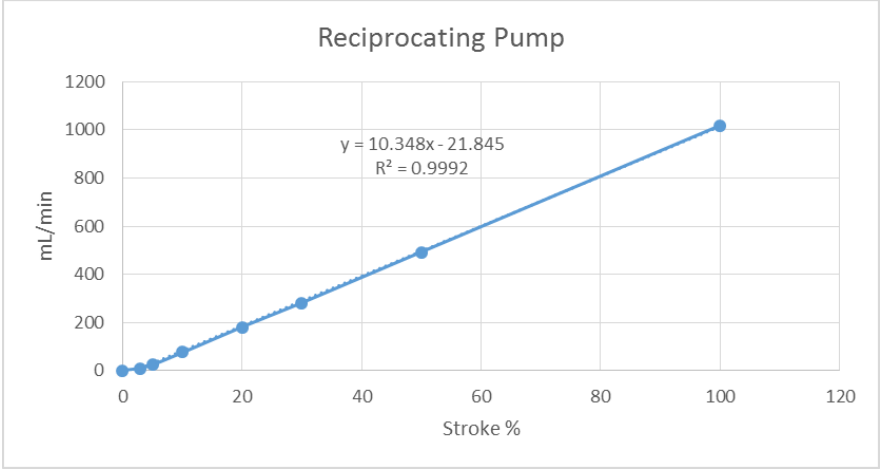

Figure 32: Reciprocating pump calibration curve

4.9.5 Quasimodo Operation Procedure

The operation of Quasimodo for these experiments can be broken down into four categories from start to finish and will be discussed in order. All valve configurations allow for flow through the shear loop and should be toggled through the manual software operations discussed in section 4.9.1.5. The categories are as follows: Pre-loading the test fluid, loading the test fluid, reciprocating/running a test and cleanout. **Figure 33** and **Figure 34** show the flow path diagrams of both the load loop and reciprocating loop for a better understanding of how the pumps and valves operate the system. Some of the operation procedures in this thesis were taken and adapted from Hutchins and Barati (75).

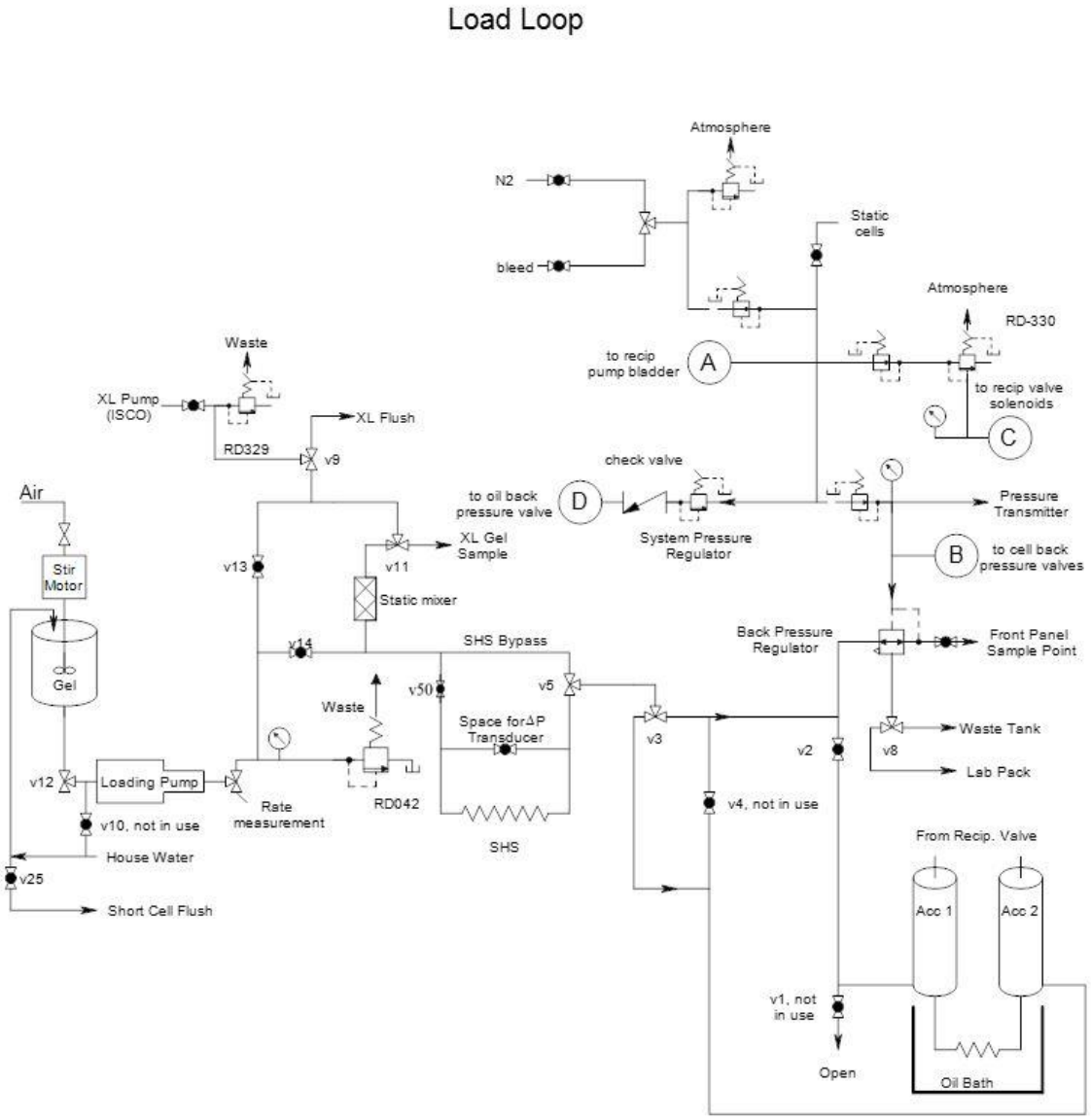

Figure 33: DFL load loop flow diagram (72)

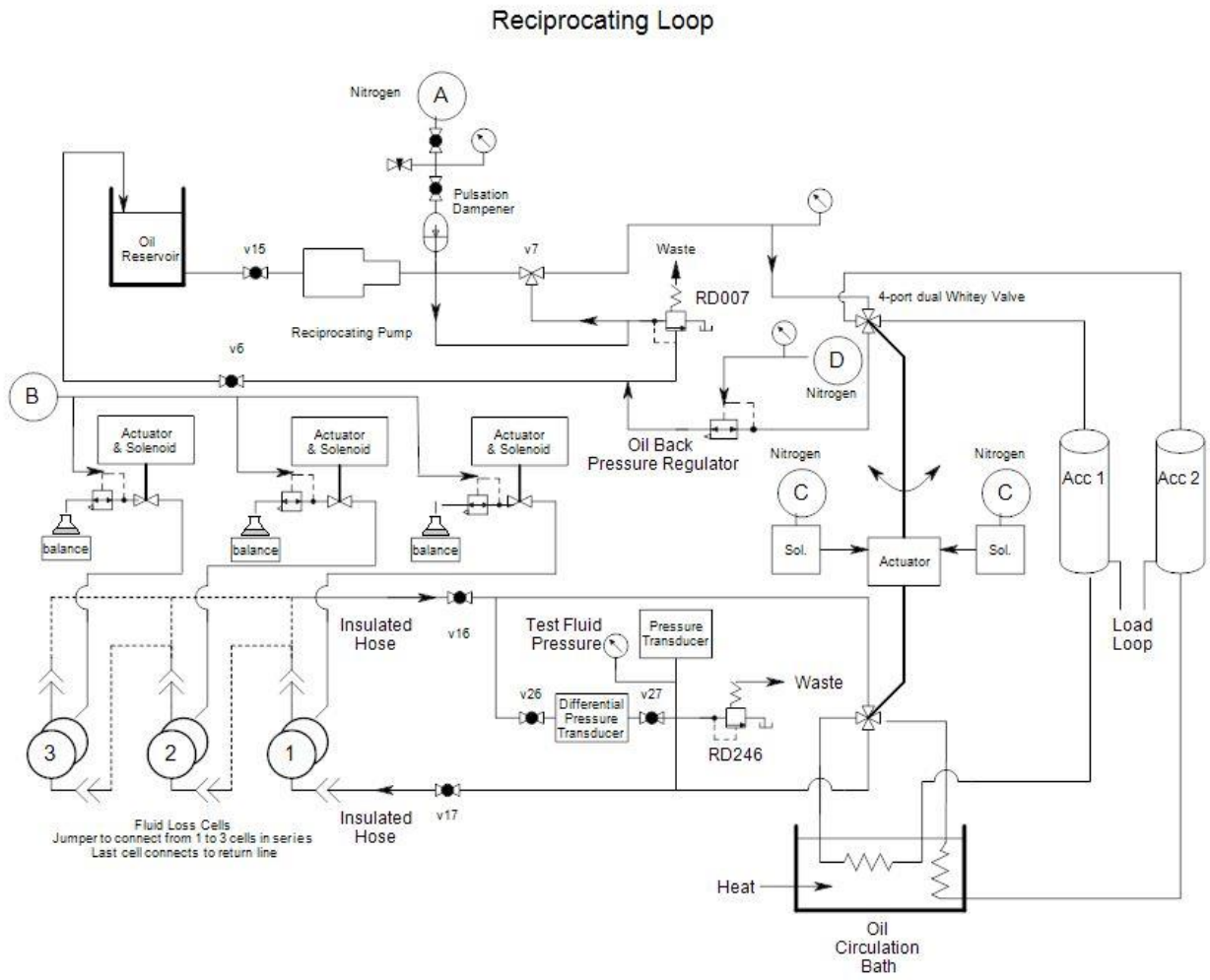

Figure 34: DFL reciprocating loop flow diagram (72)

4.9.5.1 Pre-Loading the Test Fluid

Assuming the system has been flushed with water after prior testing and both accumulator pistons are down, the purpose of pre-loading the system is to displace the water to waste while simultaneously sending the test fluid through the shear loop. This begins by pouring the test fluid into the loading reservoir connected to the load pump. The air stirrer is mounted above the reservoir for continued mixing of the fluid. The stroke of the load pump should be adjusted to the desired percentage. Power to the system should be turned on at this point. Valves should be configured the way they appear in **Figure 35,** which is also the same configuration for cleanout. Make sure that valve #50 is open in the back of the cabinet to allow flow through the shear loop. Using the switches on the front panel pictured in **Figure 36**, switch accumulator 2 into the down position. Valve 8 should be turned to waste tank and kept that way. The load pump can now be turned on and the system will begin loading. Verify that water is being expelled to the waste tank and neither magnet on the accumulators are moving. Turn on the flowline heaters to start heating the testing fluid once it reaches the flexible 3/8 inch flowlines.

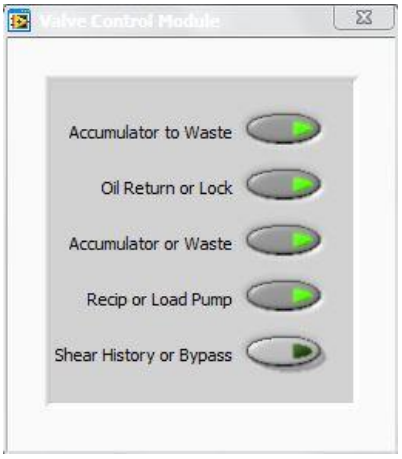

Figure 35: DFL pre load and cleanout valve configurations

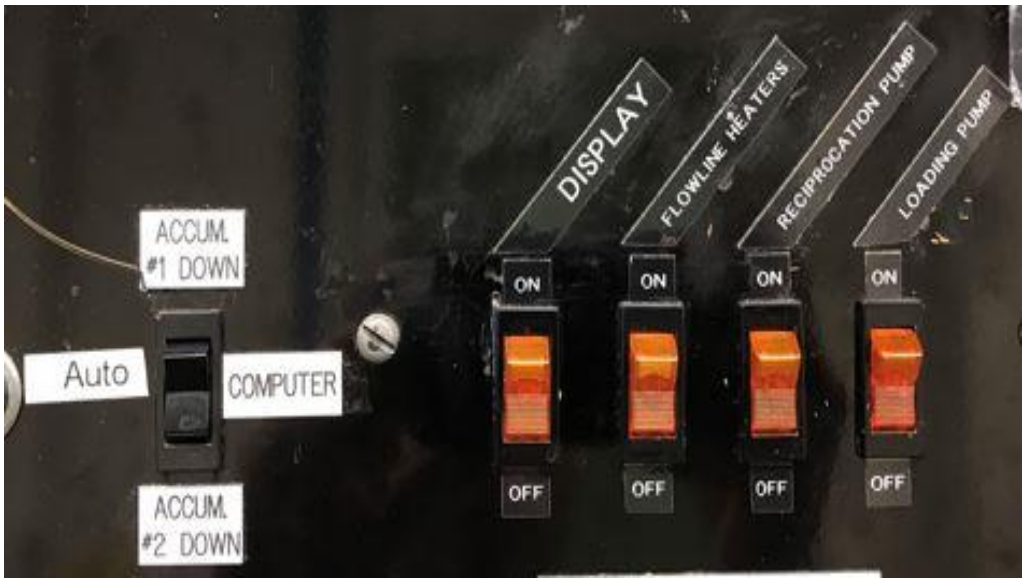

Figure 36: DFL front panel switches for accumulators, flowline heaters, reciprocation pump and load pump

Flow through the loop can take quite some time depending on the % stroke of the load pump. It is recommended that the sample port valve on the front panel be opened and emptied into a bucket for two reasons. One, to monitor the progress of test fluid moving through the system and two, in order to save room in the waste tank. Once the test fluid has made it to the sample port valve, it has filled all necessary lines for the reciprocation loop and loading of accumulator 1 can begin.

4.9.5.2 Loading the Test Fluid

The load pump should be turned off when switching between valve configurations to prevent a surge of pressure while a valve may be turning through a closed positon. Switch the valve configuration to the one pictured in **Figure 37**. This closes the fluid valve #2 to waste and allows hydraulic oil in the top of accumulator 1 to return to the oil reservoir by opening valve #6. With accumulator 2 switched to the down position, the sample port valve should be closed and the load pump turned back on. Accumulator 1 will begin to load. Verify that the magnet on accumulator 1 is moving upward signifying the movement of the accumulator piston. Once the magnet reaches

the black line at the top of accumulator 1 stop the load pump. This line indicates the 90 % fill mark of the accumulator. They should never be filled to more than 90% capacity.

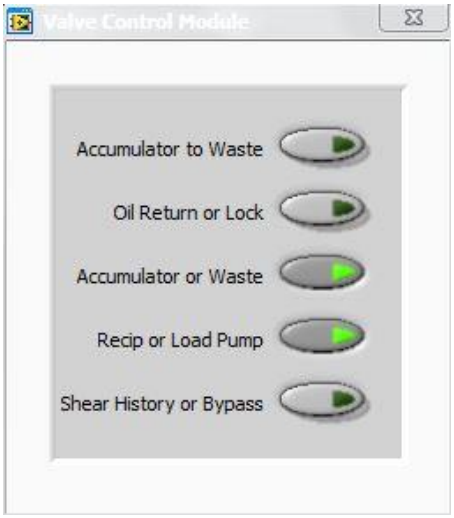

Figure 37: DFL valve configuration for loading accumulator 1

4.9.5.3 Reciprocating/Running a Test

With accumulator 1 now full, switch the valves to the configuration depicted in **Figure 38**. The reciprocation loop is now closed from the load loop. Change the accumulator switch in **Figure 36** to neutral or automatic mode. Make sure the software is in automatic mode and load a recipe then create an experiment making sure to activate all cells. For these experiments, the reciprocation pump was set to 10% stroke and a test ran for 90 minutes.

Fill the leak off side of the cells with brine by using the manual leak off switches on the front panel making sure to close the manual leak off switches when finished. Assemble the core holder with a test core inside and mount it into the heating jacket and attach the leak off quick connects. Insert the thermocouple and turn the heating jacket on. Temperatures are set to 40°C at this time. Disconnect the “To Cell” flowline from the hanging U-line and connect it to the inlet side of the

core holder which is always on bottom. Connect the jumper tubes from the outlet of one cell to the inlet of the other. Flow should always go from bottom to top of the cells.

The reciprocation pump can now be turned on and the fluid will cycle through the fluid loss cells and reciprocate between the two accumulators. Wait until the fluid and the core holders have reached the desired temperatures, then increase the fluid loss back pressure to 50 psi and the main flowline back pressure to 550 psi using nitrogen. The system will take a minute or two to rise and pump at these pressures. The "run test" button can now be pressed on the software's main screen, the system will wait two minutes then the balances will tare to zero, fluid loss valves will automatically open and the software will begin recording the data. At the end of 90 minutes, the fluid loss valves automatically close and the software completes recording the data. Stop the reciprocation pump and decrease the nitrogen pressure to zero followed by the cell back pressure. Turn off the flowline heaters and cell heaters. Wait until the cell has had time to cool off and remove the flexible flowlines and reconnect them to the hanging U-line before removing the fluid loss cell. Disassemble the cell and remove the core to be weighed with and without the filter cake as done in the static fluid loss testing. After thoroughly washing the core holder, cleanup of the system can now begin.

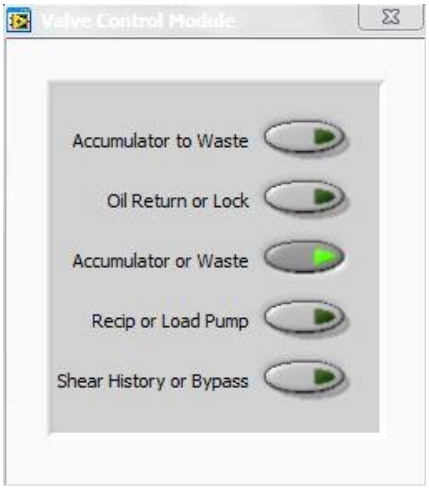

Figure 38: DFL valve configuration for reciprocation

4.9.5.4 Cleanout

The test fluid reservoir should now be filled with water and emptied into a bucket with the secondary flush valve located below the reservoir to empty any remaining test fluid. Once the loading reservoir is clean, refill it with water and configure the valves as shown in **Figure 35.** Increase the load pump stroke to 100% and repeat the same procedure as done for pre-loading. Several buckets of water should be ran through the system to ensure a thorough cleaning. Stop the load pump and configure the valves to fill accumulator 1 shown in **Figure 37**. Start the load pump and fill accumulator 1 with water. Once filled, change the valve configuration to reciprocation with the appropriate switches flipped and cycle water between the two accumulators several times. The reciprocation pump may be set to 100 % stroke to speed up the process. After cycling several times, wait until accumulator 1 has been filled and stop the pump. Manually switch accumulator 1 down, and change the valve configuration to **Figure 39.** Turn the reciprocation pump on to empty accumulator 1 to waste. Repeat this cleanout process several times to thoroughly clean the accumulators.

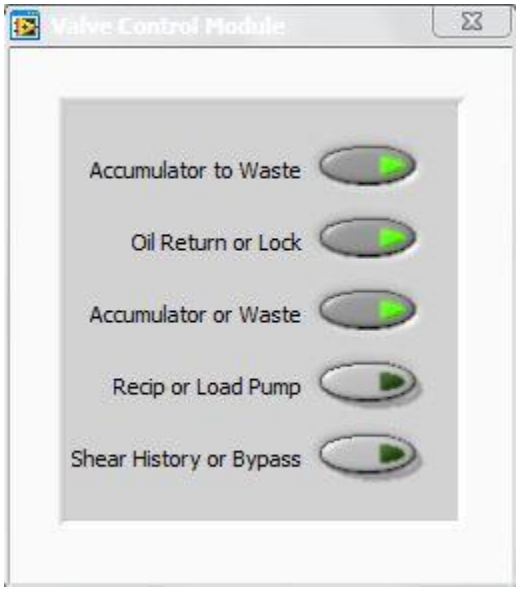

Figure 39: DFL valve configuration for emptying accumulator 1 to waste

5 Results and Discussion

5.1 PEI:DS:Brine Optimal Ratio for 3% NaCl Brine

Polyelectrolyte complex nanoparticles were generated by mixing 3 pH values of PEI in different ratios of PEI:DS:Brine. As discussed previously, ratios of PEI:DS ≥ 1 result in positively charged nanoparticles while ratios ≤ 1 result in a negative charge. Upon mixing, each sample was visually inspected for precipitation, indicating the ratio's instability. Those that did not precipitate were taken for size and zeta potential measurements. The combinations and initial stability for both positive and negative particles are arranged in **Table 3** and **Table 4.** Photos of both positive and negative PECNPs have been included in **Figure 45** and **Figure 46.**

Table 3: Positively charged nanoparticle combinations

	Initial stability (✓)		
Ratio (PEI:DS:Brine)	pH=8.5	pH=8.0	pH=7.5
1:1:0.1	×	×	×
2:1:0.1	✓	✓	✓
3:1:0.1	✓	✓	✓
4:1:0.1	✓	✓	✓

Table 4: Negatively charged nanoparticle combinations

	Initial stability (✓)		
Ratio (PEI:DS:Brine)	pH=8.5	pH=8.0	pH=7.5
1:2:0.1	×	×	×
1:3:0.1	×	×	×
1:4:0.1	×	×	×
1:5:0.1	×	×	×
1:6:0.1	✓	✓	✓
1:7:0.1	✓	✓	✓
1:8:0.1	✓	✓	✓
1:9:0.1	✓	✓	✓
1:10:0.1	✓	✓	✓

5.2 Size and Zeta Potential Measurement Results

The systems that passed initial stability visual inspection were taken for further analysis over a 24 hour period. For each system, three measurements were taken for both particle size and zeta potential and a mean average and standard deviation were calculated. After mixing each different ratio of PEI:DS:Brine, initial measurements were taken at time zero. The ratios were then allowed to mix over a 24 hour period and measurements were taken again. Any drastic increases in size over 24 hours would suggest that the particles may be flocculating. Also, any changes in zeta potentials trending toward zero would indicate the loss of particle stability over time.

5.2.1 Positively Charged Particles

Comparing all the zeta potential values for each positively charged system after 24 hours in **Figure 40**, it was determined that a PEI pH of 8.5 allowed for the highest zeta potential for each ratio. This would narrow the choices down to three systems. **Figure 41** compares those three systems' changes in zeta potential over 24 hours. Ratios of 2:1:0.1 and 3:1:0.1 showed increased zeta potential thus stability, while ratio 4:1:0.1 declined in zeta potential.

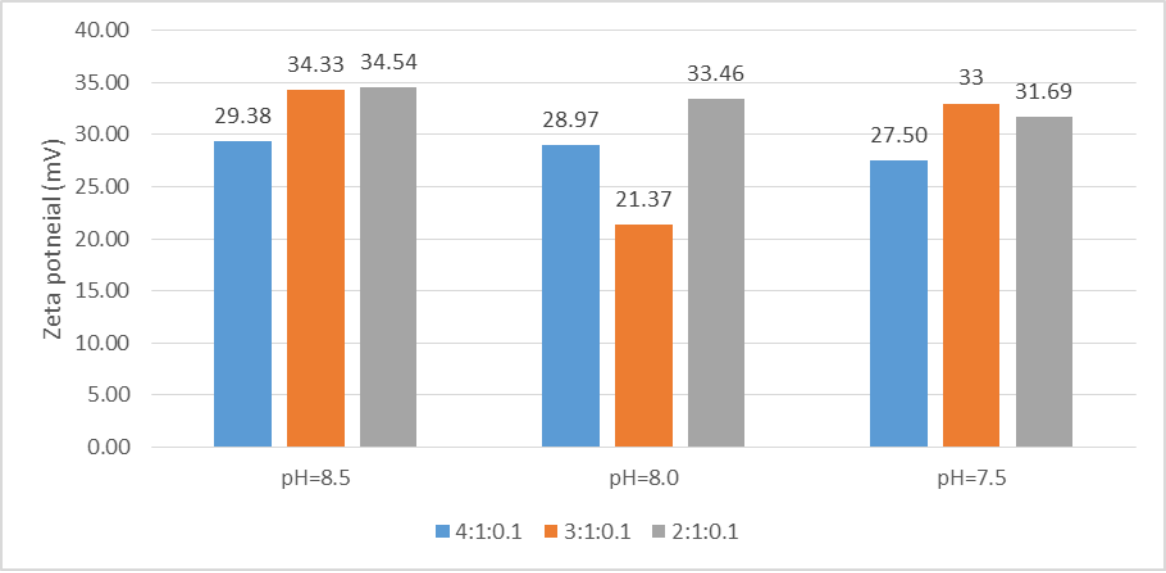

Figure 40: Comparison of each positive particle ratio at three PEI pH values after 24 hours of mixing

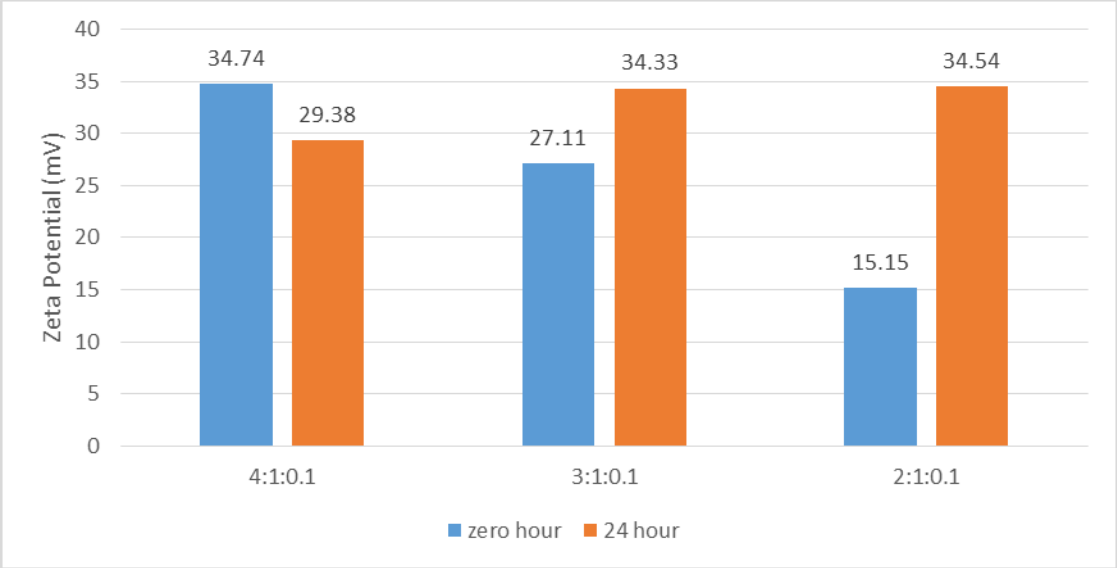

Figure 41: Comparison of positive particle ratios change in zeta potential over 24 hours at PEI pH value of 8.5

Ratios 2:1:0.1 and 3:1:0.1 were then analyzed by comparing the change in mean particle size over 24 hours. In **Figure 42** it would appear that ratio 3:1:0.1 is the better system when comparing the change in particle size to that of ratio 2:1:0.1. However, the slight increase in particle size of the 2:1:0.1 ratio is not a cause for concern. Increases of 2 or 3 times the initial particle diameter would be a greater indication of particle instability. Also with cost in mind, using the lower ratio of 2:1:0.1 would result in 33% less PEI than a ratio of 3:1:0.1 which would result in great savings when the nanoparticle system is batched on a large scale such as for drilling fluids. Therefore, the 2:1:0.1 ratio with PEI pH of 8.5 was chosen as the best system for introduction to the drill-in fluid formulation. **Table 5** summarizes the mean size and zeta potential results taken for all the positively charged systems that were measured.

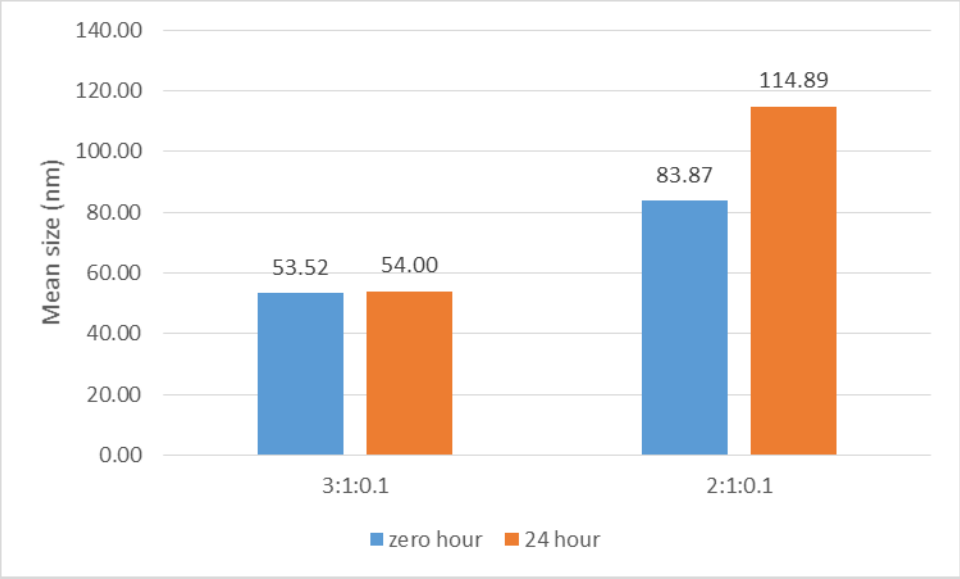

Figure 42: Comparison of changes in the mean size of positively charged particles over 24 hours for ratios 2:1:0.1 and 3:1:0.1 of PEI pH 8.5

Table 5: Summary of the zeta potential and mean particle diameter for all positive PEI:DS:Brine ratios at different pH of PEI

pH of PEI	pH after mixing	Ratio	Mean Zeta Potential (mV)	Mobility (μ/s)/(V/cm)	Mean diameter (nm)	Average Count Rate (kcps)	Polydispersity
8.5	8.57	4:1:0.1	29.38	1.49	61.43	446.93	0.30
8.5	8.65	3:1:0.1	34.33	1.61	54.00	449.87	0.29
8.5	**8.61**	**2:1:0.1**	**34.54**	**1.53**	**114.89**	**516.23**	**0.35**
8	8.13	4:1:0.1	28.97	1.63	67.39	478.77	0.29
8	8.16	3:1:0.1	21.37	1.15	65.86	450.53	0.30
8	8.24	2:1:0.1	33.46	1.47	69.35	436.83	0.34
7.5	7.67	4:1:0.1	27.50	1.44	68.65	447.83	0.31
7.5	7.71	3:1:0.1	33.00	1.85	68.68	423.57	0.30
7.5	8	2:1:0.1	31.69	1.33	78.30	488.77	0.35

5.2.2 Negatively Charged Particles

In the case of negatively charged particles, the only ratios that did not produce large amounts of precipitate had a PEI pH of 8.5 as depicted in **Table 4**. These five systems were taken for particle size and zeta potential measurements so the best system could be determined as done with the positively charged particles. It can be seen in **Figure 43** that the zeta potential for ratios of 1:7:0.1, 1:8:0.1 and 1:9:0.1 declines after a 24 hour period. This leaves a choice between ratios 1:6:0.1 and 1:10:0.1 by comparing the change in mean particle diameter over 24 hours. In **Figure 44** it can be seen that both ratios have an increase in particle size, however the 1:6:0.1 ratio size increase is much more significant. Therefore it was decided that the 1:10:0.1 ratio with PEI pH of 8.5 would be used for the negatively charged nanoparticle system introduced to the drill-in fluid formulation. **Table 6** summarizes the mean size and zeta potential results taken for all the negatively charged systems that were measured.

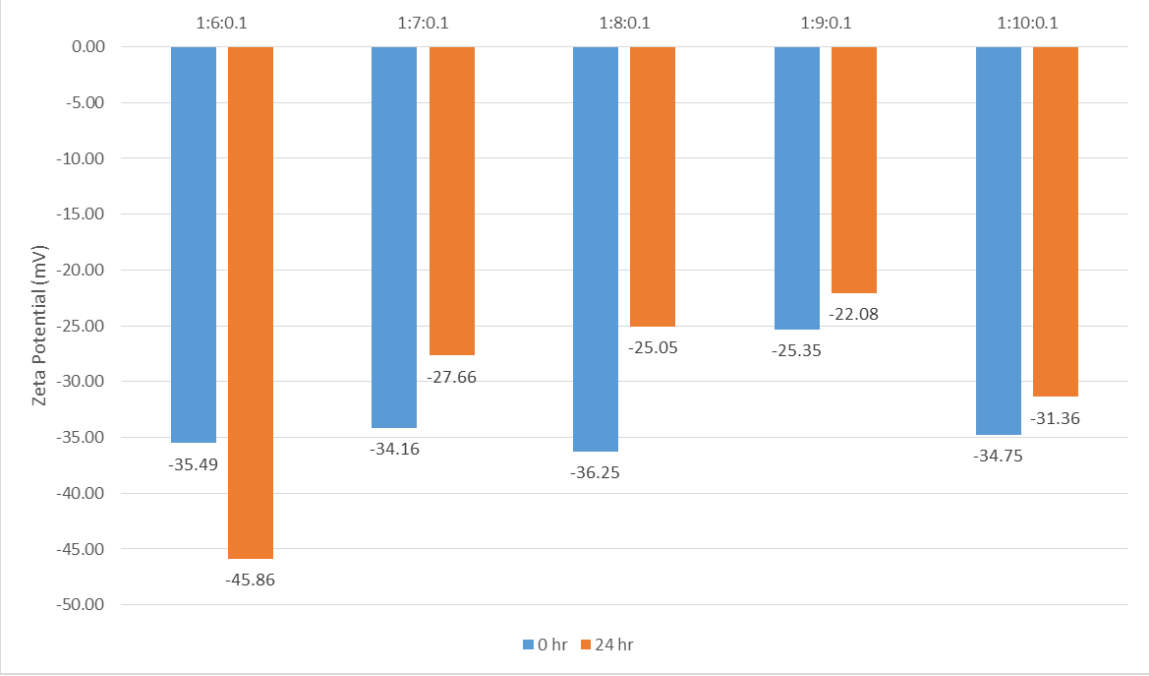

Figure 43: Comparison of zeta potential changes over 24 hours for negatively charged PEI:DS:Brine ratios

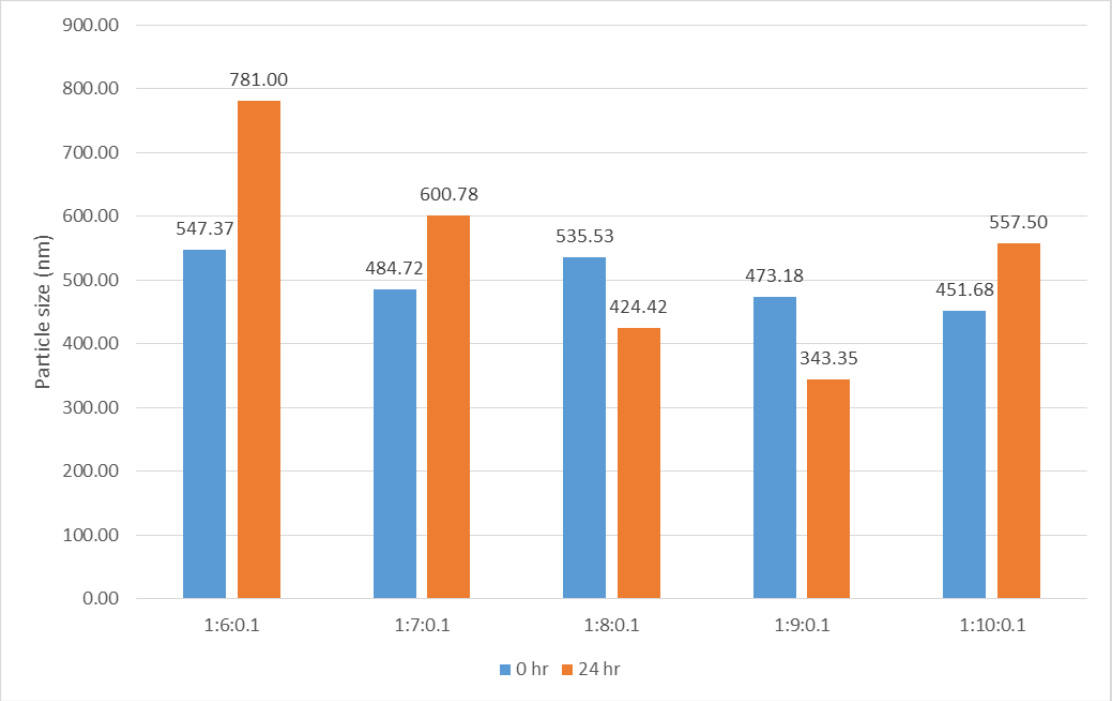

Figure 44: Comparison of mean particle size changes over 24 hours for negatively charged PEI:DS:Brine ratios

Table 6: Summary of the zeta potential and mean particle diameter for negative PEI:DS:Brine ratios at different pH of PEI

pH of PEI	pH after mixing	Ratio	Mean Zeta Potential (mV)	Mobility (μ/s)/(V/cm)	Mean diameter (nm)	Average Count Rate (kcps)	Polydispersity
8.5	9.37	6:1:0.1	-45.86	-2.45	781.00	512.83	0.17
8.5	9.37	7:1:0.1	-27.66	-1.48	600.78	482.97	0.34
8.5	9.55	8:1:0.1	-25.05	-1.34	424.42	427.90	0.37
8.5	9.55	9:1:0.1	-22.08	-1.18	343.35	506.23	0.31
8.5	9.56	10:1:0.1	-31.36	-1.68	557.50	451.83	0.37

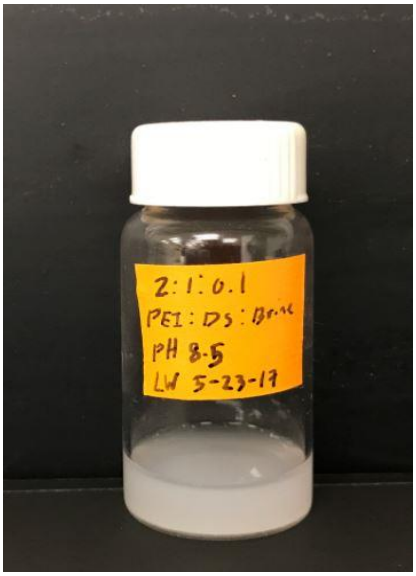

Figure 45: Positively charged PEI:DS:Brine nanoparticle systems for mixing ratios of 2:1:0.1 with PEI pH of 8.5

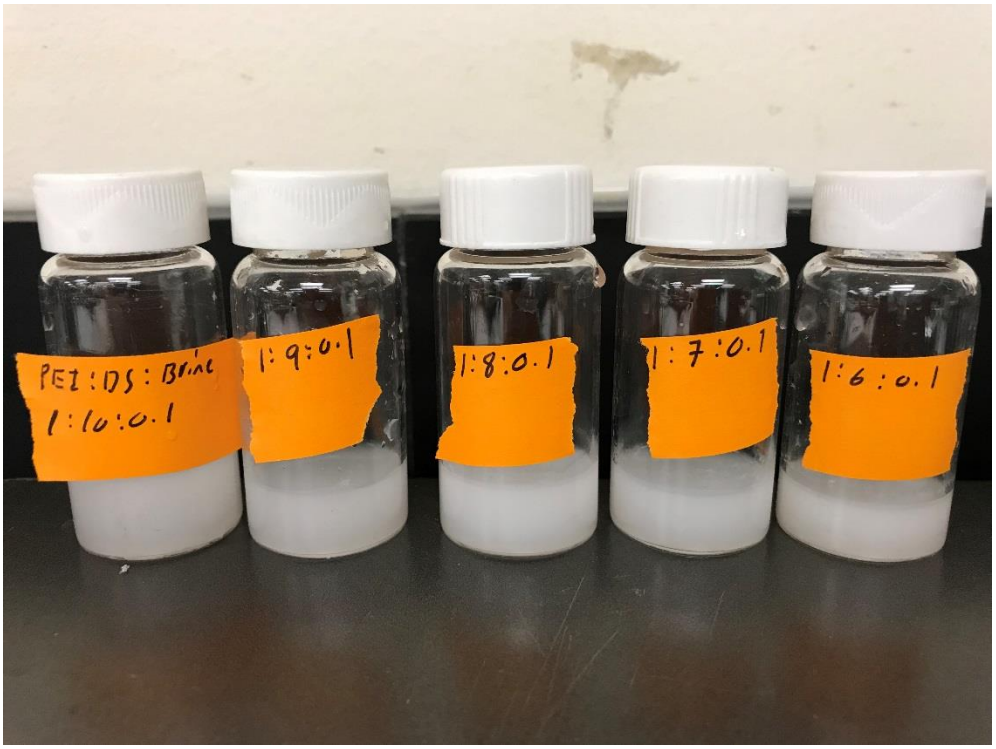

Figure 46: Negatively charged PEI:DS:Brine nanoparticle system for samples with varying mixing ratios and PEI pH of 8.5

5.3 Drill-in Fluid Rheology and Properties

It was important that the formulated drill-in fluid have the necessary rheological properties of those that are currently used in the field. Consultation with the literature provided some parameters to aim for even though the properties such as density and viscosity may vary greatly depending on the drilling scenario. Chiriac (20) provides an in depth discussion of many commercially produced drill-in fluid systems available from Schlumberger. The FlowPro NT system produced by Schlumberger is a water-based drill-in fluid with similar components to that of the fluid used in this research. Its properties are discussed by Chiriac (20) and are summarized in **Table 7.**

Table 7: Schlumberger's commercially available FloPro NT drill-in fluid system (20) (77)

Typical FloPro NT properties	
Fluid Property	Value
Fluid density (MW)	8.8 - 18.0 lb/gal
Plastic viscosity (PV)	12 - 20 cP
Yield point (YP)	20 - 35 lb/100 ft^2
Gel strength (10 s)	8 - 11 lb/100 ft^2
Gel strength (10 min)	10 - 15 lb/100 ft^2
pH	8.5-10.0
HTHP Fluid Loss	< 5.0 mL/30 min @ 150°F (66°C)

5.3.1 Density

Density of the drill-in fluid was calculated using **Equation 16** and **Equation 17.** The physical properties of the components and a sample calculation values appear in **Table 8.**

$$V_i = \frac{m_i}{\rho_i} \qquad \text{Equation 16}$$

$$\rho_f = \frac{\sum m_i}{\sum V_i} \qquad \text{Equation 17}$$

Where:

V_i = volume of a given mass, cm^3

m_i = additive mass, grams

ρ_i = additive density, g/cm^3

ρ_f = drill-in fluid density, g/cm^3

Table 8: Physical properties of the baseline drill-in fluid components and calculations for density

Drill-in Fluid Density Calculation				
Component	ρ_i	m_i	V_i	ρ_f
3% NaCl brine	1.016	100.00	98.43	value
Xanthan	1.5	0.30	0.20	
HPG	1	0.40	0.40	
CaCO3	2.71	10.00	3.69	
Sum		110.70	102.72	1.08

The calculated density comes out to be approximately 1.08 g/cm^3 which converts into 9.01 lb/gal. This value falls into the range of densities the FloPro NT system is capable of. The drill-in fluid pH was also measured and found to be 8.8 which was again comparable to FloPro NT.

5.3.2 Viscometer Results

The baseline drill-in fluid formulation as well as the formulation with nanoparticles were measured at 6 speeds available on the FANN rotational viscometer. Measurements were taken over the course of 24 hours to study the effects of aging as well. First the fluid was mixed and an initial measurement was taken followed by measurements at 4, 20 and 24 hours. In between measurements the fluids were stirred on a horizontal shaker at room temperature.

The initial readings and viscosity values for the baseline and nanoparticle fluids are found in **Table 9** and **Table 10**. When the data is plotted on a chart of shear stress versus shear rate, a curve is produced indicating the shear thinning fluid. By adding a power law trend line to the curve and displaying the equation and R^2 value on the chart, the *K* (consistency factor) and *n* (flow behavior index) are revealed in the equation. The R^2 value being ≥ 0.98 for both cases indicates that the Power Law model is a good fit for the curve. The initial baseline and PECNP drill-in fluid rheological profiles are shown in **Figure 47** and **Figure 48**.

Table 9: Baseline drill-in fluid initial viscosity measurement data with apparent viscosity calculated

Baseline Drill-in Fluid Initial Viscometer Readings				
RPM	Shear Rate (1/sec)	Shear Stress (dynes/cm^2)	Dial Reading	Apparent viscosity (cP)
600	1021	306.41	60	30
300	511	204.27	40	40
200	340	168.52	33	49.5
100	170	127.67	25	75
6	10.2	45.96	9	450
3	5.1	40.85	8	800

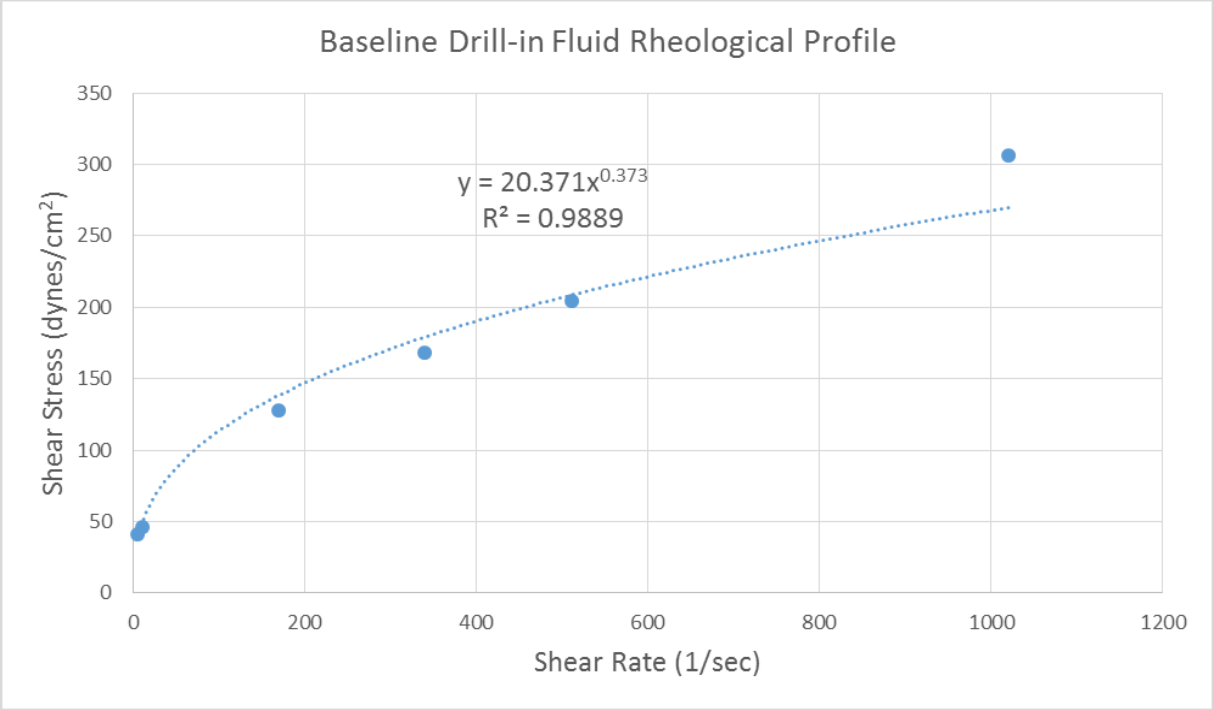

Figure 47: Baseline drill-in fluid initial rheological profile displaying shear thinning characteristics. K=20.371 , n=0.373

Table 10: PECNP drill-in fluid initial viscometer readings with apparent viscosity calculated

PECNP Drill-in Fluid Initial Viscometer Readings				
RPM	Shear Rate (1/sec)	Shear Stress (dynes/cm^2)	Dial Reading	Apparent viscosity (cP)
600	1021	316.62	62	31
300	511	204.27	40	40
200	340	173.63	34	51
100	170	132.78	26	78
6	10.2	51.07	10	500
3	5.1	40.85	8	800

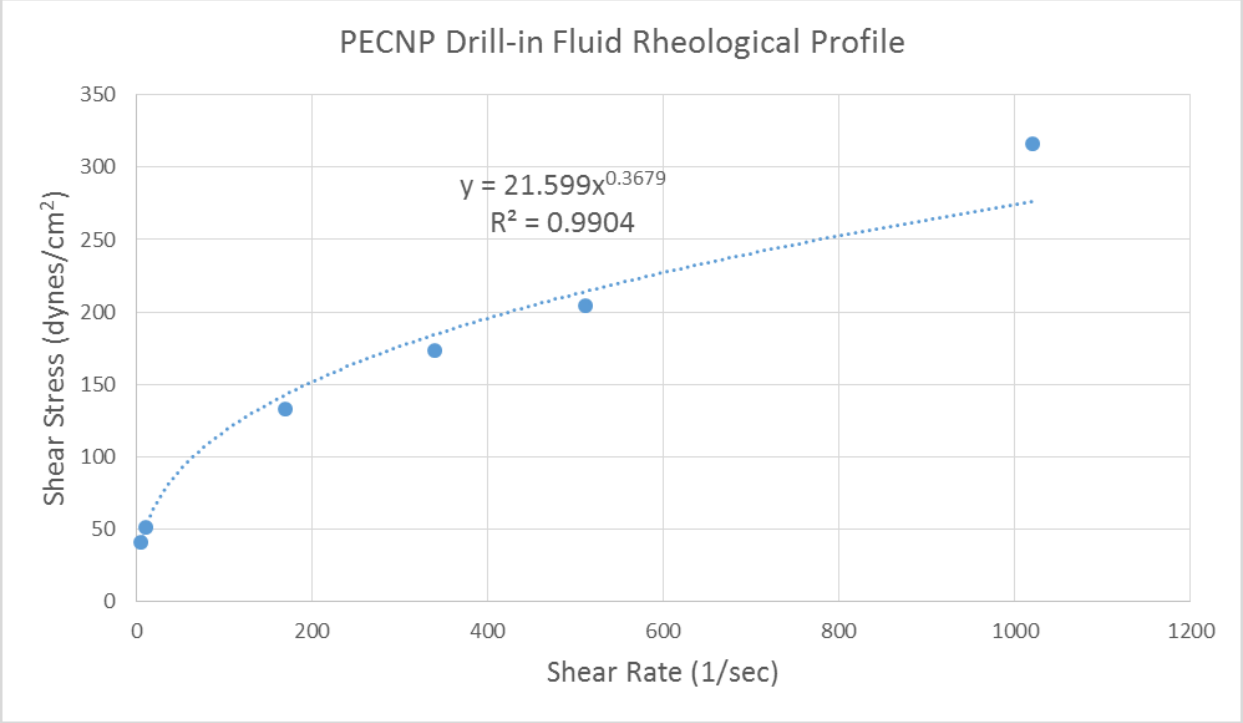

Figure 48: PECNP drill-in fluid initial rheological profile displaying shear thinning characteristics. K=21.599 , n=0.3679

The apparent viscosity, plastic viscosity, yield point, 10 second gel strength and 10 minute gel strength were also calculated from the viscometer data. The values are tabulated in **Table 11** for the baseline and PECNP fluids over 24 hours and are comparable to the FloPro NT system. Analyzing the gel strengths, the lack of a large increase from the 10 second reading to the 10

minute reading is a good sign. This is an indicator that the fluid won't gel to a significant point if the drilling has stopped for any reason. Too much gel strength can require substantial torque from the drill pipe to overcome the fluid and can even result in stuck pipe.

Figure 49 and **Figure 50** show the rheological profiles of both fluids over 24 hours. There appears to be no significant changes in the fluids behavior over a 24 hour time period indicating a stable formulation with no negative effects from addition of the nanoparticles.

Table 11: Drill-in fluid properties for baseline and PECNP fluid over a 24 hour period

	Initial		4 Hours		20 Hours		24 Hours	
	Baseline	PECNP	Baseline	PECNP	Baseline	PECNP	Baseline	PECNP
Apparent viscosity (cP)	30	31	25.5	27	24.5	27	24.5	25
Plastic viscosity (cP)	20	22	13	13	13	13	12	11
Yield point (lbf/100 ft^2)	20	18	25	28	23	28	25	28
10 sec. gel strength	9	10	9	9	8	9	8	8
10 min gel strength	14	11	10	10	10	10	10	10

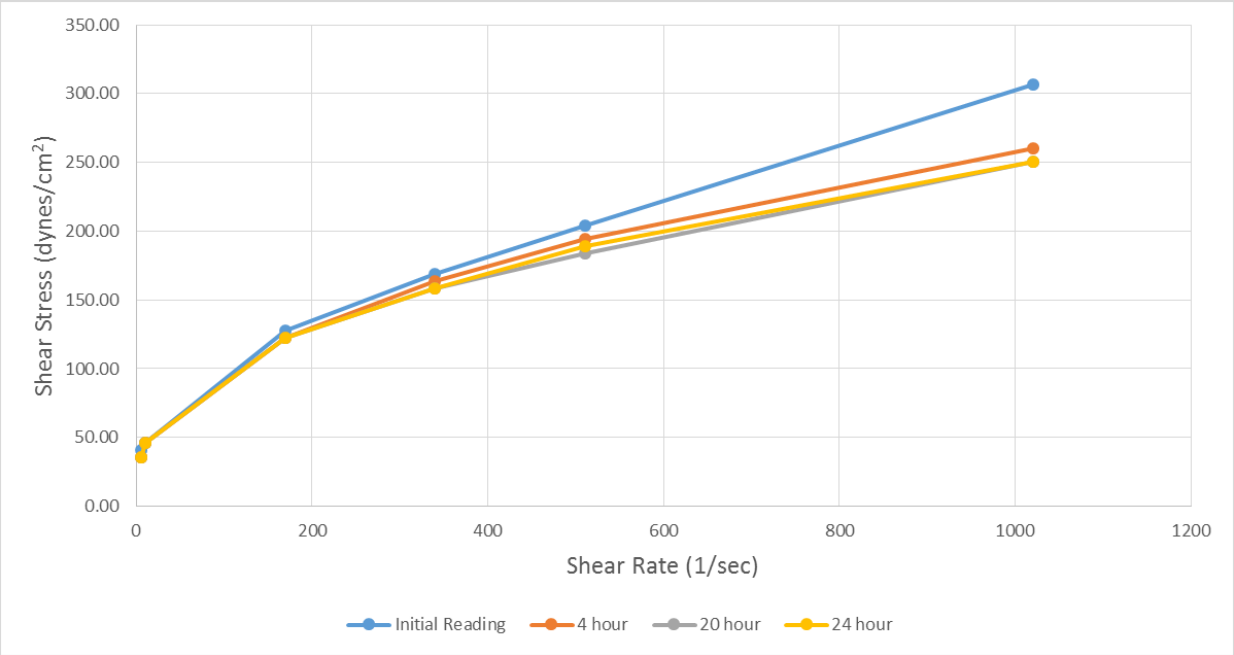

Figure 49: Baseline drill-in fluid rheology profiles over a 24 hour period

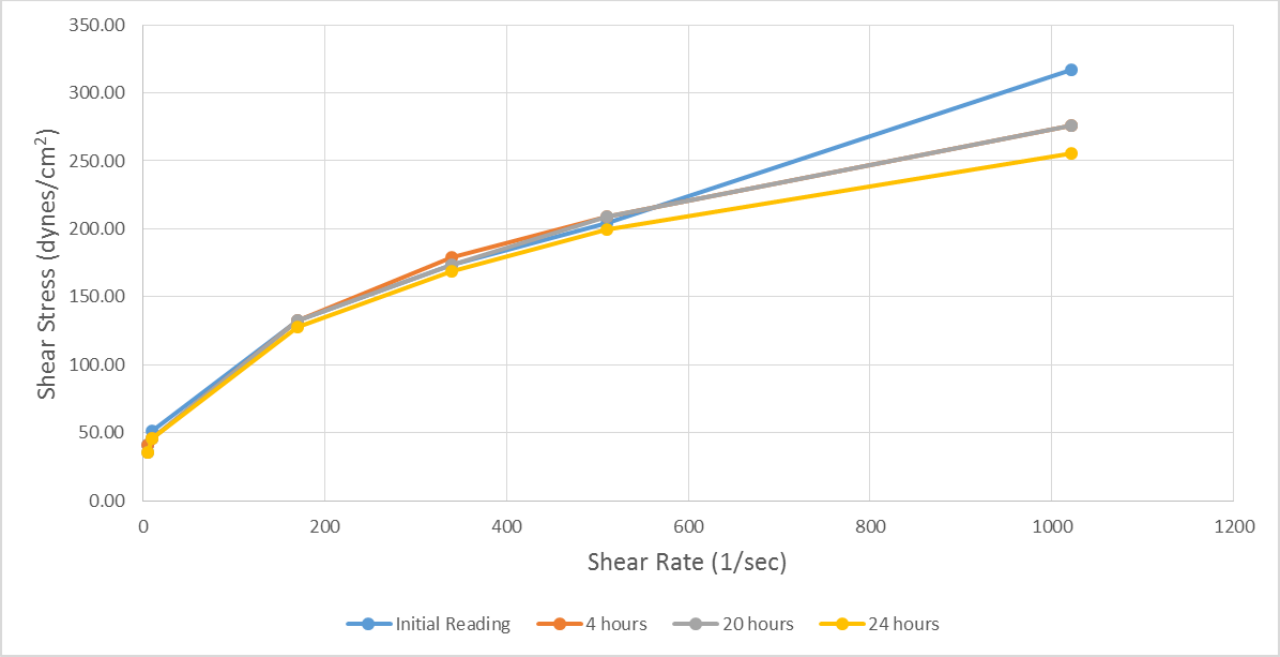

Figure 50: PECNP drill-in fluid rheology profiles over a 24 hour period

5.4 PECNP Effects on Static Fluid Loss Testing

Static fluid loss tests were performed using a baseline drill-in fluid followed by testing with the addition of nanoparticles of different dilutions. Indiana limestone (IL) and Kentucky sandstone (KC) cores were used for these tests. Initial permeabilities were measured for the core plugs and their properties will be shown in subsequent tables organized by whether positive or negatively charged PECNPs were used. Fluid loss volumes were compared alongside cleanup curves to determine which system performed the best by reducing fluid loss while causing the least amount of permeability damage. Deviation from initial permeability will determine to what degree the cores were damaged. Photos of the cores and filter cakes after a test can be found in the Appendix.

5.4.1 Static Fluid Loss Testing of Positively Charged PECNP System

Two Indiana limestone cores were used for testing the fluid loss capabilities of positively charged PECNPs. IL-9 was used for the baseline test and IL-5 was used for nanoparticle tests. IL-5 was flooded with several pore volumes after each fluid loss test to ensure the permeability returned to its initial state so that each fluid loss test would be comparable. Permeability measurements and comparisons were established using a constant flowrate of 0.25 mL/min. The initial core properties are tabulated in **Table 12**.

Table 12: Core properties for core plugs used in static fluid loss testing of positively charged PECNPs

Positive PECNP Static Fluid Loss Initial Core Properties				
Core	Length (cm)	Diameter (cm)	Porosity (%)	Permeability (mD)
IL-9	2.355	2.516	14.13	2.42
IL-5	2.228	2.515	10.73	1.88

IL-9 was tested with the baseline fluid first to serve as a comparison for subsequent PENCP testing on IL-5. The fluid loss data from each test were compiled into **Figure 51** to evaluate total fluid loss volumes over square root of time. Since fluid loss volumes for these tests were relatively low, a filter cake coefficient and spurt volume could not be calculated. After each test, the filter cake weight was calculated then the core was flooded at 0.25 mL/min while a cleanup curve was recorded. Cleanup curves were compiled into **Figure 52** to analyze the cleanup efficiency after testing of a system. **Table 13** contains key data used in determining the best nanoparticle system for further testing using the DFL equipment.

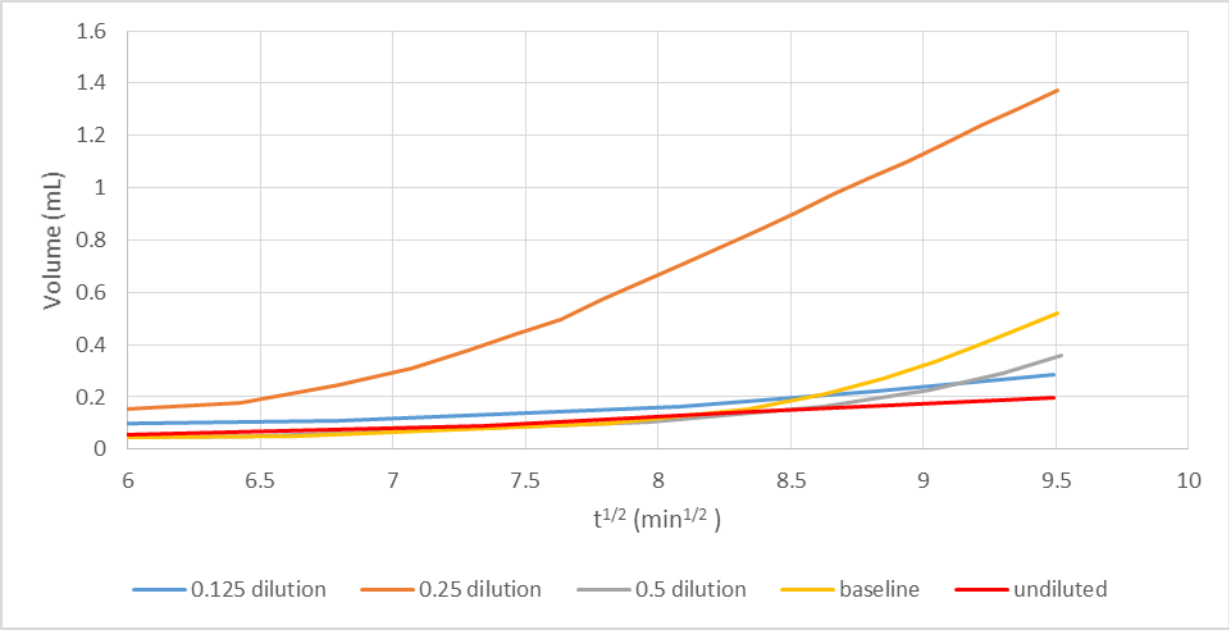

Figure 51: Fluid loss curves for baseline drill-in fluid and drill-in fluids containing positively charged PECNP dilutions

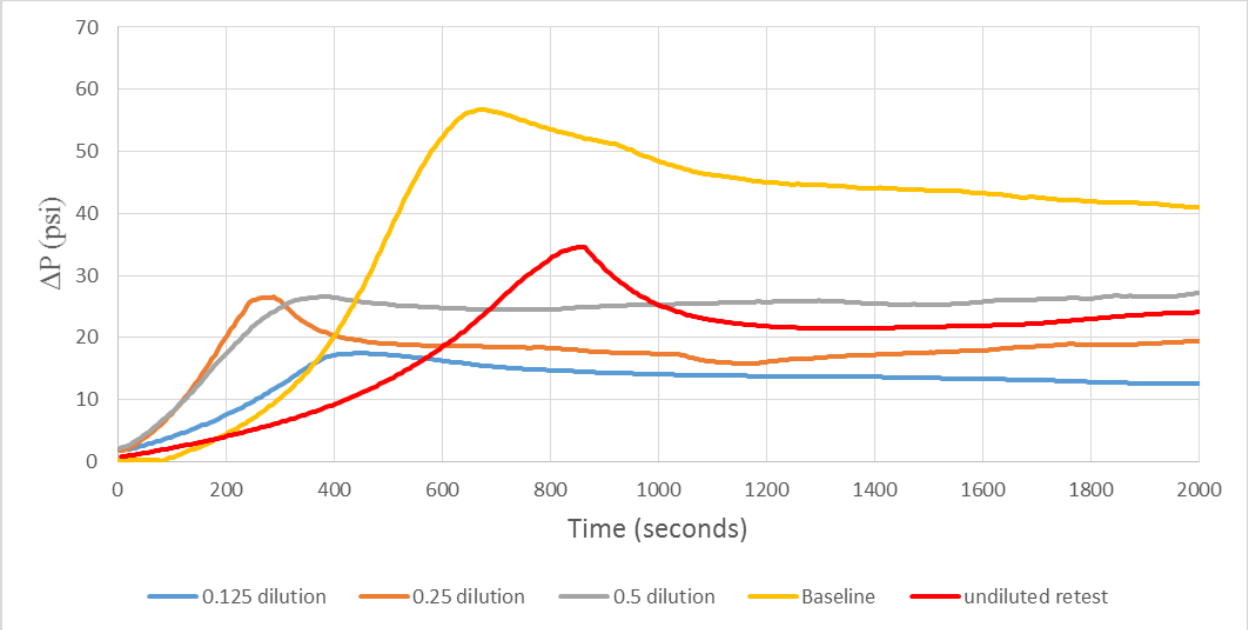

Figure 52: Cleanup curves after static fluid loss tests with baseline fluid and fluid with positively charged PECNPs added.

Table 13: Data collected after static fluid loss testing of baseline and positively charged PECNP drill-in fluids on Indiana limestone

Core	Test Fluid	Permeability before test (mD)	Permeability after test (mD)	Permeability retention %	Filter cake weight (g)	Total fluid loss volume (mL)	Peak pressure during cleanup (psi)
IL-5	80 mL Drill-in fluid + 25mL 0.5× diluted PECNPs	1.88	1.79	95.12	0.87	0.358	26.54
IL-5	80 mL Drill-in fluid + 25mL 0.25× diluted PECNPs	1.79	2.44	136.67	1.07	1.373	26.51
IL-5	80 mL Drill-in fluid + 25mL 0.125× diluted PECNPs	2.44	3.66	150.00	0.80	0.286	17.43
IL-5	80 mL Drill-in fluid + 25mL undiluted PECNPs	3.66	1.65	45.11	0.70	0.197	34.59
IL-9	80 mL Drill-in fluid + 25mL brine	2.42	1.33	54.86	0.91	0.52	56.73

Looking at the total fluid loss volumes alone, it appears that the undiluted PECNP system performed the best with the least amount of fluid loss. However, analysis of the cleanup curves reveals that the undiluted system severely damaged the core with only 45% permeability retention after cleanup. The 0.125 diluted system had the second least amount of fluid loss only slightly above that of the undiluted system. It also proved to be the least damaging system by having the lowest peak pressure required to begin cleanup of the core as seen in **Figure 52** and was able to return to its initial permeability.

When comparing the baseline test to the use of nanoparticles, it is clear that when the right dilution of PECNPs is used, better results are achieved. The baseline test had the second highest fluid loss volume and required the highest peak pressure to begin cleanup of the core. When investigating the effluent captured after passing through the baseline core, noticeable amounts of polymer and $CaCO_3$ were visible to the naked eye as pictured in **Figure 53**. This indicates filtration of these components into the pore space of the rock resulting in permeability damage during cleanup.

Filter cake thickness can sometimes be correlated to fluid loss volume by a general rule stating that the thicker the filter cake, the more fluid loss volume there will be. The logic behind this rule

stems from cake permeability. If the permeability of the cake is not decreased, the thickness will continue to build as fluid and particles filter through the cake. Assuming the thickness directly relates to weight, this correlation is found to be true as seen in **Figure 54.**

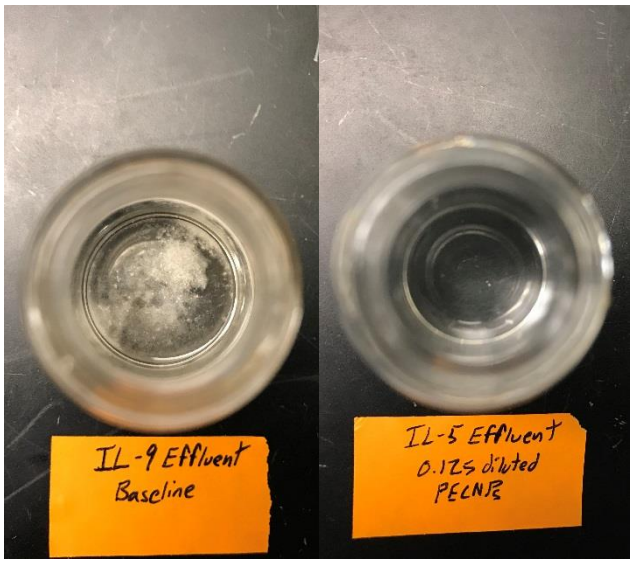

Figure 53: IL-9 baseline effluent with polymer compared with clean effluent from IL-5 0.125 diluted PECNP system

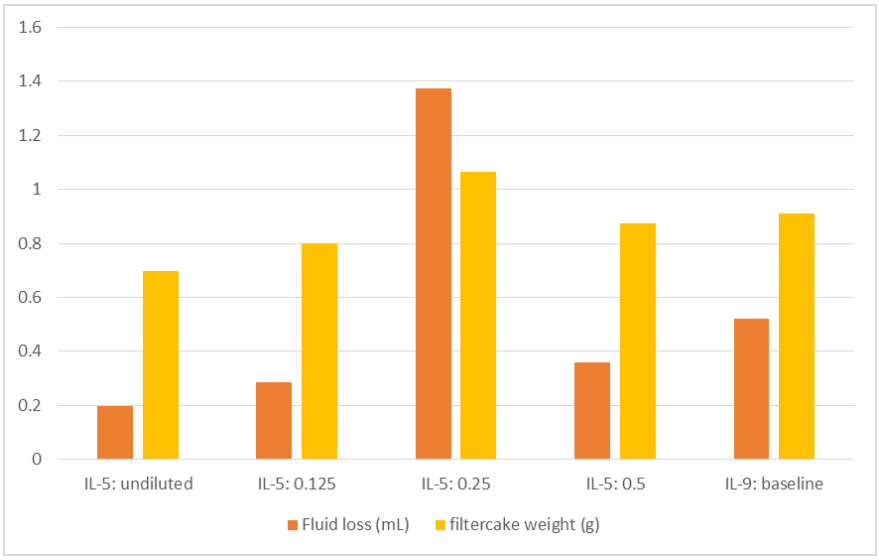

Figure 54: Correlation between filter cake weight and fluid loss volume after positive PECNP static fluid loss tests

5.4.2 Static Fluid Loss Testing on Negatively Charged PECNP System

Testing of negatively charged PECNP was done for both Indiana limestone and Kentucky sandstone cores. A different Indiana limestone core was used for each test as it was anticipated the cores would not be able to reach initial permeability values considering the potential for adsorption of the negative particles to the rock pores since limestone has a positive surface charge. Permeability measurements and comparisons were established using a constant flowrate of 0.25 mL/min for limestone and 0.1 mL/min for sandstone since it was a tighter core. The initial core properties can be found in **Table 14.**

Table 14: Core properties for core plugs used in static fluid loss testing with negatively charged

Negative PECNP Static Fluid Loss Initial Core Properties				
Core	Length (cm)	Diameter (cm)	Porosity (%)	Permeability (mD)
IL-10	2.384	2.518	10.2	6.43
IL-15	2.505	2.513	12.5	8.25
IL-17	2.516	2.513	13	9.56
IL-8	2.219	2.52	11.4	8.38
IL-16	2.423	2.52	10.7	8.65
KC-8	2.431	2.494	7.9	0.17
KC-23	2.512	2.49	8.78	0.17

5.4.2.1 Negative PECNP with Indiana Limestone

The IL-10 core was to serve as a baseline and was tested first. Tests with the addition of PECNPs of different dilutions were carried out on separate cores in the following order: undiluted, 0.125 dilution and 0.25 dilution. A secondary test was carried out on the 0.125 dilution as there was some concern about the first result in terms of the fluid loss volume. The fluid loss volumes versus square root of time were plotted in **Figure 55.** Core IL-8 with 0.25 diluted PECNP showed the best fluid loss results but once again, analysis of the cleanup curves and permeability damage is necessary to determine the full extent of a systems performance.

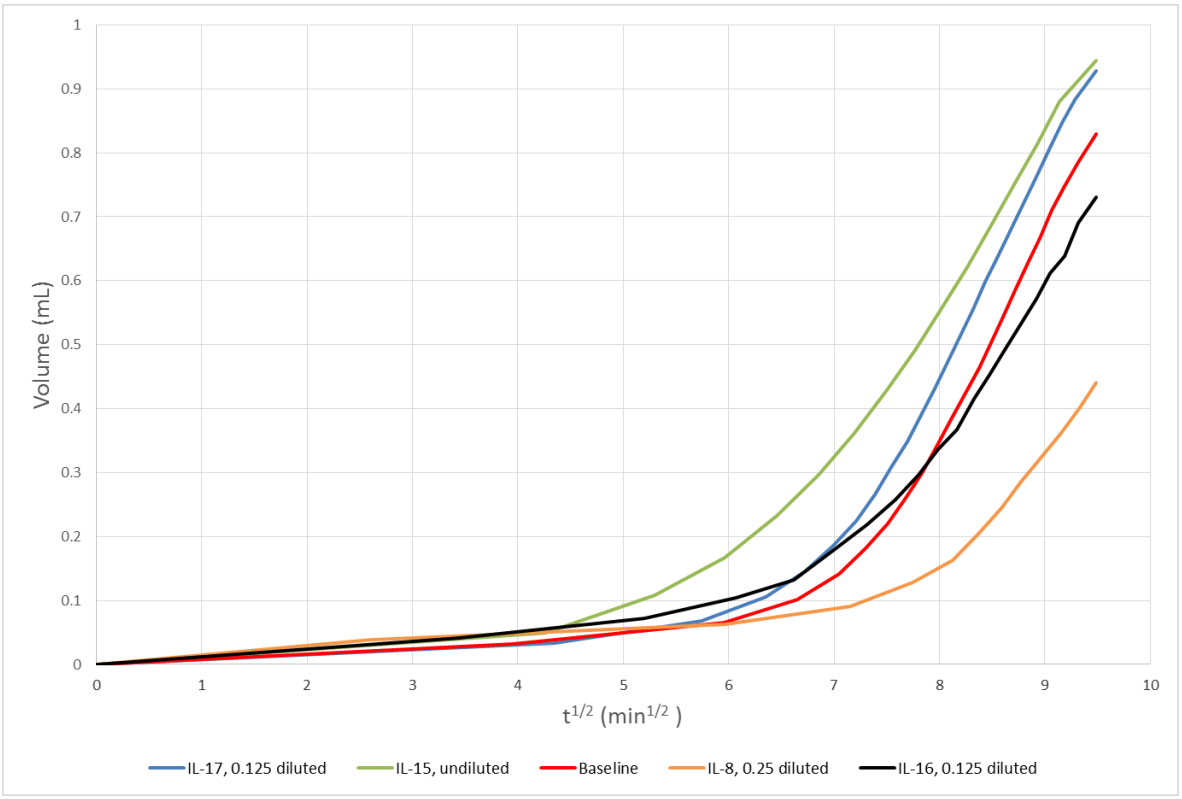

Figure 55: Fluid loss curves for baseline drill-in fluid and drill-in fluids containing negatively charged PECNP dilutions for Indiana limestone cores

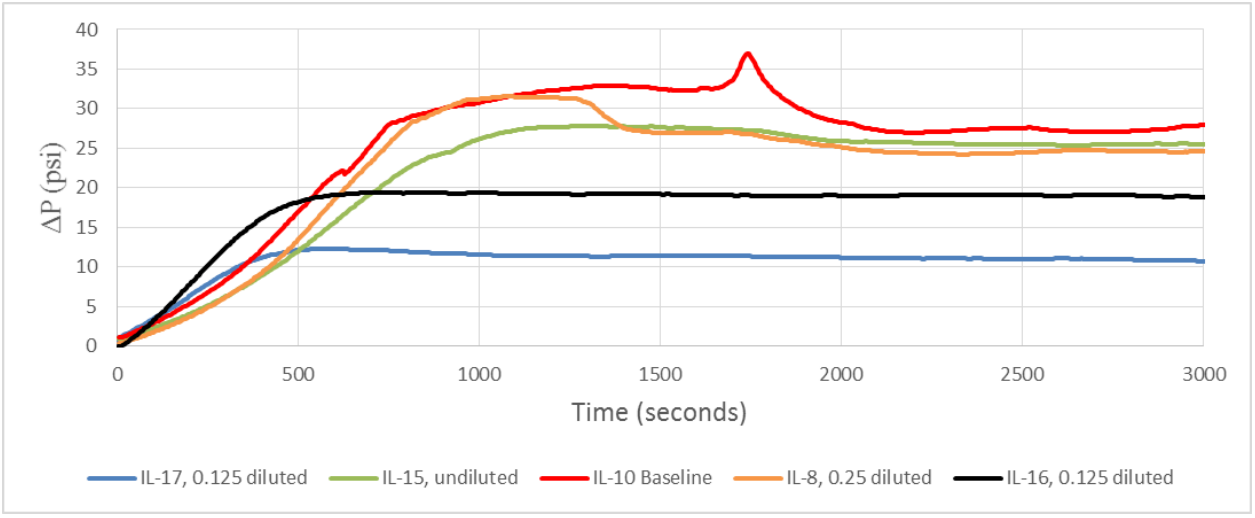

Figure 56: Cleanup curves of Indiana limestone after static fluid loss tests with baseline fluid and fluid with negative PECNPs added

Comparing the cleanup curves with the fluid loss data, cleanup of the 0.25 dilution did not go as well as the 0.125 dilutions. The peak pressures required to clean up the cores tested with 0.125 dilution were much lower than that of the 0.25 dilution. This also translates to less retention of the initial permeability value. Therefore, after a retest was performed on the 0.125 dilution, it was deemed the best system considering it had the second least amount of fluid loss and best cleanup capability. Overall, the negative PECNPs did help with fluid loss prevention but they did not perform as well as the positively charged PECNPs considering the resulting permeability damage. This was expected considering the potential for adsorption of the particles onto the rock surface. Extent of the damage and peak pressures during cleanup as well as total fluid loss volumes can be seen in **Table 15.** The same correlation of filter cake weight to fluid loss volume can also be applied to the case of negatively charged PECNPs as shown in **Figure 57**.

Table 15: Data collected after static fluid loss testing of baseline and negatively charged PECNP drill-in fluid on Indiana limestone cores

Core	Test Fluid	Permeability before test (mD)	Permeability after test (mD)	Permeability retention %	Filter cake weight (g)	Total fluid loss volume (mL)	Peak pressure during cleanup (psi)
IL-10	80 mL Drill-in fluid + 25 mL brine	6.43	1.91	29.80	0.724	0.83	36.97
IL-15	80 mL Drill-in fluid + 25 mL undiluted negative PECNP	8.25	1.94	23.53	1.065	0.945	27.77
IL-17	80 mL Drill-in fluid + 25 mL 0.125× negative PECNP	9.56	5.10	53.33	0.758	0.928	12.28
IL-8	80 mL Drill-in fluid + 25 mL 0.25× negative PECNP	8.38	1.82	21.67	0.7032	0.441	31.58
IL-16	80 mL Drill-in fluid + 25 mL 0.125× negative PECNP	8.65	2.25	25.96	0.863	0.73	19.41

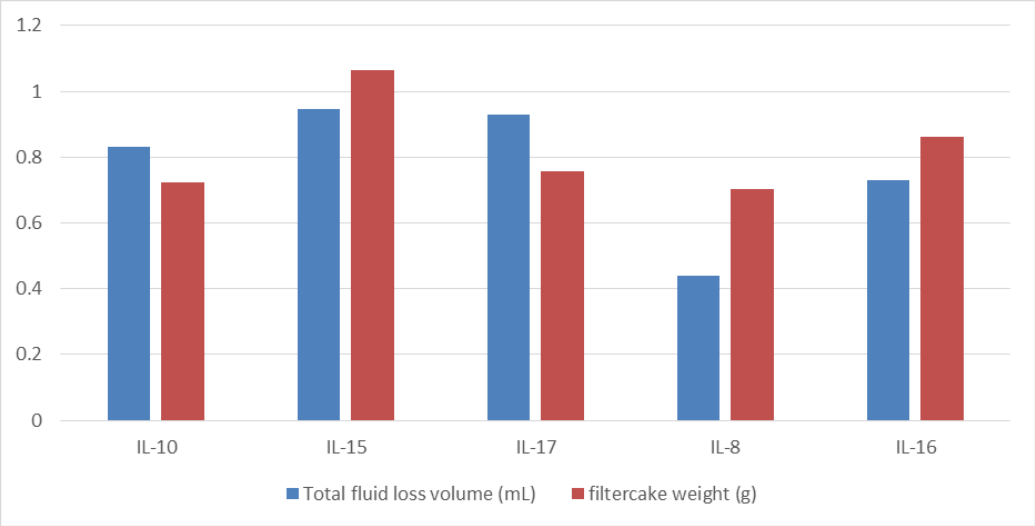

Figure 57: Correlation between filter cake weight and fluid loss volume after static fluid loss testing of negatively charged PECNP.

5.4.2.2 Negatively Charged PECNP with Kentucky Sandstone

After the damage to limestone cores by negatively charged PECNPs proved to be extensive, their use on sandstone cores was investigated considering the similar charge of the particles and the rock surface. A baseline and undiluted static test were performed on the two Kentucky cores described in **Table 14**, however no fluid loss was recorded during either test. It was surmised that the performance of the fluid and tightness of the core would not allow any further successful tests to be run.

5.5 PECNP Effects on Dynamic Fluid Loss Testing

Dynamic fluid loss tests were performed using the Quasimodo equipment described in section 4.9.1. Tests using a baseline drill-in fluid and a drill-in fluid with 0.125 diluted positive PEC nanoparticles were ran on Indiana limestone cores and a Kentucky sandstone core. The Indiana limestone cores were cleaned with bleach and flooded with several pore volumes of brine until their permeability returned to stable values comparable to their initial permeability. The Kentucky

sandstone core was freshly cut and had not been used. Three baseline fluid tests were performed followed by three PECNP fluid tests all carried out on different cores. Only one baseline and PECNP test was performed with Kentucky sandstone. Key properties of the cores used in dynamic testing can be found in **Table 16**. Photos of the cores and their filter cakes can be found in the Appendix.

Table 16: Properties of core plugs used in 90 minute dynamic fluid loss testing

Dynamic Fluid Loss Initial Core Properties				
Core	Length (cm)	Diameter (cm)	Porosity (%)	Permeability (mD)
IL-17	2.516	2.513	13	9.94
IL-9	2.355	2.516	14.13	2.58
IL-5	2.228	2.515	10.73	4.88
IL-8	2.219	2.52	11.4	6.51
IL-16	2.423	2.52	10.7	6.35
IL-6	2.587	2.482	10.2	2.91
KC-22	2.515	2.494	8.5	0.13

5.5.1 Dynamic Testing on Indiana Limestone Cores

For the purpose of reproducibility, a total of six tests were performed using Indiana limestone cores. Lengths and permeability varied slightly from core to core, so they were grouped in such a way that the baseline and PECNPs tests would cover all ranges for both test types. After a test was ran, the DFL software would create a data file containing everything recorded during the run. The file could be opened in using either the DFL software or Excel to analyze the fluid loss curves and calculate the spurt volume and wall building coefficients. Both methods were utilized to compare user calculated values to those calculated by the DFL software. Before analysis of the data, cores were removed from the fluid loss cell and taken to be weighed. The filter cake was scraped and the core was weighed again for calculation of the filter cake weight. Cores were then flooded with brine in opposite direction of the fluid loss test flow to determine any permeability damage caused during the DFL test.

The dynamic fluid loss curves of fluid loss versus square root of time can be seen in **Figure 58** and **Figure 59**. When comparing the two, an obvious variance between them is noticed in both curve height and total fluid loss volume. In the baseline cases, the initial jump in volume otherwise known as spurt is noticeably different between all three tests while the slope of the linear trend appears to be consistent. The tests using PECNPs however are very consistent in their spurt loss volumes and linear slopes as well. Slopes of the linear trend in the curves directly relate to wall building coefficients and ultimately the total fluid loss volume. **Figure 61** is a comparison of all six fluid loss curves plotted on one chart. **Figure 60** is a comparison of the averaged three curves of each test type. Comparing the curves it is clear that the baseline fluid resulted in a higher sloping trend line than the PECNP fluid thus a higher wall building coefficient. A higher wall building coefficient will result in higher fluid loss volume over time, therefore a lower wall building coefficient is desired. Even when fluid loss begins with a low spurt volume as seen with baseline test of IL-17, its total fluid loss exceeds those of the tests using PECNP fluids due to its higher wall building coefficient. **Table 17** outlines key data from DFL testing of limestone cores useful for further analysis and discussion continued below.

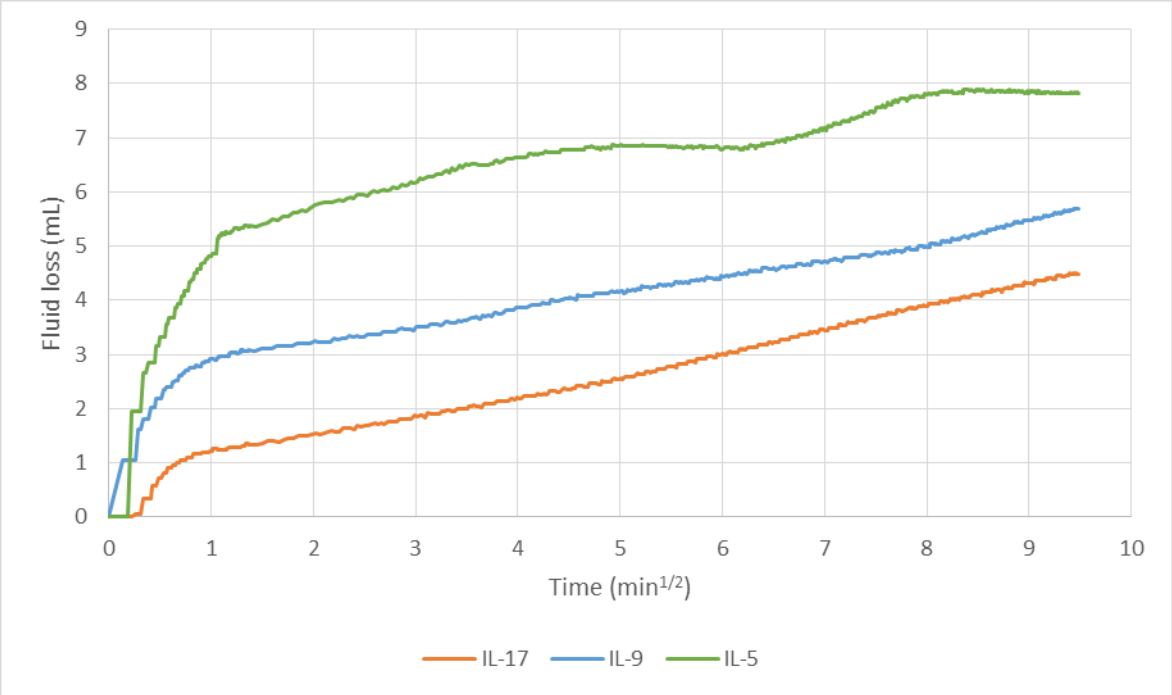

Figure 58: Dynamic fluid loss curves of three Indiana limestone cores tested using the baseline drill-in fluid

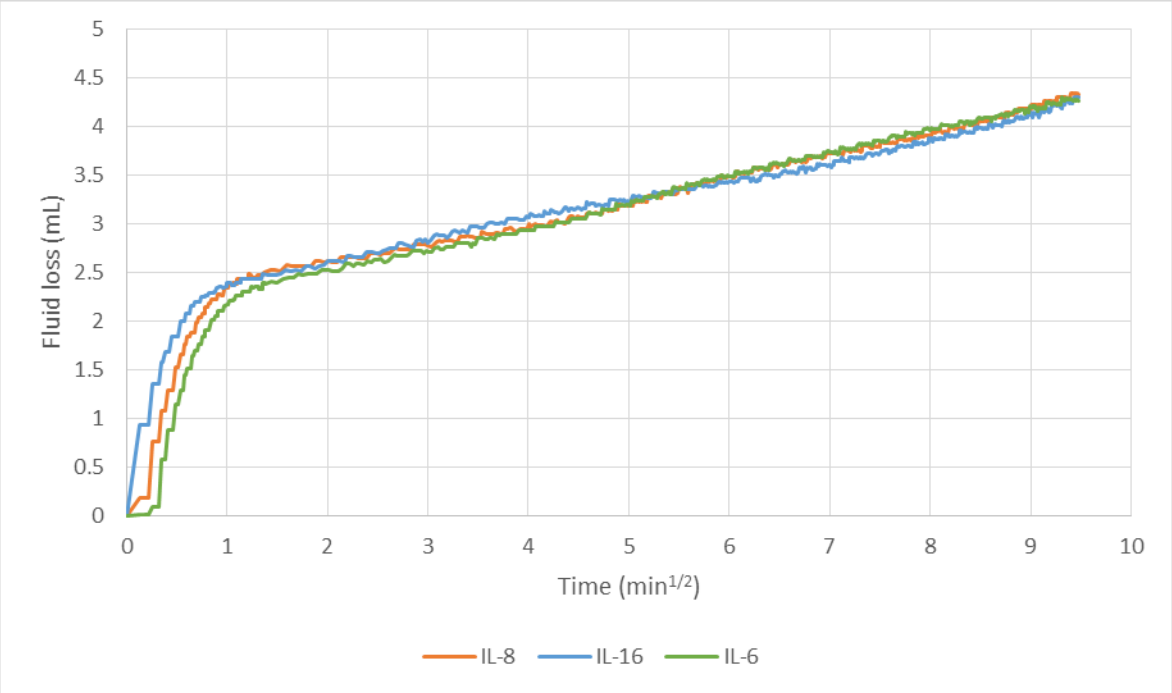

Figure 59: Dynamic fluid loss curves of three Indiana limestone cores tested using PECNP drill-in fluid

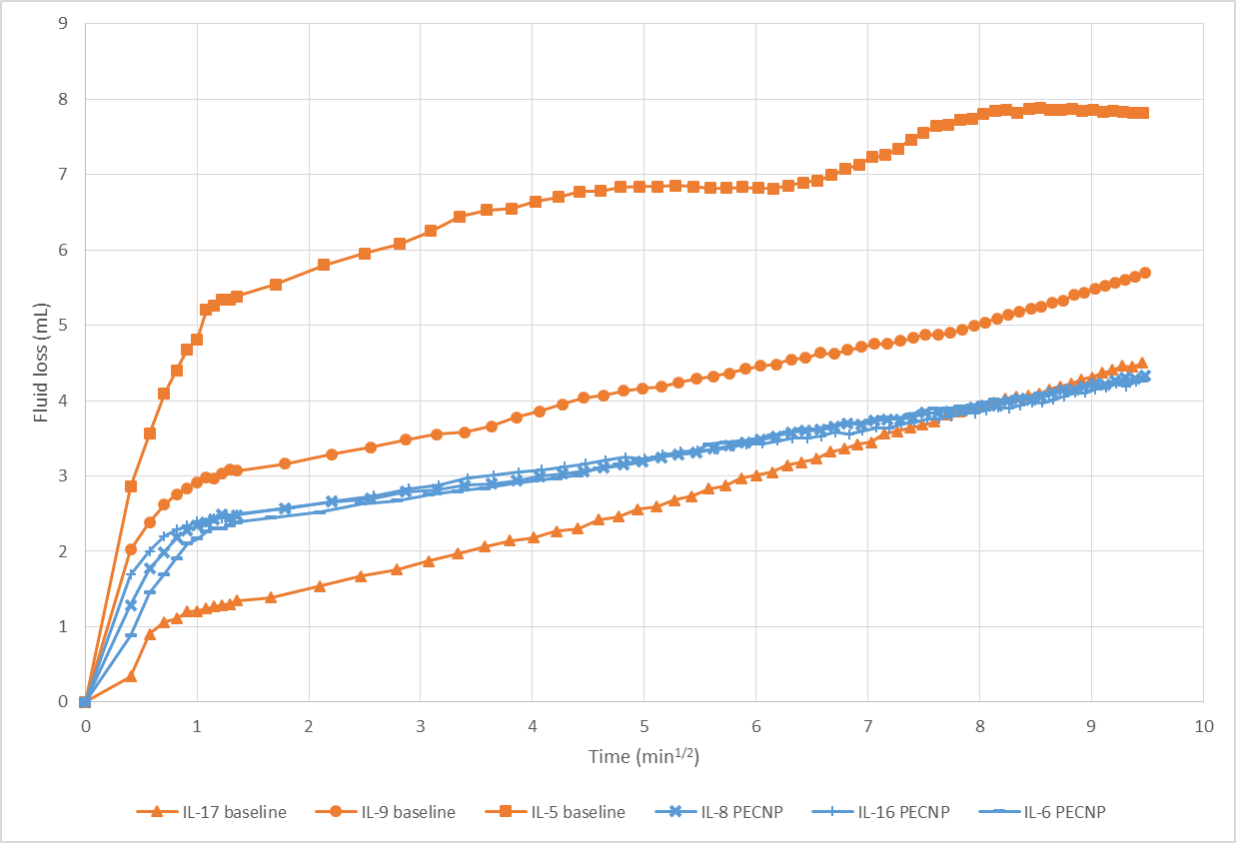

Figure 61: Dynamic fluid loss curve comparison of all 6 tests done on Indiana limestone cores using a baseline and PECNP drill-in fluid

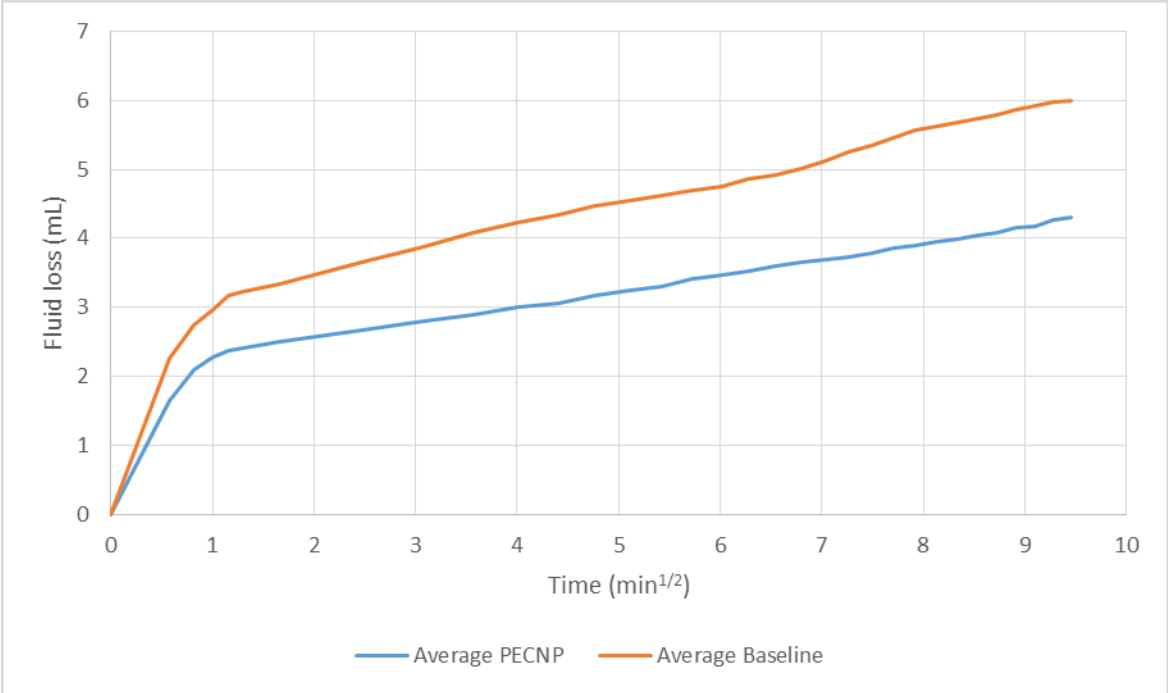

Figure 60: Average of all three baseline fluid loss curves compared with the average of all three PECNP fluid loss curves

Table 17: Dynamic fluid loss data for 90 minute tests ran using Indiana limestone cores

Core	Test Fluid	Spurt Loss (mL)	Core Length (cm)	Total Fluid Loss (mL)	C_w ft/min$^{1/2}$
IL-17	Baseline	0.71	2.516	4.5	0.00131
IL-9	Baseline	2.59	2.355	5.7	0.00103
IL-5	Baseline	5.08	2.228	7.9	0.00106
IL-6	PECNP	2.01	2.587	4.3	0.00082
IL-16	PECNP	2.17	2.423	4.31	0.00070
IL-8	PECNP	2.07	2.219	4.35	0.00077

Total fluid loss volumes are compared in **Figure 62**, **Figure 63** and **Figure 64** with an average fluid loss volume for the baseline and PECNP cases being presented in **Figure 65**. When evaluating the average fluid loss volumes in **Table 18**, the PECNP drill-in fluid clearly succeeded in lowering the filtrate volumes during DFL tests by approximately 28%.

Table 18: Total fluid loss volumes and wall building coefficients with averages and standard deviation for baseline and PECNP dynamic tests

Baseline Tests			PECNP Tests		
Core	Total Fluid Loss (mL)	C_w ft/min$^{1/2}$	Core	Total Fluid Loss (mL)	C_w ft/min$^{1/2}$
IL-17	4.5	0.00131	IL-6	4.3	0.00082
IL-9	5.7	0.00103	IL-16	4.31	0.00070
IL-5	7.9	0.00106	IL-8	4.35	0.00077
Average	6.03	0.00113	Average	4.32	0.00076
Standard deviation	1.72	0.00015	Standard deviation	0.03	0.000062

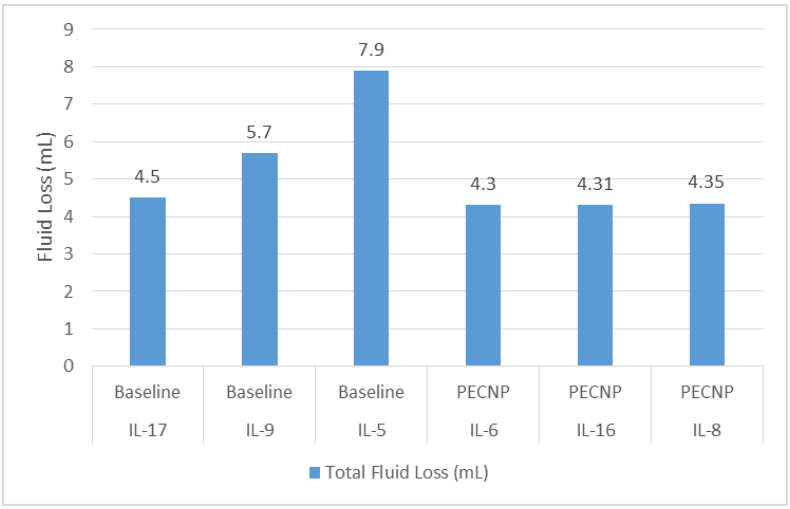

Figure 62: Total fluid loss volumes during dynamic testing of Indiana limestone cores with baseline and PECNP drill-in fluids

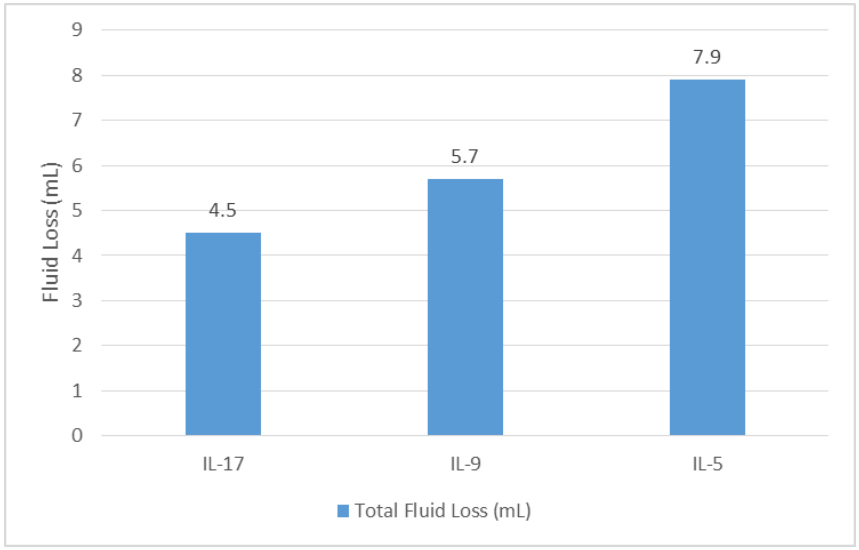

Figure 63: Total fluid loss volumes during dynamic testing of Indiana limestone cores with baseline drill-in fluid

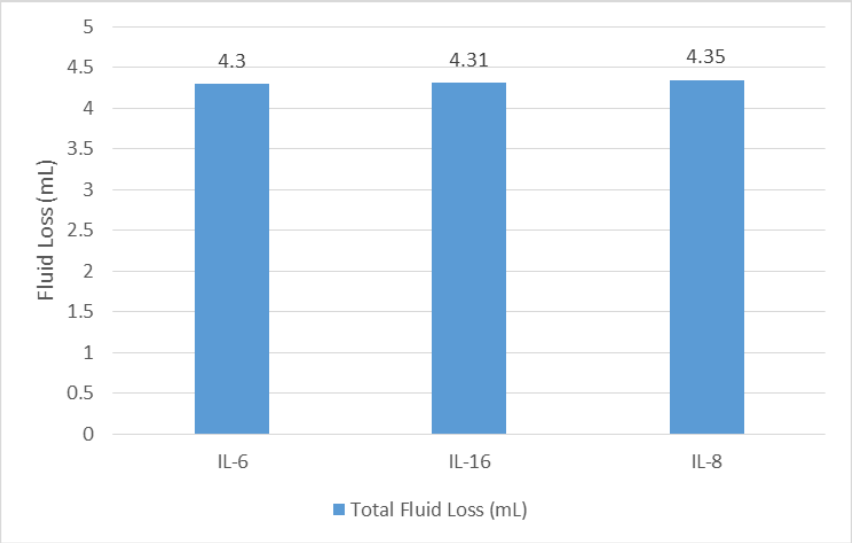

Figure 64: Total fluid loss volumes during dynamic testing of Indiana limestone cores with PECNP drill-in fluid

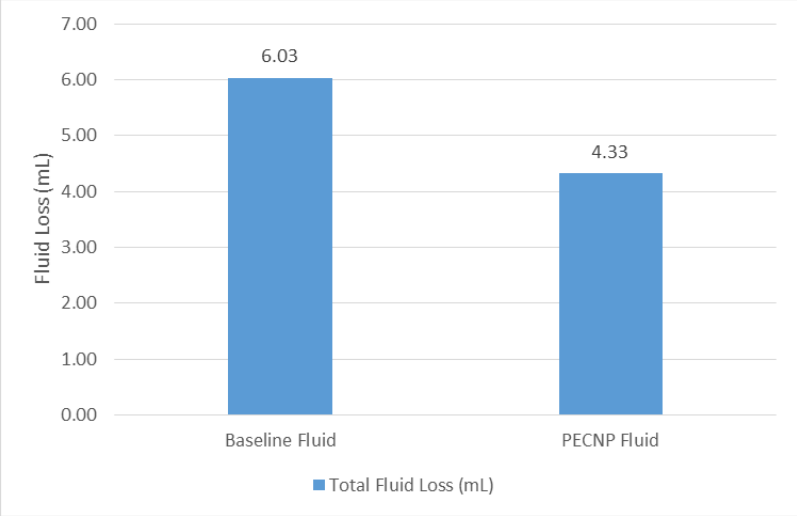

Figure 65: Average fluid loss volume for the baseline fluid case compared to the average fluid loss for the PECNP fluid after dynamic fluid loss testing

Fluid loss volumes were found to correlate with core length as seen in **Figure 66** and **Figure 67**. Longer core lengths resulted in lower fluid loss volumes, which was also observed in spurt volumes for the baseline tests. This is an indication of the filter cake quality formed by each fluid. Even when core length and permeability varied with each test, the PECNP drill-in fluid was able to quickly form a low permeability filter cake that produced consistent results of low filtrate volume.

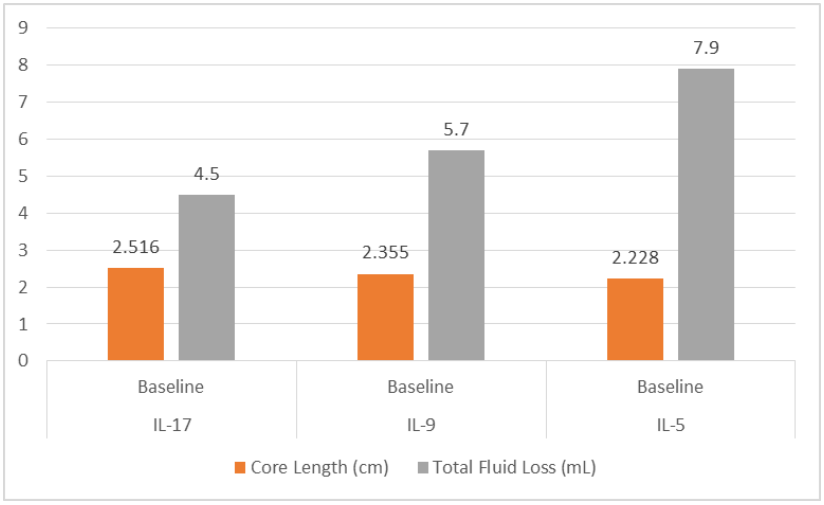

Figure 66: Correlation of fluid loss volume to core length after dynamic testing of the baseline drill-in fluid on Indiana limestone cores

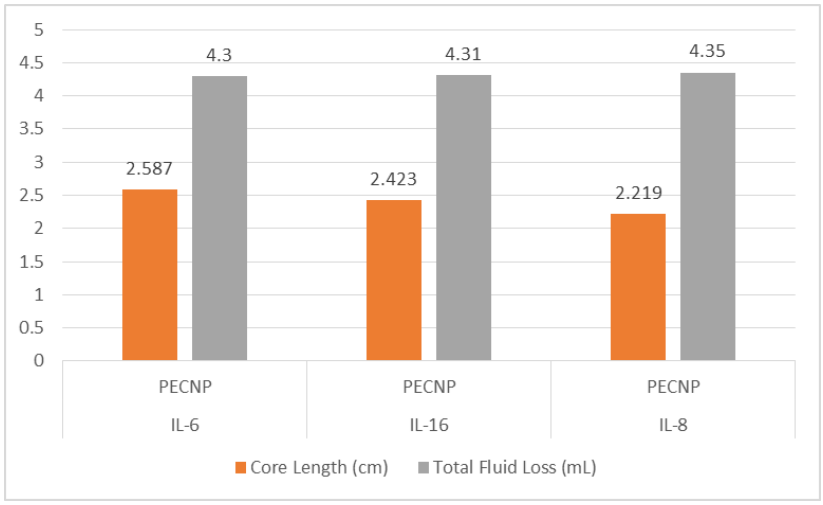

Figure 67: Correlation of fluid loss volume to core length after dynamic testing of the PECNP drill-in fluid on Indiana limestone cores

As previously mentioned, the PECNP drill-in fluid produced lower wall building coefficients in all three tests compared to the baseline cases. This is significant considering the wall building coefficient is an indicator of how much fluid loss will occur over a given period of time as represented in **Equation 18**. Filter cake development and fluid loss occur over much longer time periods than a 90 minute lab test. Therefore in a real world scenario, extrapolated fluid loss volumes of the baseline case would far exceed those of the PECNP fluid as exposure time in the borehole increased.

$$V_L = C_W \times \sqrt{t} + V_{SP} \qquad \text{Equation 18}$$

Where:

V_L = Total fluid loss volume, (gal/ft^2)

t = Total time duration of experiment, (min)

V_{SP} = Spurt loss volume, (gal/ft^2)

C_W = Wall building coefficient, (ft/min$^{1/2}$)

Wall building coefficients from these tests can be seen in **Figure 68**, **Figure 69**, and **Figure 70**. Analysis of the average coefficient of each test fluid in **Figure 71** reveals that the PECNP drill-in fluid resulted in a 32.7 % reduction of the wall building coefficient. It should be noted the dynamic regime was not reached during 90 minute tests and is further discussed in recommendations.

A filter cake weight to fluid loss correlation was not able to be made due to problems while removing the core from the fluid loss cell. Removal of the core with a completely intact filter cake proved difficult as parts of the cake would break off in the cell while dismantling the core holder. Therefore filter cake weights obtained were deemed inaccurate for developing a correlation.

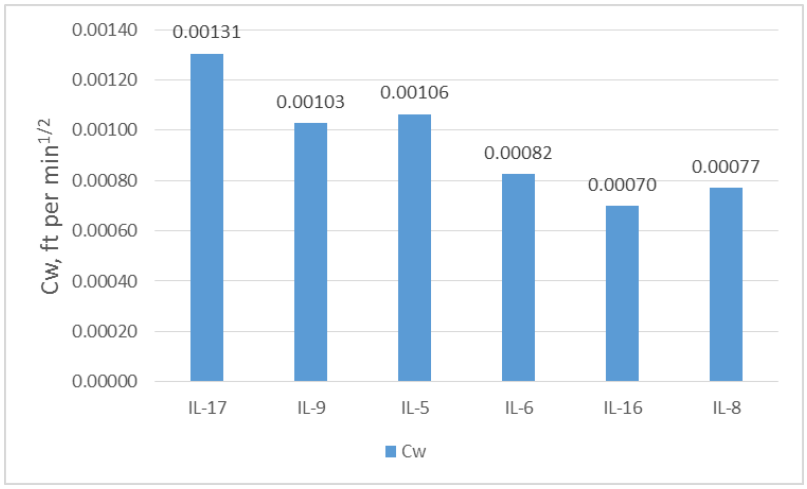

Figure 68: Wall building coefficients of both baseline and PECNP drill-in fluid tests performed on Indiana limestone cores

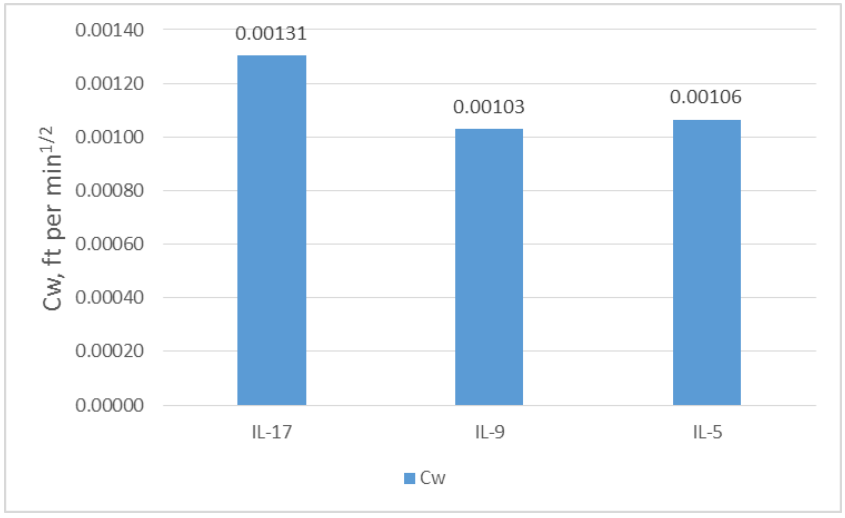

Figure 69: Wall building coefficients of baseline drill-in fluid tests performed on Indiana limestone cores

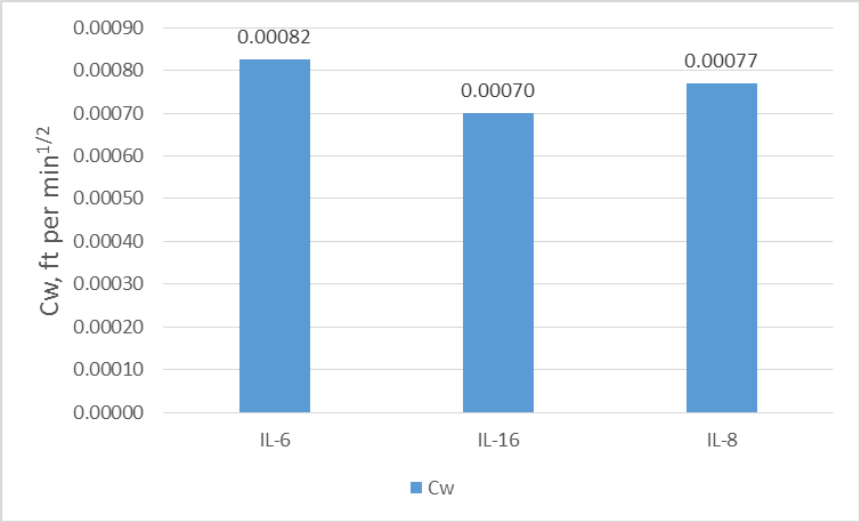

Figure 70: Wall building coefficients of PECNP drill-in fluid tests performed on Indiana limestone cores

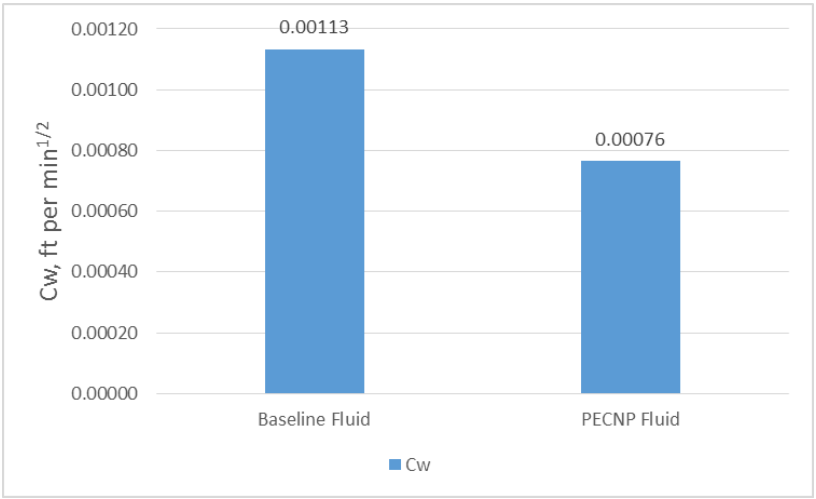

Figure 71: Average wall building coefficient for the baseline fluid case compared to the average wall building coefficient for the PECNP fluid after dynamic fluid loss testing of Indiana limestone cores

5.5.2 Dynamic Testing on Kentucky Sandstone Cores

Two dynamic tests were ran on a Kentucky sandstone core using positive PECNPs using the second fluid loss cell that was available. After the baseline test, it was discovered that no damage to the core's permeability occurred so it was used again during testing of the PECNP fluid. Since the core was tight, not much fluid loss was observed after the test was completed. As with the results from static testing, no spurt or wall building coefficient could be calculated from the gathered data. Judging from the fluid loss curve comparison in **Figure 72**, the PECNP drill-in fluid appeared to perform better by reducing total fluid loss by approximately 68%. Since the filter cakes formed during these tests were so thin, they were able to be removed without any mass being lost to the fluid loss cell and a filter cake weight to fluid loss correlation was created as seen in **Figure 73**.

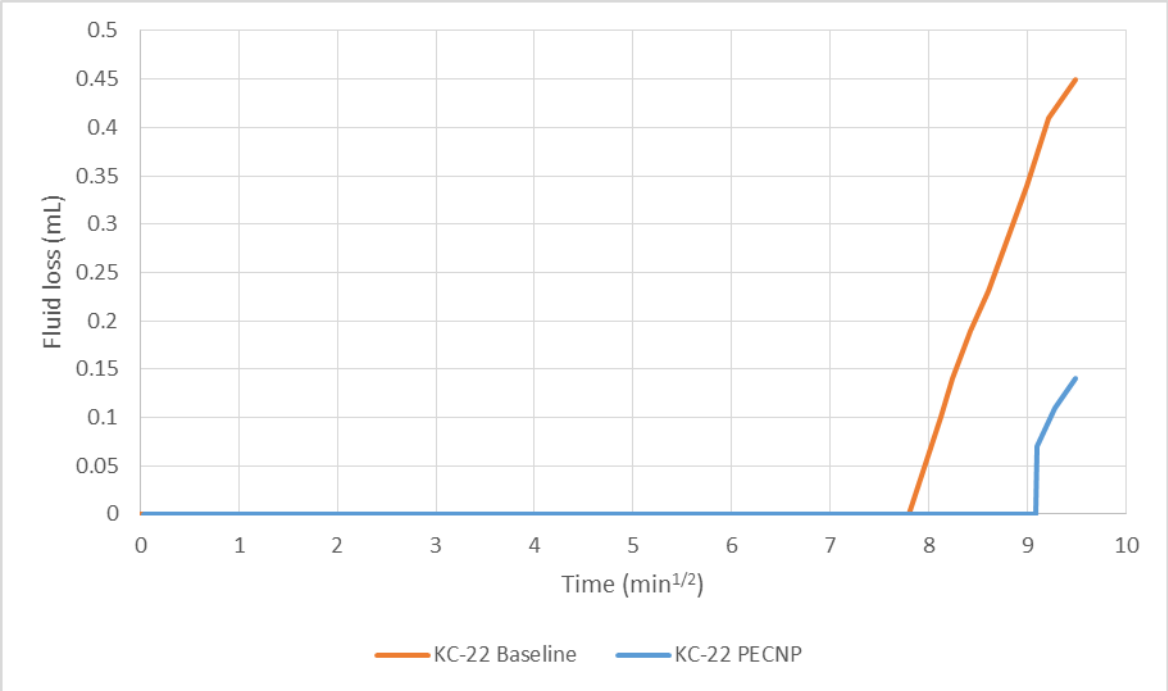

Figure 72: Dynamic fluid loss curve comparison of 2 tests done on a Kentucky sandstone core using a baseline and PECNP drill-in fluid

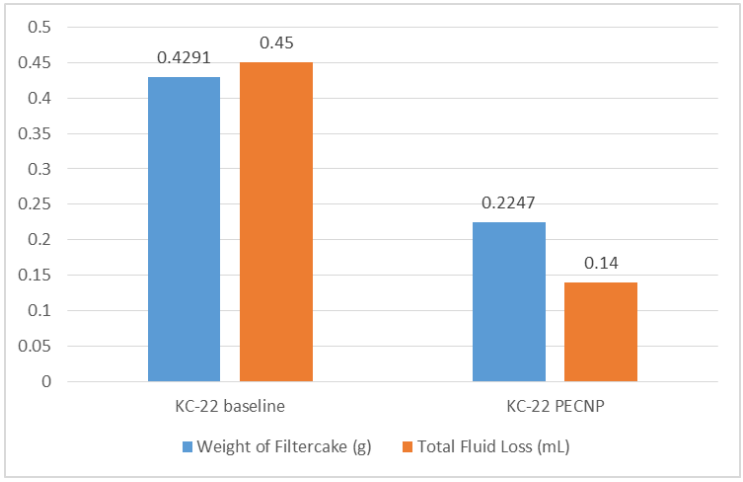

Figure 73: Filter cake weight and fluid loss correlation after dynamic fluid loss tests performed on Kentucky sandstone

5.5.3 Cleanup after Dynamic Testing

Cleanup curves between baseline and PECNP fluid tested cores were compared in pairs relative to their initial permeability values for a more accurate comparison. Curves were recorded at a flowrate of 0.25 mL/min using LabView software. Data obtained during cleanup are tabulated in **Table 19**. Comparing the cleanup curves of IL-17 versus IL-8 and IL-5 versus IL-16 one can see that the peak pressures reached during cleanup of baseline cores are higher than those of PECNP cores. This was not the case for IL-9 versus IL-6 however, the PECNP core IL-6 regained 90% of its initial permeability while the baseline only regained 62%. Cleanup curves can be seen in **Figure 74**, **Figure 75** and **Figure 76**. Comparing an overall average of permeability retention for the baseline tests (62.6%) and PECNP tests (70.3%), the cores tested using the PECNP drill-in fluid resulted in a 12.3% increase in retained permeability. As mentioned in section 5.5.2 there was no damage to the permeability after either test using the Kentucky sandstone core.

Table 19: Key data obtained before and after cleanup of Indiana limestone cores used in dynamic fluid loss testing

Core	Test Fluid	Permeability Before Test (mD)	Permeability After Test (mD)	Permeability retention %	Peak pressure during cleanup (psi)
IL-17	Baseline	9.94	5.50	55.31	12.27
IL-9	Baseline	2.58	1.60	62.07	29.25
IL-5	Baseline	4.88	3.44	70.53	17.54
IL-8	PECNP	6.51	4.61	70.90	12.10
IL-16	PECNP	6.35	3.17	50.00	15.68
IL-6	PECNP	2.91	2.62	90.00	33.83

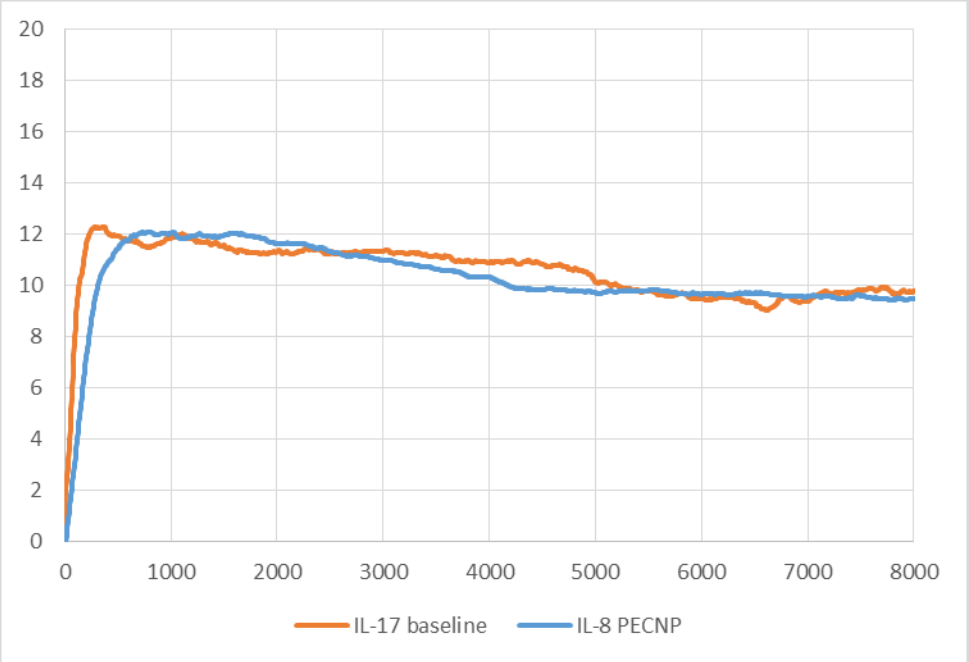

Figure 74: Comparison of IL-17 and IL-8 cleanup curves after dynamic testing, both with comparable initial permeability

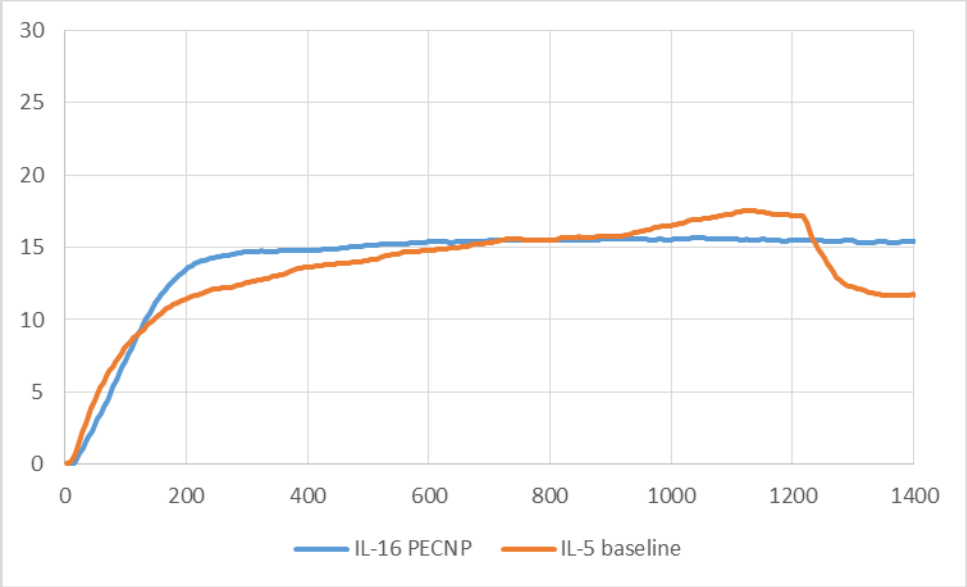

Figure 75: Comparison of IL-5 and IL-16 cleanup curves after dynamic testing, both with comparable initial permeability

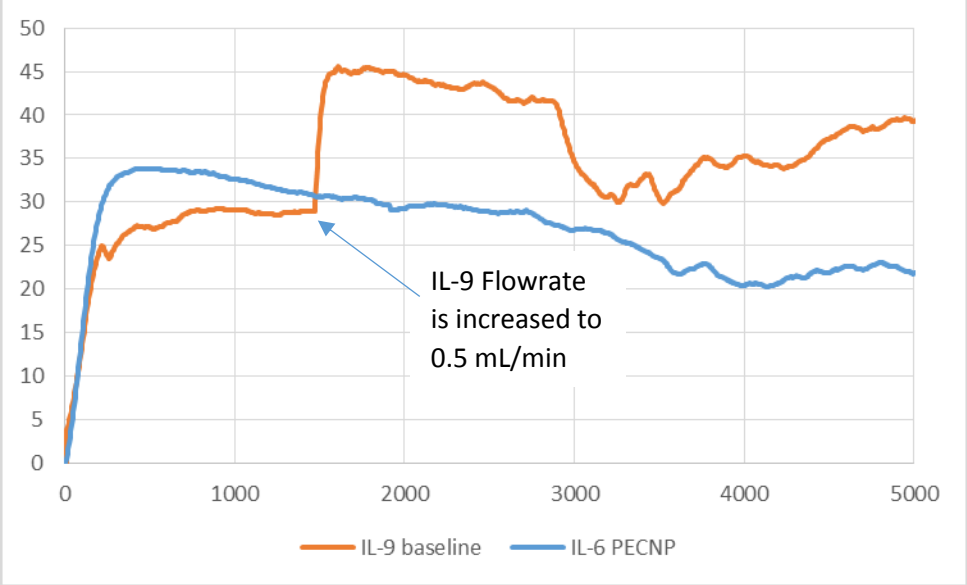

Figure 76: Comparison of IL-9 and IL-6 cleanup curves after dynamic testing, both with comparable initial permeability

Figure 77, **Figure 78** and **Figure 79** compare cleanup curves of baseline and PECNP fluids tested on core plugs of similar length. In **Figure 77** it appears the peak pressure required for cleanup of the PECNP fluid is much higher than the baseline case. This can be attributed to the initial permeability difference between the two cores as PECNP tested IL-6 has an initial permeability 3 times lower than IL-17. IL-6 also has a higher retained permeability than IL-17 after cleanup. Both comparisons in **Figure 78** and **Figure 79** show better cleanup performance of the PECNP fluid tested core plugs than the cases where the baseline fluid was used.

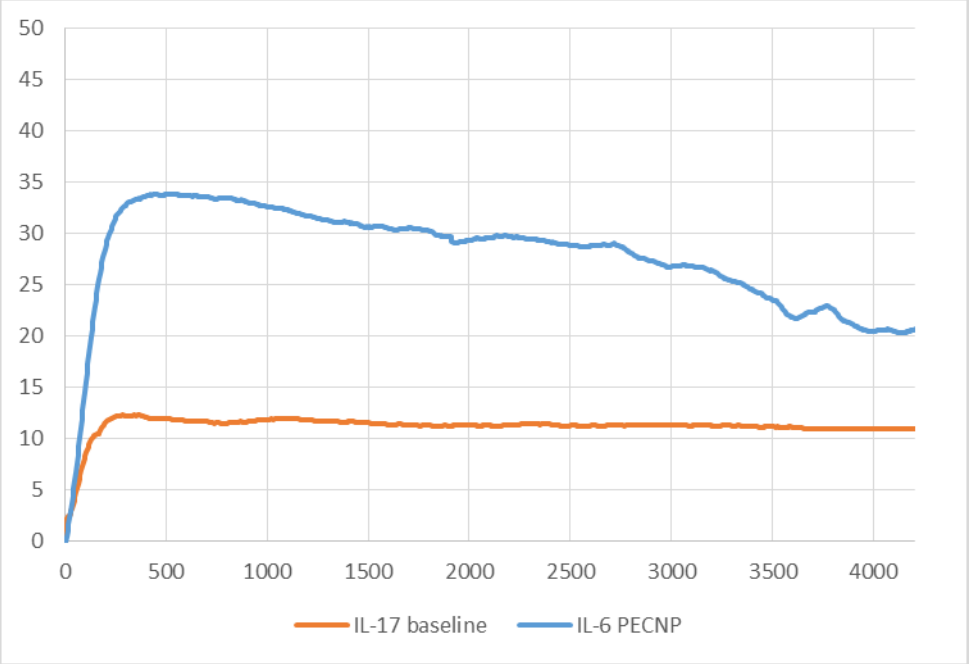

Figure 77: Comparison of IL-17 and IL-6 cleanup curves after dynamic testing, both core plugs are comparable in length

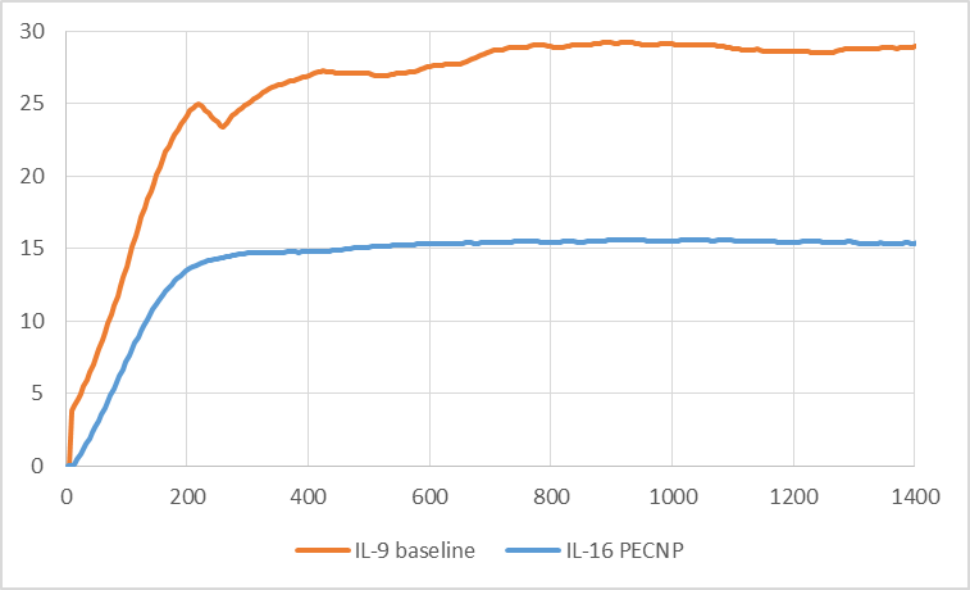

Figure 78: Comparison of IL-9 and IL-16 cleanup curves after dynamic testing, both core plugs are comparable in length

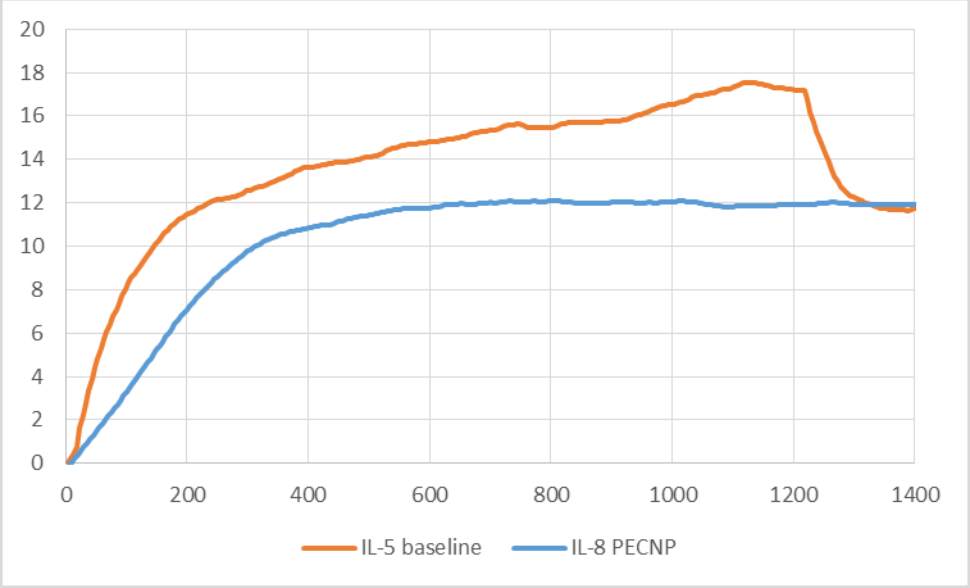

Figure 79: Comparison of IL-5 and IL-8 cleanup curves after dynamic testing, both core plugs are comparable in length

5.5.4 Result Comparison with the DFL Software

Results calculated in Excel did not differ very much from those calculated using the DFL software as seen in **Table 20**. The DFL software calculates spurt volumes in gallons per 100 square feet so the values used in Excel data had to be converted for comparison. Any differences in C_W or spurt volumes between the two data sets is likely due to user error when choosing the linear section in the DFL software. Two points are hand selected on the linear portion of the curve and the software calculates values based on a user's selection. Without the option to zoom on the chart in the software, selecting points placed directly on the curve may prove to be a source of error. With this in mind, use of Excel would be a more accurate way to analyze and interpret the data. Screenshots of the fluid loss curves plotted by the DFL software can be found in the appendix.

Table 20: Dynamic fluid loss data comparison based on how values were calculated using either Excel or DFL software

		Excel Calculated Values			DFL Software Calculated Values		
Core	Test Fluid	Spurt Loss (gal/100ft^2)	C_w	R^2 Fit Value	Spurt Loss (gal/100ft^2)	C_w	R^2 Fit Value
IL-17	Baseline	3.51	0.00131	0.995	3.883	0.00127	0.995
IL-9	Baseline	12.77	0.00103	0.995	12.45	0.00103	0.994
IL-5	Baseline	25.09	0.00106	0.943	22.99	0.00117	0.94
IL-6	PECNP	10.21	0.00082	0.998	9.767	0.000777	0.997
IL-16	PECNP	10.69	0.00070	0.995	10.378	0.000706	0.995
IL-8	PECNP	10.19	0.00077	0.995	10.612	0.000714	0.995

5.5.5 Dynamic Fluid Loss 270 Minute Tests

Two additional dynamic fluid loss tests were ran for 270 minutes to simulate areas of the well bore that are subjected to drilling fluid contact for extended periods of time. Two limestone cores of similar length and permeability were chosen as seen in **Table 21**. IL-17 was cleaned with the bleach solution discussed in section 3.8 after its previous use in 90 minute DFL testing. Testing of the baseline fluid was performed on core IL-17 while the PECNP fluid was testing on IL-7. Results were as expected with the PECNP fluid outperforming the baseline in both fluid loss and wall building coefficient reduction. Fluid loss curves for both tests can be seen in **Figure 80**. Total fluid loss volumes after 90 and 270 minutes are represented in **Table 22** and **Figure 81**. Comparing the total fluid loss volumes after 270 minutes, the PECNP fluid was able to reduce fluid loss by 14.8%. The PECNP fluid also reduced the wall building coefficient by 18.4% when comparing the values seen in **Figure 82**. The 270 minute tests are comparable to previous 90 minute testing in both fluid loss volumes and wall building coefficients which confirms result consistency while also suggesting that the PECNP filter cake performance is reliable over longer periods of time.

Error! Not a valid link.

Table 21: Initial properties of core plugs used in 270 minute DFL testing

270 Minute Dynamic Fluid Loss Initial Core Properties				
Core	Length (cm)	Diameter (cm)	Porosity (%)	Permeability (mD)
IL-17	2.516	2.513	13	5.78
IL-7	2.535	2.523	12	5.65

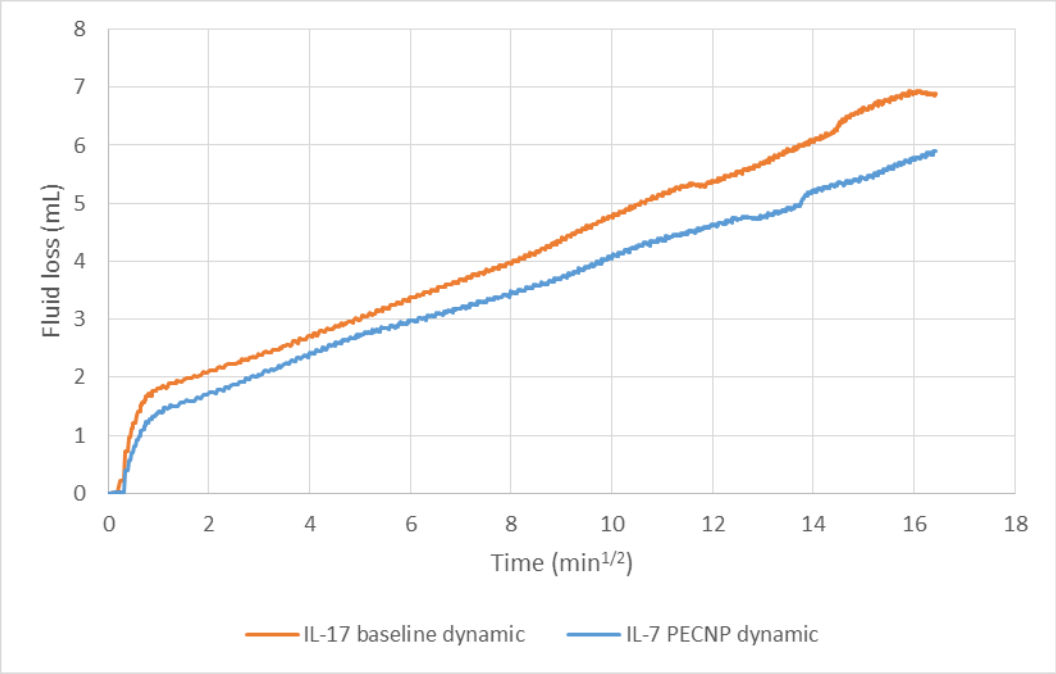

Figure 80: Dynamic fluid loss curves for 270 minute testing of baseline and PECNP fluids

Error! Not a valid link.

Table 22: Key data obtained after 270 minute DFL testing of basline and PECNP fluids

Core	Test Fluid	Spurt Loss (mL)	Core Length (cm)	90 min. Total Fluid Loss (mL)	270 min. Total Fluid Loss (mL)	C_w ft/min$^{1/2}$
IL-17	Baseline	1.3089	2.516	4.56	6.94	0.00114
IL-7	PECNP	1.2146	2.535	3.9	5.91	0.00093

Error! Not a valid link.

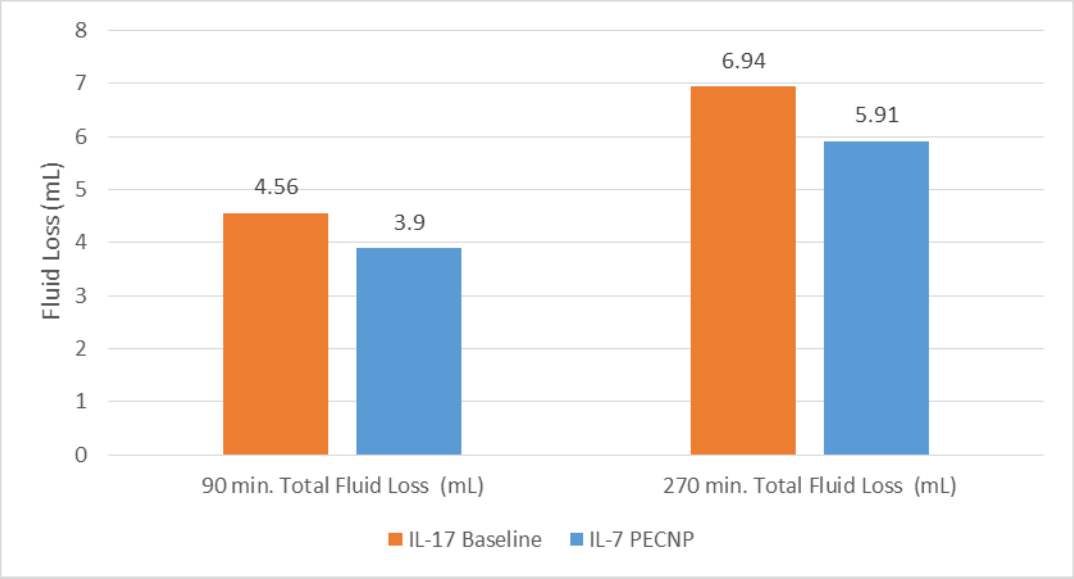

Figure 81: Total fluid loss volumes after 90 and 270 minute dynamic tests of both baseline and PECNP fluids

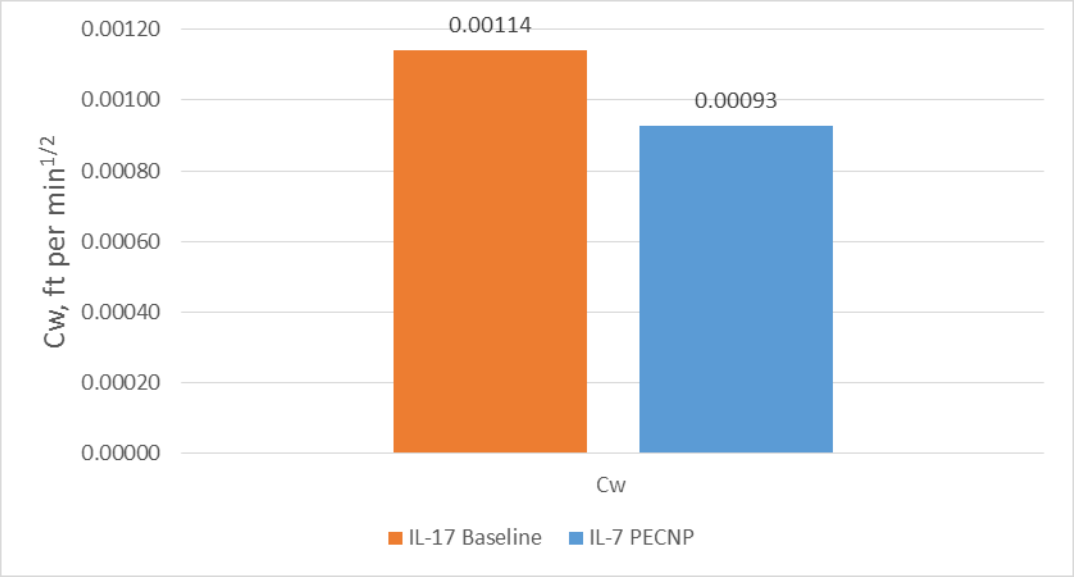

Figure 82: Wall building coefficient comparison of baseline and PECNP fluids after 270 minute DFL testing

Cleanup performance of the PECNP fluid also proved to be better than that of the baseline fluid. Although the peak pressure was higher for the PECNP cleanup, it retained more of its initial permeability than the baseline core. Cleanup data as well as the cleanup curves can be seen in **Table 23** and **Figure 83**.

Table 23: Cleanup data obtained after 270 minute DFL testing of baseline and PECNP fluids

Core	Test Fluid	Permeability Before Test (mD)	Permeability After Test (mD)	Permeability retention %	Peak pressure during cleanup (psi)
IL-17	Baseline	5.78	4.64	80.37	11.78
IL-7	PECNP	5.65	4.81	85.14	13.37

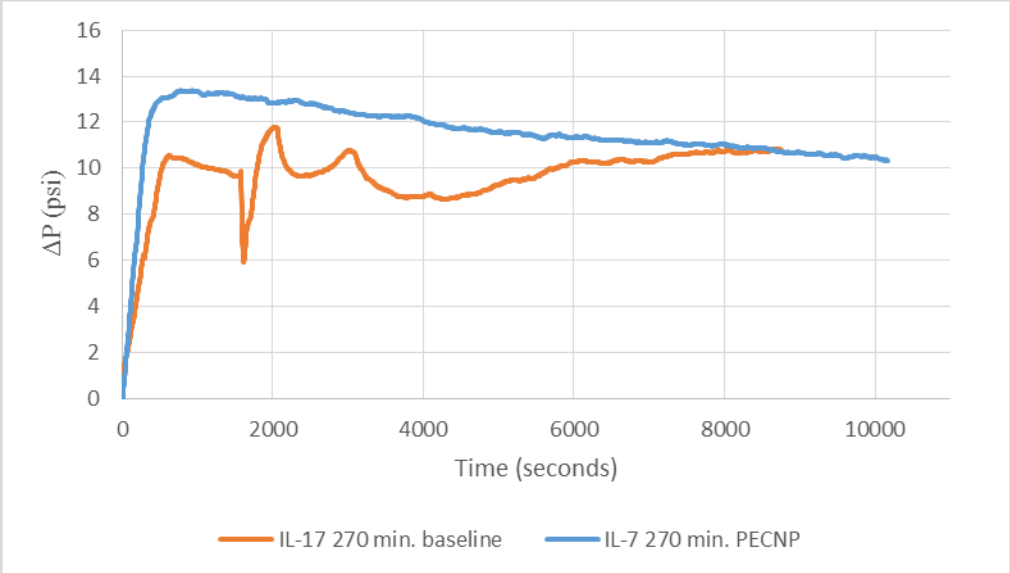

Figure 83: Cleanup curves of IL-7 and IL-17 after 270 minute DFL testing

6 Conclusions

This research investigated the addition of polyelectrolyte complex nanoparticles as a fluid loss prevention agent to a water-based biopolymer reservoir drilling fluid. Use of a PECNP drill-in fluid has the capability of reducing fluid loss while preventing formation damage to achieve higher permeability retention for flow back to the well. Every component of the fluid is degradable either by acidification or enzymatic degradation which makes for a more thorough cleanup potential of the fluid. The following conclusions can be drawn from this research:

1. **Particle size and zeta potential measurements:** The optimal PEI:DS:Brine ratios for both positive and negatively charged PEC nanoparticles in the base 3% NaCl brine and ultimately the drill-in fluid were investigated. For positively charged particles it was determined that a PEI pH of 8.5 and a PEI:DS:Brine ratio of 2:1:0.1 was the most stable system. For negatively charged particles, a PEI pH of 8.5 and a PEI:DS:Brine ratio of 1:10:0.1 was determined to be the most stable system.
2. **PECNP effect on fluid rheology:** Rheology measurements were taken for both the baseline drill-in fluid and the drill-in fluid with PEC nanoparticles added over the course of 24 hours to observe any changes that might occur between the two fluids. Analysis of the rheological profiles and calculated viscosity values revealed that no significant changes occurred in either fluid over 24 hours. This indicates that the addition of PEC nanoparticles to the fluid has no negative effects on the fluid rheology over time.
3. **PECNP effects on static fluid loss tests:** Static testing of both positive and negatively charged particles against a baseline fluid with no nanoparticles proved that the nanoparticles in correct dilution would reduce fluid loss and lower the permeability damage in limestone and sandstone cores. After analysis of fluid loss data and cleanup curves, it

was determined that a $1/8^{th}$ nanoparticle dilution allowed for the best fluid loss prevention and permeability retention performance in both positively and negatively charged PECNP cases using limestone cores. However the damage caused by negatively charged particles on limestone cores, likely due to adsorption of the particles in the pore space of the rock, was too great to consider them for further testing. Static fluid loss tests performed on tight sandstone cores were somewhat inconclusive, as no fluid loss was recorded. The PEC nanoparticle fluid did however help prevent formation damage by having 37% higher retained permeability than the baseline fluid.

4. **PECNP effects on dynamic fluid loss tests:** The best nanoparticle dilution of 0.125 determined by static testing was taken for testing in a dynamic setting. A baseline drill-in fluid and PECNP drill-in fluid were tested against three limestone cores each and in two instances sandstone cores were used. Filter cakes were successfully formed under the shear of the fluid flowing past the core face. The PECNP outperformed the baseline fluid by having lower, more consistent total fluid loss volumes as well as lower wall building coefficients which results in less fluid loss over time. Cleanup of the cores after testing also proved to be more successful when the PECNP fluid was used. In the case of Indiana Limestone cores, fluid loss volumes were reduced by 28%, wall building coefficients were reduced by 32.7 %, and retained permeability was 12.3% higher in cores tested with the PECNP drill-in fluid. In the case of Kentucky sandstone cores when PECNP fluid was used, fluid loss volumes were reduced by 68% and the core regained 100% of its initial permeability. Overall, the addition of PEC nanoparticles to the drill-in fluid was a success by creating a filter cake with consistently lower fluid loss volumes, spurt loss and wall building coefficients.

7 Recommendations

Noting the successful performance of Quasimodo after these tests and the limitations of the core holder shear rate, recommendations for future studies of drilling fluids using this system would be an increased flowrate with a new core holder designed to more closely replicate the annular space in a borehole.

Further testing using the Quasimodo setup is also recommended for longer periods of time in order to reach the dynamic fluid loss regime described in stage three of **Equation 1**. In this stage, fluid loss is no longer proportional to the square root of time and filter cake growth is controlled by the erosional forces of the fluid flowing past it. Rate of filtrate through the filter cake will follow Darcy's law, and fluid loss begins to increase. The dynamic regime did not appear to be reached even after 270 minute tests, therefore longer test times may be required or higher shear rates.

8 Nomenclature and Abbreviations

A: core cross-sectional area, cm^2

API: American Petroleum Institute

$CaCO_3$: Calcium carbonate

cm: centimeter

cP: centipoise

C_W: wall-building coefficient, $ft/min^{1/2}$

d: inner diameter of the drill pipe, inches

d_1: outer drill pipe diameter, inches

d_2: borehole diameter, inches

DFL: Dynamic fluid loss

DS: Dextran sulfate

h: height of the fracture (in this case height of the core holder slot), inches

HCl: Hydrochloric acid

HPG: Hydroxypropyl guar

HPHT: High pressure high temperature

IL: Indiana limestone

K: Consistency factor

k_1: spring torsion constant, (386 for R1-B1-F1 combination) dyne-cm/degree of reflection

k_2: effective bob surface shear stress constant, (0.01323 for R1-B1 combination) cm^{-3}

KC: Kentucky sandstone

m: slope of volume versus $t^{1/2}$

M: Mass/area of the filter cake

mD: Millidarcy

m_i: additive mass, grams

N: Rotor speed, RPM

n: Flow behavior index

NaCl: Sodium chloride

nm: nanometer

PEC: Polyelectrolyte complex

PECNP: Polyelectrolyte complex nanoparticles

PEI: Polyethylenimine

PV: Pore volume, cm^3

Q: flowrate, $in.^3$/sec

q: flowrate, gal/min

RDF: Reservoir drilling fluid

t: Total time duration of experiment, (min)

u: velocity of solvent through the filter cake

v_a: velocity in the annulus, ft/sec

V_B: Bulk volume of core, cm^3

V_i: volume of a given mass, cm^3

V_L: Total fluid loss volume, (gal/ft^2)

v_p: velocity in the drill pipe, ft/sec

V_{SP}: Spurt volume

W: width of the fracture (in this case width of the core holder slot), inches

W_D: Dry weight of core, g

W_S: Saturated weight of core, g

γ: shear rate

γ_{aw}: shear rate in the annulus, sec^{-1}

γ_{pw}: shear rate in the drill pipe, sec^{-1}

γ_{wf}: shear rate at the fracture wall, sec^{-1}

θ_N: Dial reading at N rotor speed

μ_a: Apparent viscosity, cP

μ_p: Plastic viscosity, cP

ρ: Density of saturating fluid, g/cm^3

ρ_f: drill-in fluid density, g/cm^3

ρ_i: additive density, g/cm^3

τ: shear stress, dynes/cm^2

τ: Shear stress

τ_0: Yield stress

τ_{fc}: Yield stress of the filter cake

τ_w: Fluid stress

τ_y: Yield point, lbf/100 ft^2

Φ: Porosity, %

ω: Mass fraction of solids in the fluid phase

9 Bibliography

1. Chilingarian, George V. and Vorabutr, Paul. *Drilling and Drilling Fluids.* s.l. : Elsevier Scientific Publishing Company, 1981.

2. Lummus, James L. and Azar, J.J. *Drilling Fluids Optimization: A Practical Field Approach.* s.l. : PennWell Publishing Company, 1986.

3. Darley, H.C.H. and Gray, George R. *Composition and Properties of Drilling and Completion Fluids.* Houston : Gulf Publishing Company, 1988.

4. Hill, Donald G., et al. Formation Damage: Origin, Diagnosis and Treatment Strategy. [book auth.] Michael J. Economides and Kenneth G. Nolte. *Reservoir Stimulation.* s.l. : Wiley, 2000.

5. West, Gary, Hall, John and Simon, Seaton. Drilling Fluids. [book auth.] Robert F. Mitchell and Larry W. Lake. *Petroleum Engineering Handbook Volume II.* Richardson : Society of Petroleum Engineers, 2006.

6. *Preliminary Test Results of Nano-based Drilling Fluids for Oil and Gas Field Application.* Amanullah, Md., Al-Arfaj, Mohammad K and Al-Abdullatif, Ziad. Amsterdam : Society of Petroleum Engineers, 2011.

7. *Nanotechnology for Oilfield Applications: Challenges and Impact.* Lau, Hon Chung, Yu, Meng and Nguyen, Quoc P. Abu Dhabi : Society of Petroleum Engineers, 2016.

8. *Application of nanoparticles as fluid loss control additives for hydraulic fracturing of tight and ultra-tight hydrocarbon-bearing formations.* Barati, Reza. Lawrence : Elsevier, 2015.

9. Bourgoyne Jr., Adam T., et al. *Applied Drilling Engineering.* Richardson : Society of Petroleum Engineers, 1986.

10. Spears & Associates Inc. *Oilfield Market Report.* Tulsa : www.spearsresearch.com, 2004.

11. *Particulate Invasion From Drilling Fluids.* Bailey, Louise, et al. 04, s.l. : Society of Petroleum Engineers, 2000, Vol. 5.

12. *An Overview of Formation Damage Mechanisms Causing a Reduction in the Productivity and Injectivity of Oil and Gas Producing Formations.* Bennion, D. Brant. 11, s.l. : Petroleum Society of Canada, November 2002, Journal of Canadian Petroleum Technology, Vol. 41.

13. Gatlin, Carl. *Petroleum Engineering: Drilling and Well Completions.* Englewood Cliffs : Prentice-Hall, Inc., 1960.

14. *Optimizing Filtrate Design to Minimize In-Situ and Wellbore Damage to Water-Wet Reservoirs During Drill-In.* Dalmazzone, Christine, et al. 01, s.l. : Society of Petroleum Engineer, 2006, Vol. 21.

15. Azar, J.J. Drilling Problems Solutions. [book auth.] Robert F. Mitchell and Larry W. Lake. *Petroleum Engineering Handbook Volume II.* Richardson : Society of Petroleum Engineers, 2006, 10.

16. *Effect of Drilling Fluids on Rock Surface Properties.* Cuiec, L. 01, s.l. : Society of Petroleum Engineers, 1989, Vol. 4.

17. *The Alteration of Rock Properties Due to Interactions With Drilling Fluid Components.* Sharma, M. M. and Wunderlich, R. W. s.l. : Society of Petroleum Engineers, 1985.

18. Dandekar, Abhijit Y. *Petroleum Reservoir Rock and Fluid Properties.* s.l. : CRC Press, 2013. 13: 978-1-4398-7645-9.

19. *Limiting, Treating Formation Damage in Horizontal, Extended Reach Wells.* Le Blanc, Leonard. 6, June 1996, Offshore, p. 56.

20. Chiriac, Alexandru . Reservoir Drill-in Fluids, Completion and Workover Fluids. Aberdeen : Aalborg University Esbjerg, 2014.

21. *Enzymes Breakers for Viscosity Enhancing Polymers.* Battistel, Ezio, et al. 1, s.l. : Elsevier, 2011, Vol. 77.

22. *Drilling Fluids: State of the Art.* Caenn, Ryen and Chillingar, George V. 3-4, s.l. : Elsevier, May 1996, Journal of Petroleum Science and Engineering, Vol. 14, pp. 221-230.

23. Nowak, T.J. and Kruegar, R.F. The Effect of Mud Filtrates and Mud Particles upon the Permeabilities of Cores. New York : American Petroleum Institute, 1951.

24. *Microbial Polysaccharides.* Linton, J.D., Ash, S.G. and Huybrects, L. 1991, Biomaterials: Novel Materials from Biological Sources, pp. 215-261.

25. *Binding of Bivalent Cations by Xanthan in Aqueous Solution.* Bergmann, Dirk, Furth, Guido and Mayer, Christopher. 3, s.l. : Elsevier, October 2008, International Journal of Biological Macromolecules, Vol. 43, pp. 245-251.

26. Laroche, Celine and Michaud, Philippe. Microbial Polysaccharides. *Comprehensive Food Fermentation and Biotechnology.* New Delhi : Asiatech Publisher Inc., 2010, 8.

27. *Evaluation of Rheological Properties of the Exopolysaccharide of Sphingomonas paucimobilis GS-1 for Application in Oil Exploration.* Shah, A. K. and Ashtaputre, A. A. . 1999, Journal of Industrial Microbiology and Biotechnology.

28. Company, Drilling Specialties. Flowzan Biopolymer. *Technical Sheet.* s.l. : Chevron Phillips Chemical Company.

29. Schlumberger. Oilfield Glossary. [Online] Schlumberger, 2017. http://www.glossary.oilfield.slb.com/Terms/x/xanthan_gum.aspx.

30. *Field Experience Validates Effectiveness of Drill-In Fluid Cleanup System.* Beall, Brian B., Tjon-Joe-Pin, Robert and Brannon, Harold D. San Antonio : Society of Petroleum Engineers, 1997.

31. Gulbis, Janet and Hodge, Richard M. Fracturing Fluid Chemistry and Proppants. [book auth.] Michael J. Economides. *Reservoir Stimulation.* s.l. : John Wiley & Sons, Inc., 2000.

32. *Empirical Correlation to Predict Viscosity Breaking Ratio of Guar-Based Biodegradable Drilling Fluid.* Cai, Jihua, Liu, Hao and Gu, Sui. s.l. : IEEE Conference Publications, 2010.

33. *Solutions of xanthan gum/guar gum mixtures: shear rheology, porous media flow, and solids transport in annular flow.* Amundarain, J. L., et al. 5, s.l. : Springer-Verlag, June 2009, Rheologica Acta, Vol. 48.

34. Barati, Reza. Fracturing Fluid Cleanup by Controlled Release of Enzymes from Polyelectrolyte Complex Nanoparticles- PhD Thesis. Lawrence : University of Kansas, 2010.

35. *Chemically Modified Natural Gum for Use in Well Stimulation.* Githens, C. J. and Burnham, J. W. 01, s.l. : Society of Petroleum Engineers, 1977, Society of Petroleum Engineers Journal, Vol. 17.

36. *Breaker Concentrations Required to Improve the Permeability of Proppant Packs Damaged by Linear and Cross-linked Fracturing Fluids.* Brannon, H.D. and Pulsinelli, R. J. 4, 1992, SPE Production Engineering, Vol. 7, pp. 338-342.

37. Geo Drilling Fluids, Inc. Product Sheet. [Online] 2010. http://geodf.com/wp-content/uploads/2017/09/CALCIUM-CARBONATE.pdf.

38. *Mud Design to Minimize Rock Impairment Due to Particle Invasion.* Abrams, A. 05, s.l. : Society of Petroleum Engineers, 1977, Journal of Petroleum Technology, Vol. 29.

39. *Optimizing the Selection of Bridging Particles for Reservoir Drilling Fluids.* Dick, M. A. , et al. Lafayette : Society of Petroleum Engineers, 2000.

40. Hughes, Baker. *Drilling Fluids Reference Manual.* s.l. : Baker Hughes, 2006.

41. Calcium Carbonate Data Sheet. *MiSWACO.* [Online] [Cited: December 6, 2017.] http://www.slb.com/~/media/Files/miswaco/ps-specialized-tools/calcium_carbonate.ashx.

42. *Cleanup of Wall-Building Filter Cakes.* Zain, Zulkeffeli M. and Sharma, Mukul. Houston : Society of Petroleum Engineers, 1999.

43. *New Treatment for Removal of Mud-Polymer Damage in Multilateral Wells Drilled Using Starch-Based Fluids.* Driscoll, K. P., Amin, N. M. and Tantawi, I. Y. . 03, s.l. : Society of Petroleum Engineers, 2000, SPE Drilling and Completion, Vol. 15.

44. *Application of Polymer Specific Enzymes To Clean Up Drill-In Fluids.* Suhy, Thomas E. and Harris, Ramon P. s.l. : Society of Petroleum Engineers, 1998.

45. *Using a Physical Wellbore Model To Study Formation Damage Problems in Well Completions.* Burnett, D.B. 01, s.l. : Society of Petroleum Engineers, 1995, SPE Drilling and Completion, Vol. 10.

46. *Characterization of Xanthan Gum Degrading Enzymes from a Heat-stable, Salt-tolerant Bacterial Consortium.* Ahlgren, Jeffrey A. 1993, Developments in Petroleum Science, Vol. 39.

47. *Modification of guar galactomannan with the aid of Aspergillus niger pectinase.* Shobha, M. S. , et al. 1, s.l. : Elsevier, December 2005, Carbohydrate Polymers, Vol. 62.

48. *Filtration From Mud During Drilling.* Ferguson, C.K. and Klotz, J.A. 2, s.l. : Society of Petroleum Engineers, February 1954, Journal of Petroleum Technology, Vol. 6.

49. *Optimum Fluid Characteristics for Fracture Extension.* Howard, George C. and Fast, C.R. s.l. : American Petroleum Institute, 1957, Drilling and Production Practice, pp. 261-270.

50. Constein, Vernon G., et al. Performance of Fracturing Materials. [book auth.] Michael J. Economides. *Reservoir Stimulation.* s.l. : Wiley, 1987.

51. *Filter-Cake Formation of Fracturing Fluids.* Prud'homme, R.K. and Wang, J.K. New Orleans : Society of Petroleum Engineers, 1993.

52. *Dynamic Fluid Loss in Hydraulic Fracturing Under Realistic Shear Conditions in High-Permeability Rocks.* Navarrete, R.C., Cawiezel, K.E. and Constien, V.G. 3, s.l. : Society of Petroleum Engineers, 1996, Vol. 11.

53. *Preliminary Test Results of Nano-based Drilling Fluids for Oil and Gas Field Application.* Amanullah, Md, AlArfaj, Mohammed K. and Al-abdullatif, Ziad Abdullrahman. Amsterdam : Society of Petroleum Engineers, 2011.

54. *Nanoparticle-Based Drilling Fluids for Minimizing Formation Damage in HP/HT Applications.* Mahmoud, Omar, et al. Lafayette : Society of Petroleum Engineers, 2016.

55. Ismail, Abdul Razak, et al. Nanoparticles Performance as Fluid Loss Additives in Water Based Drilling Fluids. *Materials Science Forum.* 2016, Vol. 864, pp. 189-193.

56. *Fluid filtration and rheological properties of nanoparticle additive and intercalated clay hybrid bentonite drilling fluids.* Barry, Matthew M., et al. s.l. : Elsevier, 2015, Journal of Petroleum Science and Engineering, Vol. 127, pp. 338-346.

57. Koetz, Joachim and Kosmella, Sabine. Introduction and Objective. *Polyelectrolytes and Nanoparticles.* s.l. : Springer Laboratory, 2007.

58. *Multifunctional Nanoparticulate Polyelectrolyte Complexes.* Hartig, Sean M., et al. 12, s.l. : Springer, December 2007, Pharmaceutical Research, Vol. 24.

59. *Formulation and characterization of DNA–polyethylenimine–dextran sulfate nanoparticles.* Tiyaboonchai, Waree, Woiszwillo, James and Middaugh, Russell C. 4, s.l. : Elsevier, July 2003, European Journal of Pharmaceutical Sciences, Vol. 19.

60. Dextran Sulfate. *Sigma Aldrich.* [Online] Sigma Aldrich, 2017. https://www.sigmaaldrich.com/technical-documents/protocols/biology/dextran-sulfate.html.

61. *Insulin containing polyethylenimine–dextran sulfate nanoparticles.* Tiyaboonchai, Waree, et al. 1-2, s.l. : Elsevier, 2003, International Journal of Pharmaceuticals, Vol. 255, pp. 139-151.

62. *Delayed HPAM Gelation via Transient Sequestration of Chromium in Polyelectrolyte Complex Nanoparticles.* Cordova, Mary, et al. 12, Lawrence : American Chemical Society, May 17, 2008, Macromolecules, Vol. 41, pp. 4398-4404.

63. Sigma Aldrich. *PEI Product Specification Sheet.* [Online] 2017. https://www.sigmaaldrich.com/Graphics/COfAInfo/SigmaSAPQM/SPEC/40/408727/408727-BULK_____ALDRICH__.pdf.

64. *Application of Nanoparticles as Proppants and Breaker Encapsulating Agents.* Bose, Charles. Lawrence : University of Kansas, 2016.

65. *Drill-in fluid reduces formation damage, increases production rates.* Hands, Nick, et al. s.l. : Oil & Gas Journal, 1998, Oil & Gas Journal.

66. *ECOPOL-400DS Hydroxypropylated Guar Product Data Sheet.* Houston, TX : s.n., 2017.

67. *Malvern.* 2017.

68. Zeta Potential. *Wikipedia.* [Online] [Cited: December 6, 2017.] https://en.wikipedia.org/wiki/Zeta_potential.

69. FANN Instrument Company. *FANN Model 35 Viscometer Instruction Manual.* [Online] 2016.

70. Hutchins, R. E. *Notes for Schlumberger Static Fluid Loss Cell.* 2010.

71. *The Effects of Fluid Preconditioning and Test Cell Design on the Measurement of Dynamic Fluid Loss Data.* McGowen, J.M. and McDaniel, B.W. Houston : Society of Petroleum Engineers, 1988.

72. Hutchins, R.D. and Roberson, Andre. *Improvements to the Dynamic Fluid Loss Equipment (Quasimodo).* s.l. : Schlumberger, 2009.

73. *Reservoir Drilling Fluids-Designing for Challenging Wells in a Remote Location.* Knox, David Alexander, et al. s.l. : Society of Petroleum Engineers, 2005.

74. Grant Prideco. Drill pipe data tables. [Online] http://www.oilproduction.net/files/casing_drilling/GrantPrideco_Drill_Pipe_Data_Tables.pdf.

75. Hutchins, R.D. and Barati, Reza. *Parametric Study of Factors Influencing Dynamic Fluid Loss Using a Novel Fluid Loss Additive.* s.l. : Schlumberger Report DL 11371, June 24, 2008.

76. Sigma Aldrich . *DS product information sheet.* [Online] 2017. https://www.sigmaaldrich.com/content/dam/sigma-aldrich/docs/Sigma/Product_Information_Sheet/d8906pis.pdf.

77. Schlumberger. Technical Report of FloPro NT fluid performance in the field. [Online] http://www.slb.com/~/media/Files/miswaco/tech_reports/flopro-nt-slavetskoye-field-tr.pdf.

78. Hutchins, R.E. *Notes on the Schlumberger Static Fluid Loss Apparatus.* 2010.

Appendix

A. Filter Cake Images after Static Fluid Loss Testing with Positively Charged PECNPs

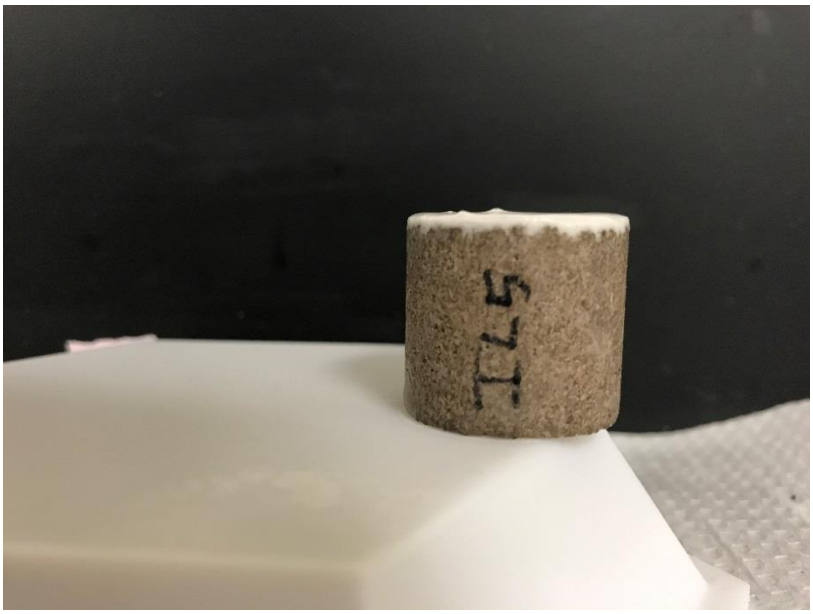

Figure A-1: Filter cake formed on IL-5 core after static fluid loss testing using an undiluted positive PECNP drill-in fluid

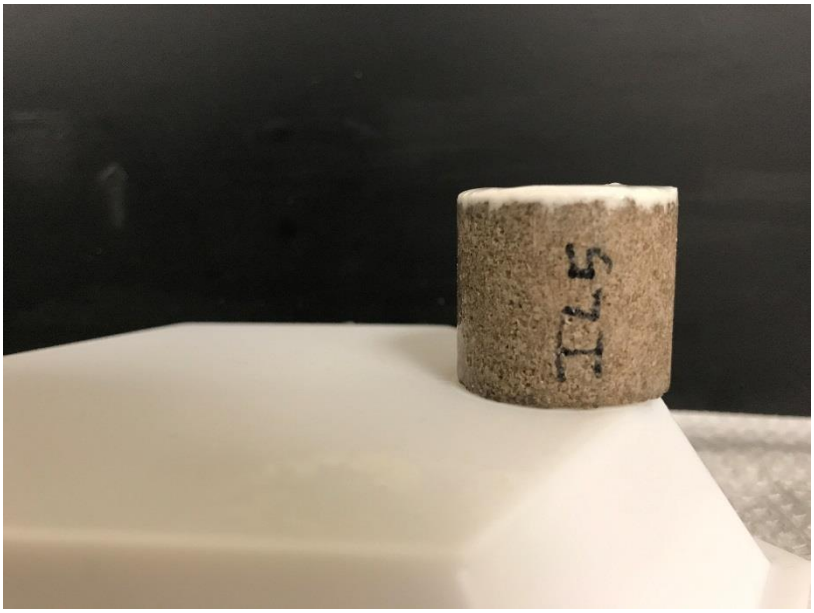

Figure A-2: Filter cake formed on IL-5 core after static fluid loss testing using a 0.125 diluted positive PECNP drill-in fluid

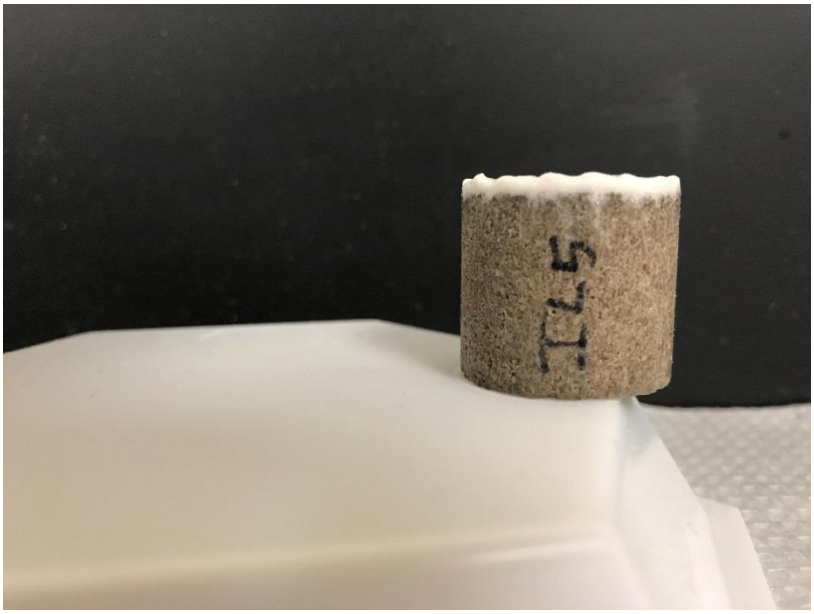

Figure A-3: Filter cake formed on IL-5 core after static fluid loss testing using a 0.25 diluted positive PECNP drill-in fluid

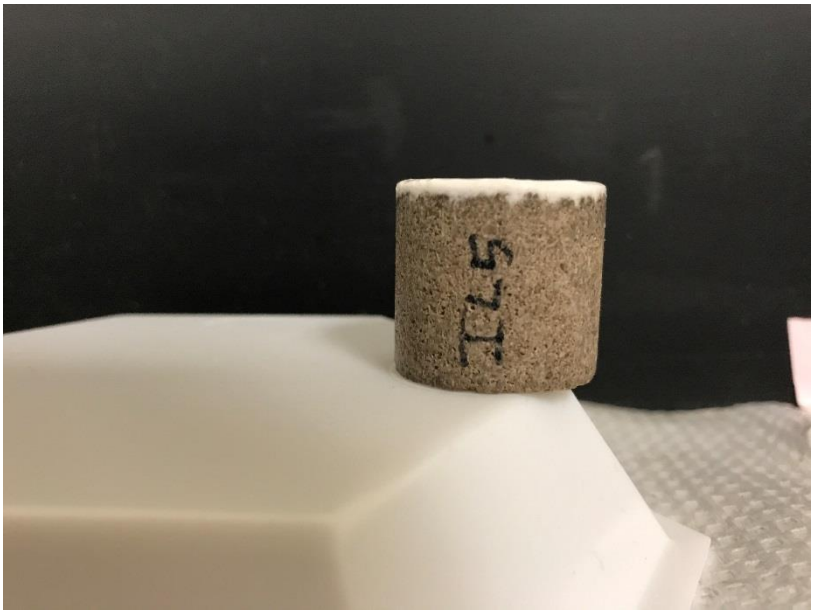

Figure A-4: Filter cake formed on IL-5 core after static fluid loss testing using a 0.5 diluted positive PECNP drill-in fluid

B. Filter Cake Images after Static Fluid Loss Testing with Negative PECNPs

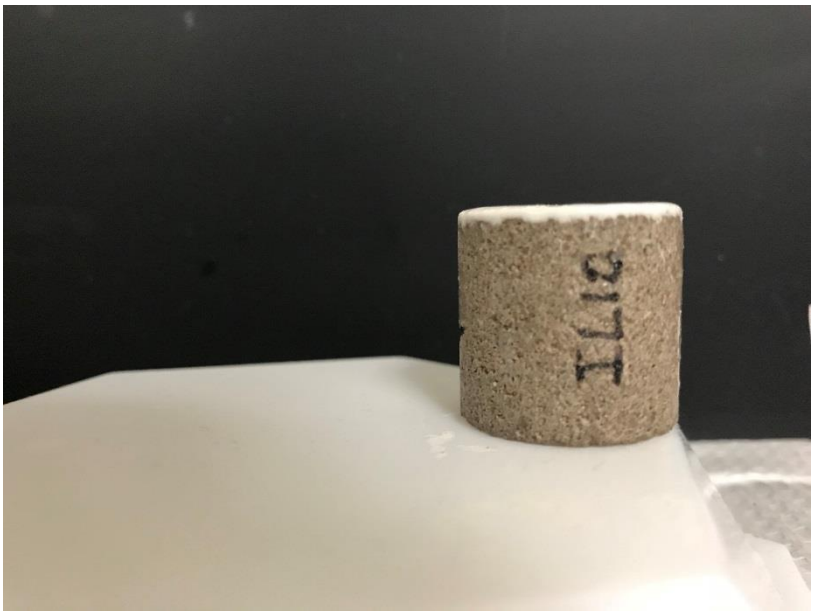

Figure B-1: Filter cake formed on IL-10 core after static fluid loss testing using a baseline drill-in fluid

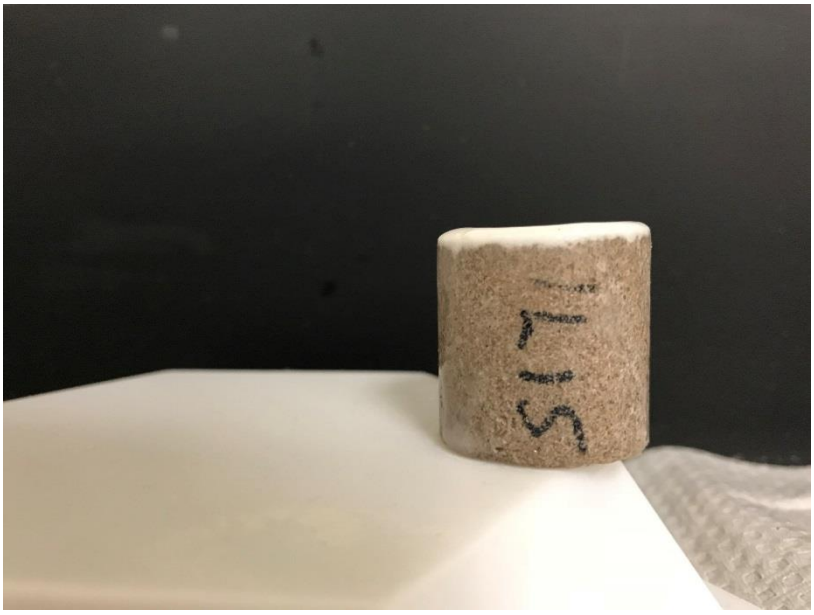

Figure B-2: Filter cake formed on IL-15 core after static fluid loss testing using an undiluted negative PECNP drill-in fluid

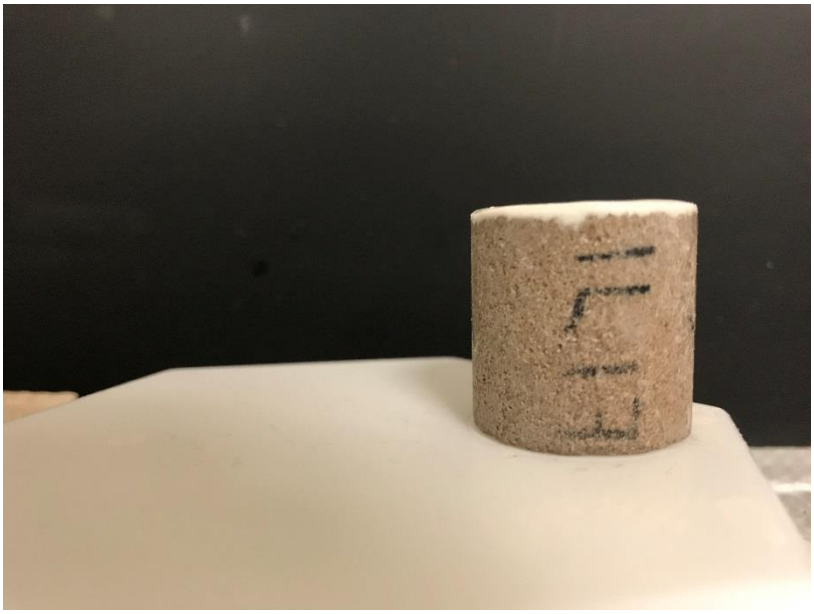

Figure B-3: Filter cake formed on IL-17 core after static fluid loss testing using a 0.125 diluted negative PECNP drill-in fluid

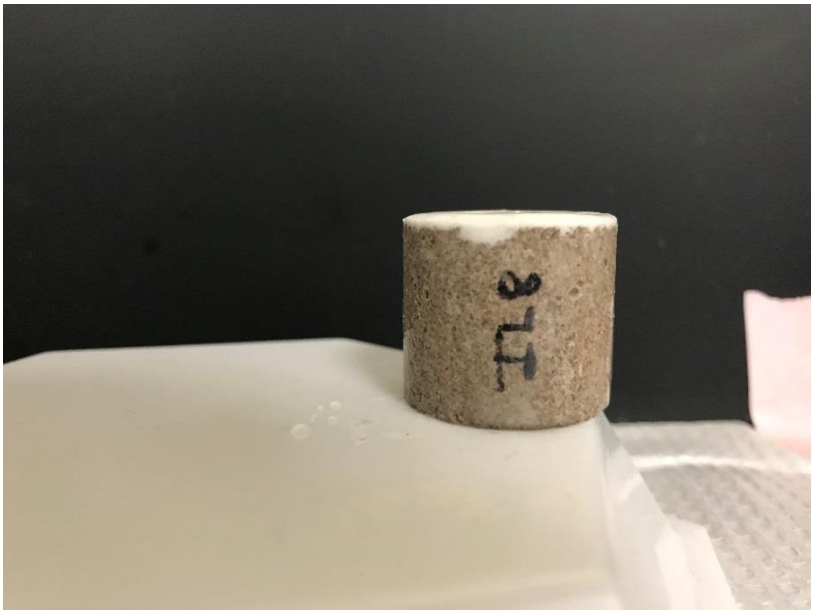

Figure B-4: Filter cake formed on IL-8 core after static fluid loss testing using a 0.25 diluted negative PECNP drill-in fluid

Figure B-5: Filter cake formed on KC-8 core after static fluid loss testing using a baseline drill-in fluid

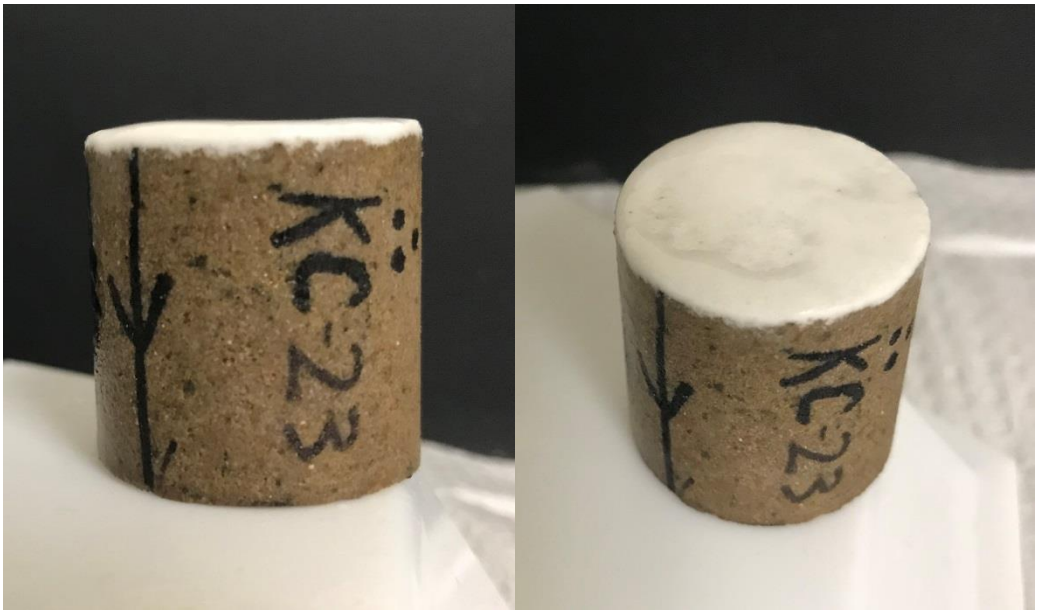

Figure B-6: Filter cake formed on KC-23 core after static fluid loss testing using an undiluted PECNP drill-in fluid

C. Filter Cake Images after Dynamic Fluid Loss Testing

Figure C-1: Filter cake formation after dynamic fluid loss testing on core IL-17 using a baseline drill-in fluid

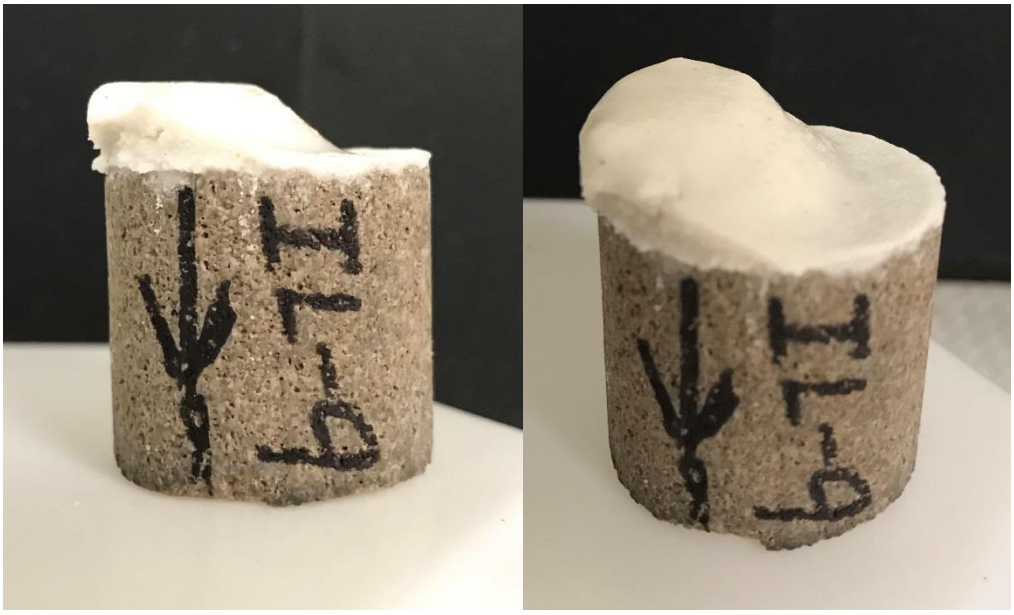

Figure C-2: Filter cake formation after dynamic fluid loss testing on core IL-9 using a baseline drill-in fluid

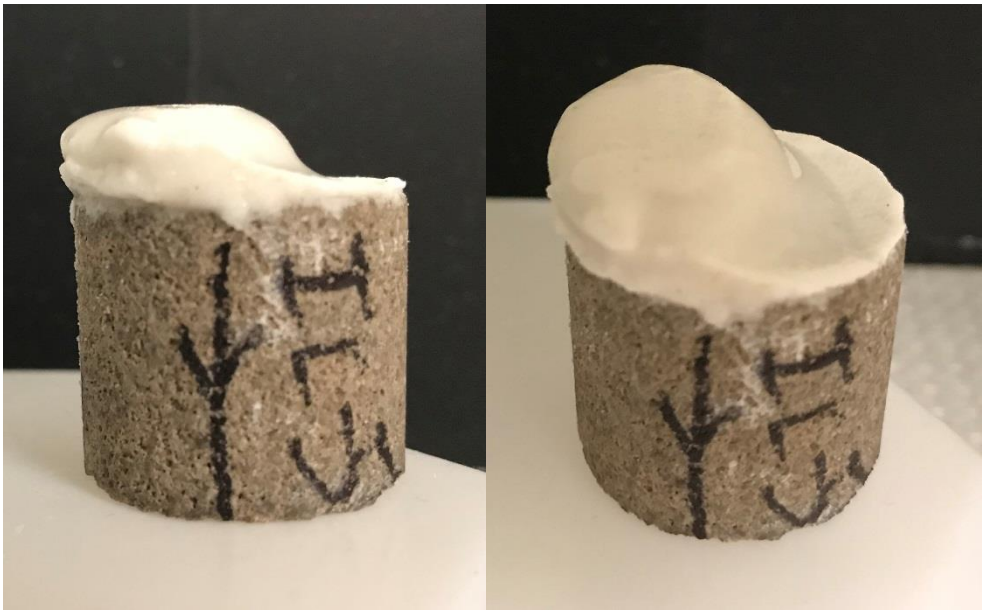

Figure C-3: Filter cake formation after dynamic fluid loss testing on core IL-5 using a baseline drill-in fluid

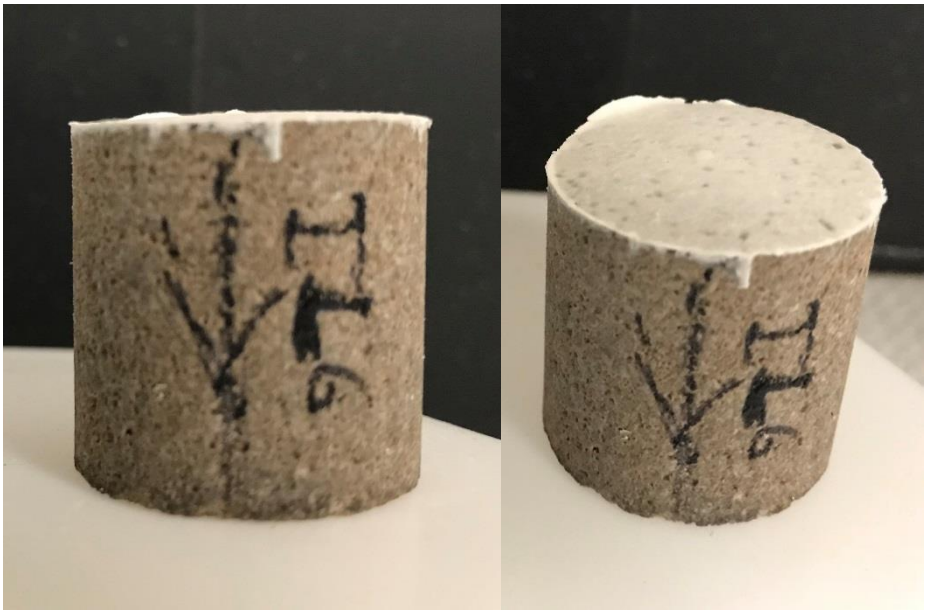

Figure C-4: Filter cake formation after dynamic fluid loss testing on core IL-6 using a 0.125 diluted PECNP drill-in fluid

Figure C-5: Filter cake formation after dynamic fluid loss testing on core IL-16 using a 0.125 diluted PECNP drill-in fluid

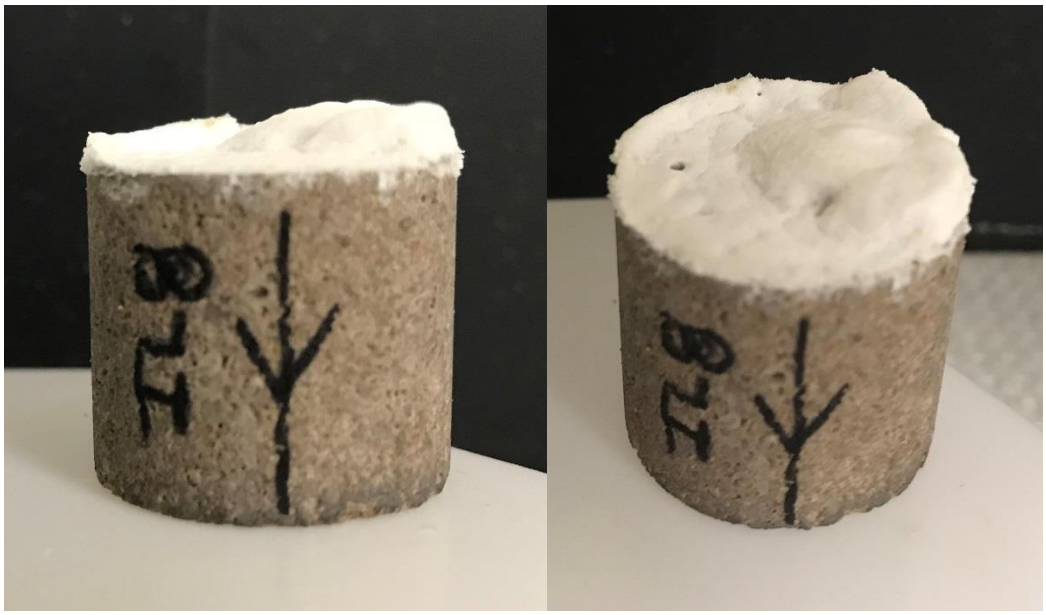

Figure C-6: Filter cake formation after dynamic fluid loss testing on core IL-8 using a 0.125 diluted PECNP drill-in fluid

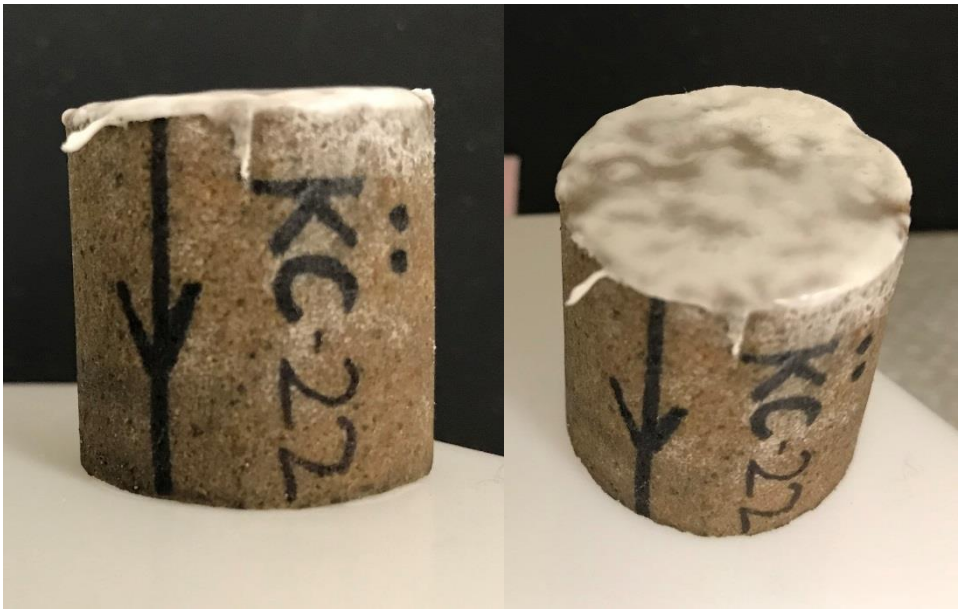

Figure C-7: Filter cake formation after dynamic fluid loss testing on core KC-22 using a baseline drill-in fluid

Figure C-8: Filter cake formation after dynamic fluid loss testing on core KC-22 using a 0.125 diluted PECNP drill-in fluid

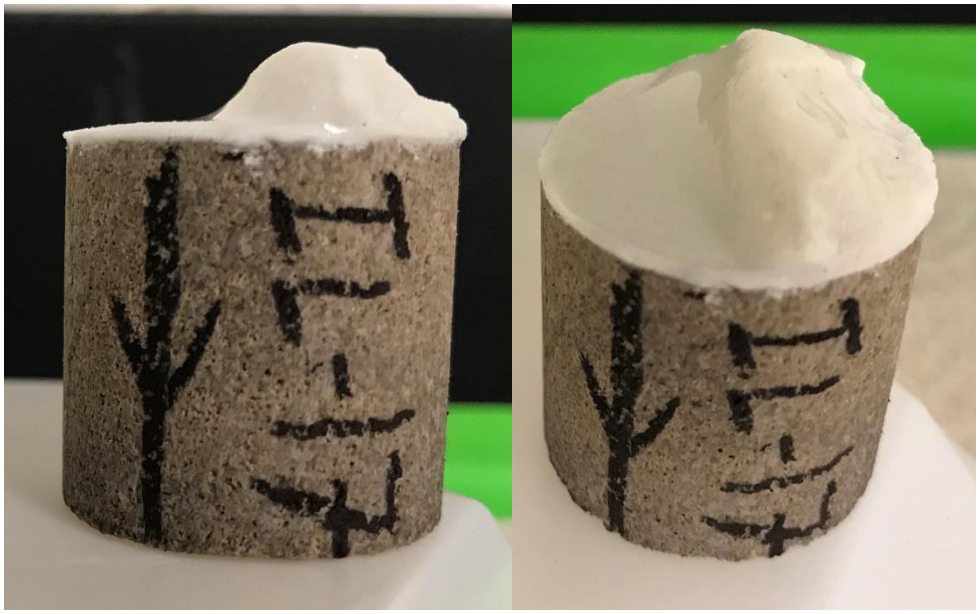

Figure C-9: Filter cake formation after dynamic fluid loss testing on core IL-17 using a baseline drill-in fluid

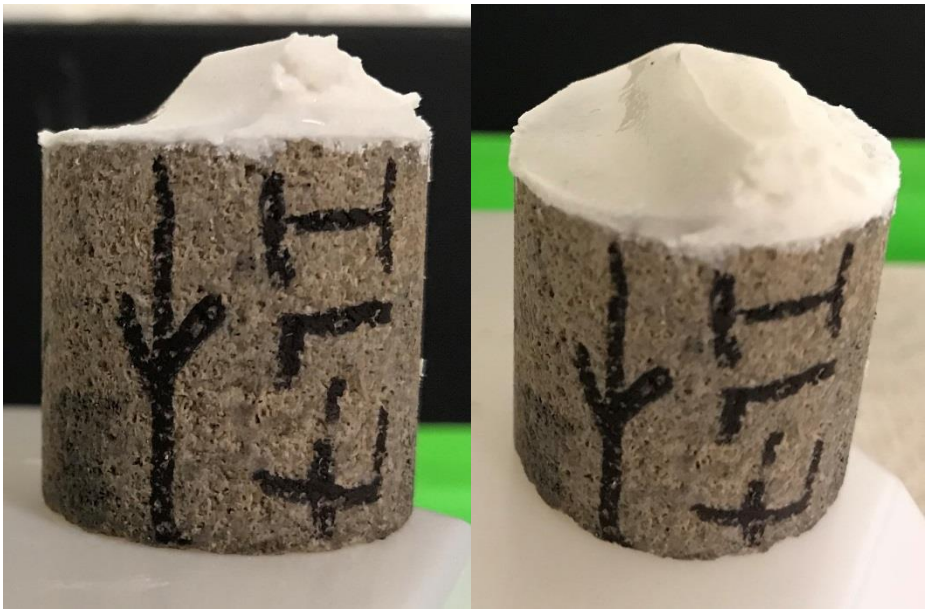

Figure C-10: Filter cake formation after dynamic fluid loss testing on core IL-7 using a 0.125 diluted PECNP drill-in fluid

D. Fluid Loss Curves Plotted by DFL Software

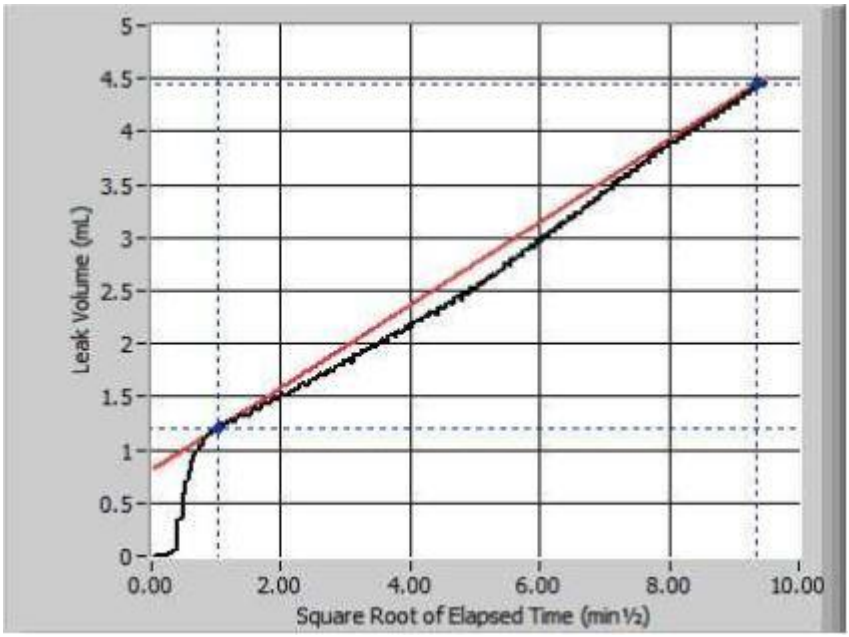

Figure D-1: IL-17 baseline test fluid loss curve plotted by DFL software

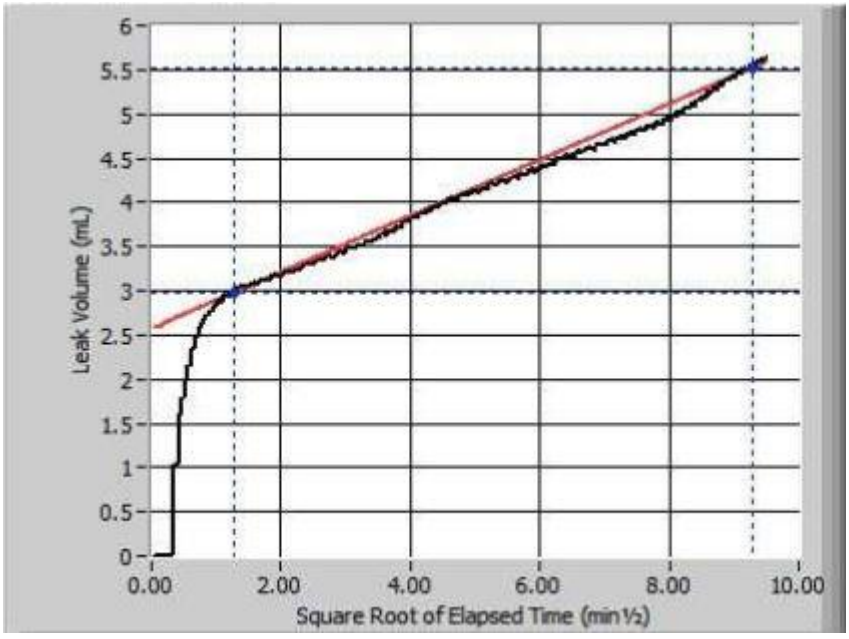

Figure D-2: IL-9 baseline test fluid loss curve plotted by DFL software

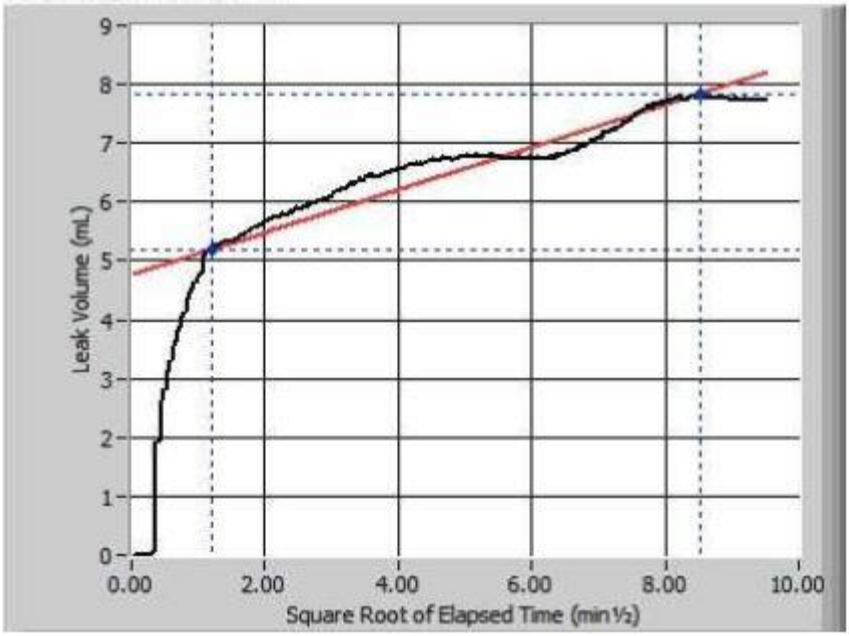

Figure D-3: IL-5 baseline test fluid loss curve plotted by DFL software

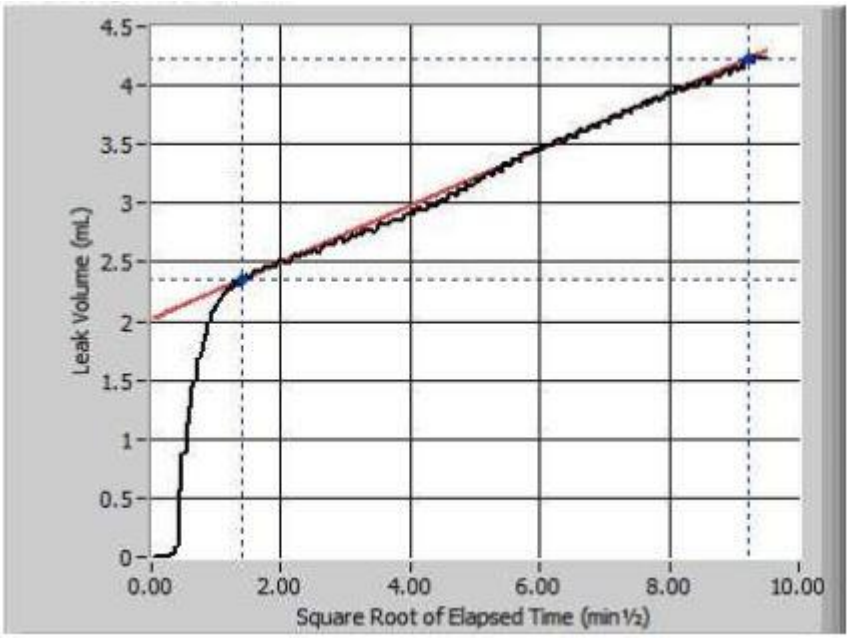

Figure D-4: IL-6 PECNP test fluid loss curve plotted by DFL software

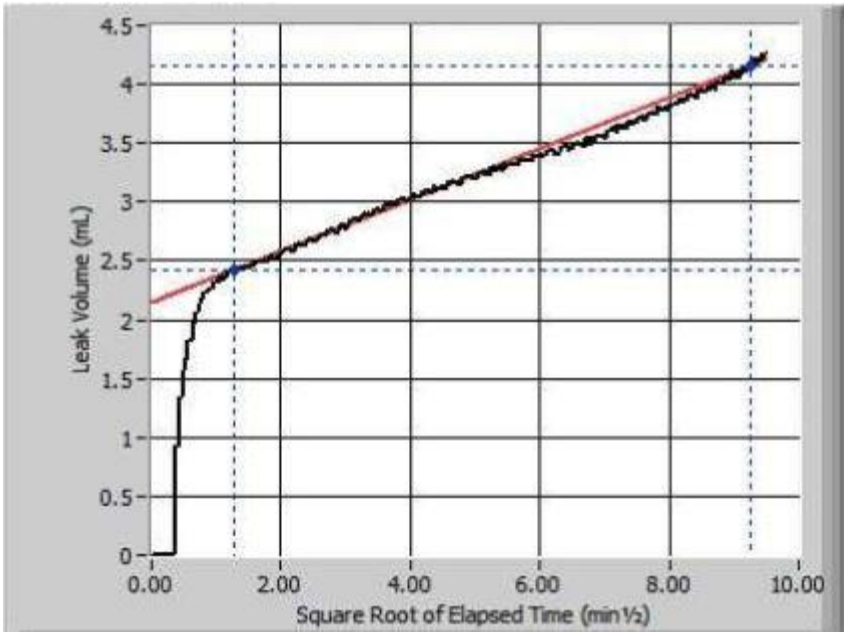

Figure D-5: IL-16 PECNP test fluid loss curve plotted by DFL software

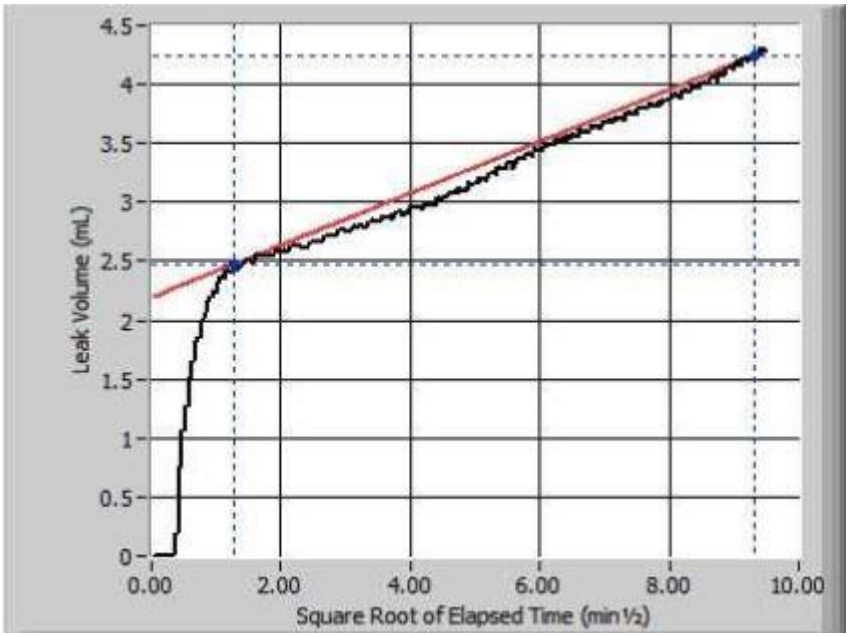

Figure D-6: IL-8 PECNP test fluid loss curve plotted by DFL software